# THE CALCULATION OF VAPOR-LIQUID EQUILIBRIA FOR PURE METAL SYSTEMS FROM PHYSICAL PRINCIPLES

By

MARK MONTOYA

A DISSERTATION PRESENTED TO THE GRADUATE SCHOOL
OF THE UNIVERSITY OF FLORIDA IN PARTIAL FULFILLMENT
OF THE REQUIREMENTS FOR THE DEGREE OF
DOCTOR OF PHILOSOPHY

UNIVERSITY OF FLORIDA

1994

ACKNOWLEDGMENTS

I would like to thank my colleagues in the Chemical Engineering Department at the University of Florida. In particular, I would like to thank Dr. Tim Anderson for his professional advice and guidance. Conversations with Dr. Mark Orazem, Dr. David Micha, Dr. Gar Hoflund, and Dr. Lewis Johns over my six year stay at the University of Florida have been both helpful and enlightening. Dr. Oliver Moghissi, Dr. Matthew Esteban, S. Ajith Perera, and Pankaj Agarwal have also contributed to my project and are heartily thanked. I would also like to thank the students at the Quantum Theory Project and the Physics Department for their perspectives, Dr. Keith Runge has helped with this project extensively--and deserves special note.

I also wish to thank a few members of the Gainesville Community. Jack Saarela, Vincent Lane, and Joe Messer have helped to maintain my sanity, by offering me the opportunity to focus on projects other than this dissertation. I thank Dr. Peter Andersen for his keen eye when it comes to spotting fish. I also thank those hackers that put up with my terrible outside shooting over the years, I promise that now that the distraction of this thesis is gone my shooting will improve, if only slightly.

My family has always believed I would finish my education, and I thank them for their support. Kristin Lundgren has also believed, her help and encouragement during the past several months is appreciated immensely.

TABLE OF CONTENTS

ACKNOWLEDGMENTS ii

LIST OF TABLES v

LIST OF FIGURES vi

ABSTRACT x

CHAPTERS

1 INTRODUCTION 1

2 STATISTICAL MECHANICAL CONSIDERATIONS 10

3 THE GENERAL MONTE CARLO METHOD 22

The Necessity of the Monte Carlo Method 22
The Metropolis Algorithm - Weighted Sampling 24
Monte Carlo Error Analysis 31

4 THE MONTE CARLO METHOD IN TWO-PHASE CALCULATIONS 36

Theory 37
Systems Previously Studied with the Gibbs Ensemble Simulation Method 49
Apparent Weaknesses of the Gibbs Ensemble Simulation Method 50
Extension of Parameter Space in the Simulation 51

5 ASSESSMENT OF FLUID MODEL POTENTIALS 54

Introduction 54
The Lennard-Jones Potential 54
The Empty-Core Pseudopotential 57

6 THE GIBBS-BOGOLIUBOV METHOD 73

Theoretical Outline of the Gibbs-Bogoljubov Method 74
The Ideal Gas Vapor Phase 81
A Simple Model for Dimers 85

7 APPLICATION OF THE GIBBS ENSEMBLE METHOD 91

Implementation of the Gibbs Ensemble Technique 91
The Lennard-Jones One Component System 93
Metal Systems - General Features 97

Initial Conditions for Metal Simulation in the Gibbs Ensemble ... 100
The Sodium System ... 101
The Aluminum System ... 106

8 APPLICATION OF THE GIBBS-BOGOLJUBOV METHOD ... 124

Structure Trends in the Periodic Table of the Elements ... 124
Outline of the Gibbs-Bogoljubov Calculation ... 127
Group IA Metals ... 128
Group IIA Metals ... 131
Group IIIA Metals ... 132
Group IVA Metals ... 133
Summary of Results ... 135

9 FUTURE CONSIDERATIONS ... 160

10 SUMMARY AND CONCLUSIONS ... 166

APPENDICES

A THE DIRECT CORRELATION FUNCTION OF A HARD-SPHERE FLUID ... 172

B APPROXIMATIONS TO THE EMPTY-CORE PSEUDOPOTENTIAL ... 174

C CALCULATION OF THE RADIAL DISTRIBUTION FUNCTION ... 185

REFERENCES ... 190

BIOGRAPHICAL SKETCH ... 195

## LIST OF TABLES


| Table | Caption | Page |
|---|---|---|
| 7-1 | Lennard-Jones parameters for various systems These parameters are used to reduce experimental quantities to dimensionless form | 113 |
| 8-1 | Parameters used for Gibbs-Bogoljubov calculation. Where parameters are not available for the diatomic vapor species the vapor is assumed to be an ideal monatomic gas The experimental internal energies are from J M Zinan [73] Diatomic spectral data are from Huber and Herzberg [74] Core radii are the values given by Hafner [41] All other property data are taken from the CRC Handbook of Chemistry and Physics, 74th Edition [64]. | 138 |
| 8-2 | Regression fits for liquid density Density is given in g/cm$^3$ Experimental curves are from the CRC Handbook of Chemistry and Physics, 74th edition [64] | 139 |
| 8-3 | Regression fits for saturated vapor pressure described by the Antoine equation, given by $\log_{10}(P) = A + B/T$, where the pressure is in atmospheres, and the temperature in K | 140 |
| 8-4 | Ionization energy values, calculated to fit experimental data at the boiling temperature Also included are the predicted melting temperatures from the Antoine equation curve fits listed in table 8-3 Experimental curves are from the CRC Handbook of Chemistry and Physics, 74th edition [64] | 141 |
| B-1 | Coefficients for the numerator of the rational polynomial representation of the dielectric function | 181 |
| B-2 | Coefficients for the denominator of the rational polynomial representation of the dielectric function. | 183 |

LIST OF FIGURES


| Figure | Caption | Page |
|---|---|---|
| 7-1 | Reduced temperature versus reduced density plot for a pure Lennard-Jones fluid, calculated using the Gibbs ensemble simulation method. Note that near the critical point the simulations do not match. Relative errors in the density calculations are very small (< 0.5 %) and are not shown to reduce the clutter at the data points. The simulations shown are results for 300 particle systems, with $2 \times 10^5$ calculation iterations. | 109 |
| 7-2 | $\log_{10}$(reduced pressure) versus reduced temperature plot for a pure Lennard-Jones fluid, calculated using the Gibbs ensemble simulation method. Error bars are too small to be seen on the plot and are no more than 0.3%. The simulations shown are results for 300 particle systems, with $2 \times 10^5$ calculation iterations. | 110 |
| 7-3 | Reduced temperature versus reduced density plot for various materials. Experimental data are taken from N.B. Vargaftik [61]. | 111 |
| 7-4 | $\log_{10}$ (reduced pressure) versus inverse reduced temperature for various materials. Experimental data are from N.B. Vargaftik [61]. | 112 |
| 7-5 | Sodium pair potential (a.u.) versus radial distance (a.u.) for various densities. | 114 |
| 7-6 | Pair potential (a.u.) versus radial distance for various densities of aluminum. | 115 |
| 7-7 | Typical calculated radial distribution function versus radial distance ($r$) for a simulated sodium system. The simulation temperature of this system was 373 K, and the ionization energy $E_{ion}$ = -5.143 eV. The tail end of the distribution function shows artifacts due to the method used to estimate the distribution. | 116 |
| 7-8 | A snapshot of a sodium liquid configuration from a Gibbs ensemble simulation at 373 K. The core radius, $R_c$ = 1.70 a.u., is used to size the spheres. Note the voids in the system, which indicate that the liquid is not a homogeneous phase. | 117 |
| 7-9 | Potential energy contributions to the volume energy of sodium (Hartrees) versus number density (atoms/m$^3$). | 118 |

| Figure | Caption | Page |
|---|---|---|
| 7-10 | Potential energy contributions to the volume energy of aluminum (Hartrees) versus number density (atoms/m$^3$) | 119 |
| 7-11 | Aluminum number density (atoms/m$^3$) versus temperature (K) for $E_{tot}$ = -54 477 eV Experimental values are from the CRC Handbook of Chemistry and Physics [73] | 120 |
| 7-12 | Aluminum $Log_{10}$(pressure in atmospheres) versus inverse temperature (K$^{-1}$) for $E_{tot}$= -54 477 eV Selected values are from Hultgren *et al* [74] | 121 |
| 7-13 | Radial distribution function versus radial distance in meters for the aluminum system This simulation was conducted with a 300 particle system at 934 K | 122 |
| 7-14 | A snapshot of an aluminum liquid configuration from a Gibbs ensemble simulation at 934 K. The core radius, $R_c$ = 1 11 a.u., is used to size the spheres The phase resembles solid aluminum | 123 |
| 8-1 | Temperature (K) versus number density (atoms/m$^3$) phase diagram for sodium Experimental data are from N B Vargaftik [61] | 142 |
| 8-2 | $Log_{10}$ (pressure in atmospheres) versus inverse temperature (K$^{-1}$) for sodium Experimental data are from N.B Vargaftik [61] | 143 |
| 8-3 | Vapor fraction of monatomic sod diatomic species for sodium plotted versus temperature in Kelvin Also included is the experimental and calculated compressibility Z of the vapor phase. Selected values are from Hultgren *et al* [65] | 144 |
| 8-4 | Calculated upper bound for the Gibbs energy per atom (J) versus temperature (K) for sodium The Gibbs energy at the melting temperature is chosen as the reference energy Selected values are from Hultgren *et al* [65] | 145 |
| 8-5 | Temperature (K) versus number density (atoms/m$^3$) for magnesium. The experimental curve is from the CRC Handbook of Chemistry and Physics, 74th edition [64] | 146 |
| 8-6 | $Log_{10}$ (pressure in atmospheres) versus inverse temperature (K$^{-1}$) for magnesium Selected values are from Hultgren *et al.*[65] | 147 |

| Figure | Caption | Page |
|---|---|---|
| 8-7 | Vapor fractions of species versus temperature for magnesium. Also shown is the compressibility $Z$ for the system | 148 |
| 8-8 | Gibbs energy (J) versus temperature (K) for magnesium. The Gibbs energy at the melting temperature is chosen as the reference energy. Selected values are from Hultgren *et al.* [65] | 149 |
| 8-9 | Temperature (K) versus liquid number density (atoms/m$^3$) for aluminum. The experimental curve is from the CRC Handbook of Chemistry and Physics [64] | 150 |
| 8-10 | Log$_{10}$ (pressure in atmospheres) versus inverse temperature (K$^{-1}$) for aluminum. Selected values are from Hultgren *et al.* [65] | 151 |
| 8-11 | Calculated fraction of atomic species versus temperature (K) for aluminum. The calculated compressibility $Z$ is also shown. | 152 |
| 8-12 | Calculated Gibbs energy per atom (J) versus temperature (K) for aluminum. The Gibbs energy at the melting temperature is chosen as the reference energy. Selected values are from Hultgren *et al.* [65] | 153 |
| 8-13 | Temperature (K) versus liquid phase density (atoms/m$^3$) for silicon. Note the difference between the experimental curve fits. The experimental curves (Experiment I and Experiment II) are from the CRC Handbook of Chemistry and Physics [64] | 154 |
| 8-14 | Log$_{10}$ (pressure in atmospheres) versus inverse temperature for silicon. Selected values are from Hultgren *et al.* [65] | 155 |
| 8-15 | Calculated vapor fraction of species versus temperature (K) for silicon. The compressibility $Z$ for the vapor phase is also shown. | 156 |
| 8-16 | Calculated Gibbs energy per atom (J) versus temperature (K) for silicon. The Gibbs energy at the melting temperature is chosen as the reference energy. Selected values are from Hultgren *et al.* [65] | 157 |
| 8-17 | Calculated number density (atoms/m$^3$) versus temperature (K) for silicon. It appears that experimental error in the measurement of the internal energy of the silicon system at its melting temperature (internal energy u in Hartrees) can have a profound effect on the calculated value for liquid density | 158 |

| Figure | Caption | Page |
|---|---|---|
| 8-18 | $\text{Log}_{10}$(pressure in atmospheres) versus inverse temperature ($K^{-1}$) for the saturated sodium system for several values of internal energy. Higher internal energies raise the slope of the vapor pressure curve, indicating a rise in the magnitude of the heat of vaporization for the system. The Experiment I and Experiment II curves are from the *CRC Handbook of Chemistry and Physics* [64]. | 159 |

Abstract of Dissertation Presented to the Graduate School of the University of Florida in Partial Fulfillment of the Requirements for the Degree of Doctor of Philosophy

THE CALCULATION OF LIQUID-VAPOR EQUILIBRIA FOR PURE METAL SYSTEMS USING PHYSICAL PRINCIPLES

By

MARK MONTOYA

AUGUST 1994

Chairman Tim Anderson
Major Department Chemical Engineering

Liquid-vapor equilibria for pure metals are examined using two previously developed modeling methods. The Gibbs Ensemble Monte Carlo model is an approach to the direct calculation of liquid-vapor equilibria from a particle representation of the metal system. This method combines characteristics of different statistical mechanical ensembles to calculate saturated properties without simulating an interface. The second method is an application of the Gibbs-Bogoljubov inequality, a perturbative method useful for estimating the Helmholtz energy of a liquid system. The Gibbs-Bogoljubov method imposes a reference liquid structure on a system with a known interatomic potential, allowing an upper bound to the Helmholtz energy of a liquid system to be calculated. Both

methods incorporate a representation of the potential energy of the metal system, for this project the empty-core pseudopotential model for nearly free electron metal systems is chosen as a compromise between accuracy and simplicity

Results for the Gibbs-Bogolyubov method are in good agreement with experimental observations of liquid density, vapor density, and system pressure The calculated ionization energy also agrees closely with experiment Calculations for test cases from the Group IA, IIA, IIIA, and IVA metals are performed The liquid structure of group IA and IIA metals is represented well by the hard sphere reference system The group IIIA and IVA systems begin to show substantial deviations from experimental results suggesting the hard-sphere fluid is not an accurate representation of these metals The vapor phase has been modeled both as a monatomic ideal gas and an associated solution of monomers and dimers Allowance for dimerization leads to results in better agreement with experimental data

Results from the Gibbs ensemble method are more ambiguous. The changes in density characteristic of the Gibbs ensemble method amplify the weaknesses in the empty-core pseudopotential representation of potential energy The rise in potential energy contributions due to dropping density are too small to overcome the decrease in energy due to pair-potential energy contributions. Representative calculations are included for the sodium and aluminum systems Methods to overcome the problem of simulating a liquid metal with the empty-core pseudopotential model using the Gibbs ensemble technique are discussed

# CHAPTER 1
# INTRODUCTION

Chemical engineers apply knowledge of the liquid-vapor transition in separation processes, and many semiconductor processing steps, such as melt-zone refinement, rapid thermal processing, and bulk crystal growth, require knowledge of the vapor pressure of a liquid metal melt. In volatile organic molecular systems, the liquid-vapor equilibrium curve is important in the calculation of flash-points. The rate of development of novel solid materials, such as compound semiconductors and complex metal alloys, has grown much faster than the current laboratory capacity for thermodynamic measurements. As a result, little is known about the thermodynamic and kinetic properties of these systems, and since the determination of system properties allows for more efficient process design, the development of effective means for bulk manufacture of the new materials has suffered accordingly. The vapor-liquid coexistence curve for many of the metal and semiconductor mixtures is difficult to determine experimentally, since the combination of highly reactive pure components coupled with the severe temperatures and corresponding high vapor pressures at which the liquid and vapor exist makes the design of a suitable measurement apparatus very difficult.

The objective of this thesis is to assess two of the theoretical methods that have yielded successful general procedures for the calculation of phase-coexistence. The first is the Gibbs ensemble method [1], a computationally expensive, brute-force particle method

for the direct simulation of liquid-vapor equilibria. The Gibbs method has not been applied to systems with complicated potentials, and there have been no previous attempts to test the method with the potential energy functions characteristic of metals. The second method is a more elegant approach based on the calculation of a lower bound to the Helmholtz energy of a system using the Gibbs-Bogoljubov inequality. This method was developed to study the bulk thermodynamic properties of metals, and previous calculations for the sodium and sodium-potassium alloy systems have been published [2,3]

The Gibbs ensemble method is a procedure that allows for the calculation of phase coexistence for any potential energy function, should this equilibrium exist. Two phases are defined in the Gibbs approach, one modeling the high density "liquid" phase and one modeling the low density "vapor" phase. Transitions are defined that allow the calculation of pressure and chemical potential for each phase at a given temperature. Hundreds of thousands of applications of each of the transitions are necessary to approximate the behavior of a real system.

The Gibbs ensemble method has several advantages. Traditional Monte Carlo approaches to the calculation of phase coexistence have relied on the creation of a **PVT** equation of state by several dozen simulations over various values of volume and temperature. Phase equilibria were found by locating two points on the **PVT** curve that have equivalent chemical potentials. The Gibbs ensemble eliminates the need for multiple simulations; each simulation yields a point that lies on the phase coexistence curve. Structure in a fluid phase is determined solely by the potential energy defined for the

simulated system Thus, model potentials must be very accurate to deliver results that agree with experiment over a wide range of temperatures Data can be accumulated that allow comparison of experimental structure with structure determined by the Gibbs ensemble method Often shortcomings in the definition of the potential energy of a system become apparent by such analysis. The Gibbs system is perfectly general The only parameters needed to begin a simulation are the chosen potential energy function and an initial system configuration

The Gibbs method also has several disadvantages Only the liquid-vapor or liquid-liquid transition can be studied with the Gibbs method Transitions corresponding to the maintenance of constant chemical potential between the systems are unlikely when one of the phases exhibits an unusually high density Simulation size effects (the number of particles) become crucial for simulations near the critical point of a liquid, where potential functions with substantial long range effects can significantly alter the properties of the calculated critical point Accurate potential energy functions must be defined over the entire range of conditions for a simulation. This is often not feasible. The Gibbs method in its current formulation does not allow for accurate calculation of the properties for systems with non-spherical, multi-segment, or strongly interacting particles

The second method proposed for study allows for the direct calculation of the thermodynamic properties of a system, using the Gibbs-Bogoljubov inequality to supply an upper bound estimate to the Helmholtz free-energy of a liquid system [2] Once this estimate is given differentiation of the Helmholtz energy yields the entropy and pressure for the liquid system The pressure and chemical potential of the vapor phase is found by

using a simple equation of state, this dissertation shows results for both an ideal gas vapor phase and an associated solution model that includes effects due to dimerization, a phenomenon that has been observed experimentally in metal vapors [4]. Once a temperature is assumed for each calculation, the problem becomes one of searching for a liquid specific volume that has the same chemical potential and pressure as the vapor phase.

The Gibbs-Bogoliubov inequality defines a perturbation calculation that relies on a choice of a reference system for liquid structure. Experiments, in the form of X-ray and neutron diffraction studies, have provided some of the information necessary for the choice of the reference fluid. Experimental structure factors for Group IA, IIA, and IIIA metals exhibit many of the qualitative characteristics of a hard-sphere fluid. These metals have a structure factor which is symmetric about the first maximum. The ratio of the positions of the first and second peaks is around 1.86. The number of atoms in the first coordination shell is between nine and eleven. Crystalline forms of these elements choose a close packed arrangement, such as a face-centered cubic, body-centered cubic, or hexagonal arrangement. The hard sphere fluid reference system seems to be a suitable choice as a reference system for these metals.

Group IVA metals present a more difficult situation. The first maximum on the experimental structure factor shows an anomalous shoulder. The liquid is loosely packed, with coordination number between six and eight. The crystalline forms of these metals show multiple structures, ranging from face-centered cubic, to the more open diamond arrangements. Bonding, especially near the melting temperature, shows a more covalent

character than the other metal melts. Because of their high boiling temperatures, experimental data over the range of liquid-vapor coexistence for these metals is scarce. For these metals, this project will address the sensitivity of the Gibbs-Bogoljubov method to the choice of a hard-sphere reference system by comparing calculations to the limited available experimental data.

Both the Gibbs-Bogoljubov method and the Gibbs ensemble method rely on the choice of a potential energy function ("potential") to describe the liquid phase of a metal system. This potential can be calculated through the inversion of an experimental structure factor, which varies with liquid temperature and pressure. Experimental structure factors must be available for all thermodynamic conditions; the need to obtain such an abundance of structure data destroys the predictive capability of the techniques in this thesis. A second method of obtaining a potential energy function is to choose a promising theoretical method which yields results close to physical reality. Ideally, the potential is also simple to calculate, which ensures calculations using the Gibbs method will not be computationally prohibitive.

Experimentally, potential energy functions for metal systems are known to have two important characteristics. First, there is a contribution to the potential energy due to the density of the system. This contribution is called the volume energy, and is due to the contributions of the free-electron gas to the system and the interactions of an atom with its own screening cloud of electrons. The second characteristic is the presence of oscillations at long-range in the potential energy function describing pair interactions. These oscillations are called Friedel oscillations, and are a characteristic resulting from a

discontinuity in the dielectric function of the electron gas expressed as a function of wavevector

The simplest theoretical representation that yields both Friedel oscillations and a density dependent contribution to the potential energy of a metal is the Ashcroft empty-core pseudopotential model [5] This simple model represents atoms as charged spheres in an electron gas Within the sphere, all potential energy contributions are present. Outside the sphere, the potential energy of the system is due to the many interactions between a system of charged hard spheres and a surrounding electron gas medium. The total potential energy in the Ashcroft model is the sum of volume contributions due to the presence of the electron gas energy effects due to exchange and correlation between electrons, Coulombic interactions between the core spheres and interactions between the core spheres and the electron cloud A small contribution to the potential energy of the metal system would be expected due to exchange and correlation contributions from core spheres; these effects are not included in the traditional Ashcroft model Perturbation theory is used to calculate the mathematical expression for the empty-core pseudopotential. In this dissertation, this approach is taken and terms to second order are included in the analysis

Parameters for the empty-core pseudopotential are calculated from the properties of a crystalline solid, and are most often determined from the partial volume derivative of the equilibrium binding energy It is not known just how well the Ashcroft form will describe liquid metals, though molecular dynamics studies in systems constrained by simulation volume have shown that the experimental structure factors of complicated

metal systems such as germanium can be represented to first approximation by the empty-core pseudopotential [6] The Gibbs ensemble simulation method should determine the usefulness of the empty-core pseudopotential as a stand-alone representation of a liquid metal.

Calculations using the Gibbs ensemble method are attempted to determine the phase coexistence curves for the sodium and aluminum systems The two systems studied are chosen to exploit the qualitative differences between the pair potentials of the liquid phase calculated at the metal's melting temperature. The potential energy function incorporated is a true density dependent potential since both the pair-potential terms and the volume energy of the system are dependent on the specific volume of the system These calculations will be the first to study realistic volume dependent potentials using the Gibbs ensemble method

The Gibbs-Bogoljubov method has been previously applied to calculate liquid-vapor coexistence properties for the sodium system [3,7] This thesis describes a systematic study of the periodic table by examining elements from Groups IA, IIA, IIIA, and IVA. Predictions not only account for liquid density, pressure, and Gibbs energy as functions of temperature, but information is also gathered concerning the ionization potential for a pure metal modeled by the empty-core pseudopotential Modeling the vapor phase using an associated solution model yields information about the concentration of monatomic and diatomic species in the vapor phase of the metal

Since this thesis outlines work that is outside the traditional scope of the chemical engineering discipline, two introductory chapters are included to provide background

information on the techniques needed to apply the Gibbs Ensemble Monte Carlo method The second chapter addresses some of the statistical mechanical relations used to calculate bulk thermodynamic properties from simulation. Chapter 3 is a description of the general Monte Carlo method, and a simple application of the Monte Carlo method is examined before extending the method to the evaluation of statistical mechanical integrals Chapter 4 is an introduction of the Gibbs Monte Carlo method The theory behind the method is outlined and successful applications of the method are listed

In chapter 5 the potential energy functions considered for the representation of the metal system are examined Since the empty-core pseudopotential model is quite complicated most of the chapter is devoted to the expressions needed to calculate the volume energy and pair-potential characteristic of the real space formulation of this potential representation Chapter 6 is an outline of the Gibbs-Bogoljubov method and presents two models for the vapor phase of the system the ideal vapor phase and the associated solution model The basics of the hard sphere fluid are presented, and a reciprocal space formulation of the empty-core pseudopotential is also covered

Chapter 7 includes a discussion of the results of Gibbs ensemble calculations for the sodium and aluminum systems, both chosen for the relative relation of the first potential minimum to the first peak of the radial distribution function After a brief discussion of liquid metal structure, chapter 8 presents the results of the application of the Gibbs-Bogoljubov method to metal systems In chapter 9 suggestions are made for future work, and chapter 10 lists the conclusions of this dissertation. Appendix A calculates the direct correlation function for a single component hard-sphere fluid An approach to the

integration of the real-space formulation of the pair potential is given in Appendix B Appendix C is a collection of the information necessary to calculate the radial distribution function of a liquid system

## CHAPTER 2
## STATISTICAL MECHANICAL CONSIDERATIONS

In order to discuss the computational issues examined in this thesis, some basic statistical mechanical relations and properties must be introduced. These relations will describe how a model constructed for atomic level interactions will allow for the calculation of the macroscopic properties of the system. To begin this discussion, a typical system for atomistic simulation must be described. Once this system is defined, classical mechanics can be used to analyze the system, and eventually some basic statistical mechanical results will be used to define the macroscopic thermodynamic properties of the atomistic system. These results will be presented in a computational context to demonstrate how they will be used to calculate phase properties of the system. Finally, the atomistic system properties that allow comparison of experimental results to the models used in atomistic simulation will be reviewed.

A system for the purpose of atomistic simulation consists of a cubic region in space of length $L$ and volume $V$ which contains $N$ atoms. The position vector of each atom is given from a common origin situated at the center of the cube, and represented by the symbol $r_i$, where $i$ is a unique integer index assigned to each atom. To be rigorous, each atom also has a momentum vector $p_i$, though this quantity is ignored by assumptions explained later when calculating bulk thermodynamic properties using the Monte Carlo

method For the purposes of this thesis, it is assumed that each atom interacts with other atoms through pair interactions only, that is, the dynamic description of the many-body system is concerned with forces that arise from the study of pairs of atoms only The system can also be assigned a volume dependent energy, which is an energy that depends on the specific volume of the system, given by $V/N$ Unless otherwise specified, each atom is assumed to be an infinitesimal point in space. The temperature $T$ of the system for Monte Carlo simulations will always be fixed.

The behavior of a much larger simulation system is approximated by using periodic boundary conditions, a method which artificially surrounds a simulation cube with 6 perfect replicas of itself and calculates the interaction of the atoms within the simulation cube with the nearest of the atoms artificially surrounding the cube Though this method introduces a periodicity to the liquids simulated, the contributions of this periodicity to the system energy and structure are assumed to be small - much smaller than the total energy of the system

Since the system is now defined, the methods of statistical thermodynamics can be applied to calculate the equilibrium properties of the system [8] Statistical thermodynamics is a field that allows the calculation of a system's thermodynamic properties given the Hamiltonian, or equation of energy, for the system Given a Hamiltonian $\mathcal{H}$ which consists of the sum of $n$ energy levels $\mathcal{E}_1 + \mathcal{E}_2 + \mathcal{E}_3 + \quad + \mathcal{E}_n$, the probability $\mathcal{P}$ that a system lies at an energy $\mathcal{E}_i$ can be calculated to be

$$\mathcal{P}_i = \frac{\exp\left(-\frac{\mathcal{E}_i}{k_B T}\right)}{\sum_{j=1}^{} \exp\left(-\frac{\mathcal{E}_j}{k_B T}\right)} \tag{2-1}$$

where $k_B$ is Boltzmann's constant and $T$ is the absolute temperature of the system. Knowing this distribution of energies allows for the calculation of the average properties of a system. If each contribution to the property $\mathcal{A}_i$ is calculated for an energy $\mathcal{E}_i$, then the calculated $\mathcal{A}_i$ can be weighted according to the probability for occupation given by (2-1), giving the system average

$$\langle \mathcal{A} \rangle = \frac{\sum_{i=1}^{} \mathcal{A}_i(\mathcal{E}_i) \exp\left(-\frac{\mathcal{E}_i}{k_B T}\right)}{\sum_{i=1}^{} \exp\left(-\frac{\mathcal{E}_i}{k_B T}\right)} \tag{2-2}$$

Both the simple test systems and the more complex metal systems studied are represented by a continuum of energy levels, a consequence of the classical representation of pair potentials assumed to represent the system. If the energy levels of a system are closely spaced, as in the quantum energy levels of a complex molecule, or are represented by functions defined over all energy levels, the sums in equation (2-2) can be replaced by integration over all energy levels

$$\langle \mathcal{A} \rangle = \frac{\int_{\mathcal{E}}^{} \mathcal{A}(\mathcal{E}) \exp\left(-\frac{\mathcal{E}}{k_B T}\right) d\mathcal{E}}{\int_{0}^{} \exp\left(-\frac{\mathcal{E}}{k_B T}\right) d\mathcal{E}} \tag{2-3}$$

Equation (2-3) will allow for the evaluation of the pressure and chemical potential of the systems of interest

Monte Carlo simulation depends exclusively on the potential energy of the system of atoms As stated before, this thesis is mainly concerned with volume dependent energies and energies due to the interaction of pairs of atoms The potential energy of interaction between pairs of atoms is called a pair potential, and is a function of the scalar distance between atoms. Let $v(r)$ be the potential energy of interaction between a pair of atoms separated by the scalar distance $r$, so that the total system energy due to the pair potential can be calculated by

$$\mathcal{V}_{sys} = \frac{1}{2}\sum_{i=1}^{N}\sum_{\substack{j=1 \\ j\neq i}}^{N} v\left(\left|\mathbf{r}_i - \mathbf{r}_j\right|\right) \qquad (2\text{-}4)$$

This expression gives the potential energy due to fluid structure for a system described by pair potentials Not all the terms in the pair potential sum contribute significantly to total potential of the system, and depending on the potential chosen to represent the system, a cut-off radius is generally introduced that separates the quickly varying potential contributions due to an atom s nearest neighbors from the more slowly varying long-range contributions

Certain statistical mechanical theorems allow alternative, simpler methods for the calculation of average properties, and these method will also be used to calculate thermodyname properties from Monte Carlo simulations One such theorem is the virial theorem Assume that a system can be represented by a Hamiltonian $\mathcal{H}$ defined as a function of the position vector r and the momentum vector p, or $\mathcal{H} = \mathcal{H}(r, p)$ Then each component of the variable vectors p or r is related to the system temperature by

$$\left\langle r_k \frac{\partial \mathcal{H}}{\partial r_k} \right\rangle = k_B T \tag{2-5}$$

$$\left\langle p_k \frac{\partial \mathcal{H}}{\partial p_k} \right\rangle = k_B T \tag{2-6}$$

for the coordinates $r_k$ and the momenta $p_k$. It is through the virial theorem that the momentum of a system is related to the temperature of a system by the simple relation

$$\left\langle \sum_{i=1}^{N} \frac{|p_i^2|}{m_i} \right\rangle = 2\langle \mathcal{T} \rangle = 3N k_B T \tag{2-7}$$

where $m_i$ is the mass of a particle, and $\mathcal{T}$ is the instantaneous kinetic energy of the system.

Monte Carlo simulations do not calculate the kinetic temperature of the system, but the virial theorem can also use the position vectors of atoms in a closed system to calculate the equilibrium pressure of that system. Hamilton's equations of motion can be written as a sum of two contributions $\mathcal{T}$ and $\mathcal{V}$, which represent the kinetic and potential energy of the system, respectively. If it is assumed that the kinetic energy is dependent on momentum only and the potential energy is dependent only on the position of the particle in the system, the system Hamiltonian can be written

$$\mathcal{H}(\mathbf{r}, \mathbf{p}) = \mathcal{T}(\mathbf{p}) + \mathcal{V}(\mathbf{r}) \tag{2-8}$$

If only the coordinate derivatives are considered, the virial equation reduces to

$$-\frac{1}{3}\left\langle \sum_{i=1}^{N} \mathbf{r}_i \bullet \nabla_{r_i} \mathcal{V}(\mathbf{r}) \right\rangle = \frac{1}{3}\left\langle \sum_{i=1}^{N} \mathbf{r}_i \bullet \mathbf{f}_i^{int} \right\rangle = -N k_B T \tag{2-9}$$

with $\mathbf{f}_i^{tot}$ representing the total force on a particle, including external forces such as electric and magnetic fields. If the effect of molecular collisions with container walls is considered, the external pressure can be calculated by

$$\frac{1}{3}\left\langle \sum_{i=1}^{N} \mathbf{r}_i \bullet \mathbf{f}_i^{wall} \right\rangle = -PV \tag{2-10}$$

The internal virial $\mathcal{W}$ can be defined similarly by

$$\mathcal{W} = -\frac{1}{3}\sum_{i=1}^{N} \mathbf{r}_i \bullet \nabla_{\mathbf{r}_i} V = -\frac{1}{3}\sum_{i}^{N} \mathbf{r}_i \bullet \mathbf{f}_i \tag{2-11}$$

where the forces considered are the interatomic forces only. The forces on each atom may divided into interatomic and external contributions, which allows the pressure equation to be rewritten

$$PV = N k_B T + \langle \mathcal{W} \rangle \tag{2-12}$$

Again the pressure can be divided into an instantaneous pressure equation

$$P = \rho k_B T + \frac{W}{V} = P^{virial} + P^{external} \tag{2-13}$$

valid for any system configuration, which has the property of returning the average pressure of the system when averaged over all configurations. In a system with periodic boundary conditions, there are no container walls with which to reckon, and thus there are no external forces. Despite this difference in system description, the same equations can be used to calculate the pressure of the system. By using the virial theorem, a continuum description for pressure has been transformed into an average of the virial calculated for discrete configurations of the atomic system.

If only pairwise interactions are studied, a few shortcuts may be provided for the calculation of the virial which are computationally more convenient than those for

generalized potentials, this assumption expedites the calculation of pressure. Define the pairwise potential interaction as a function of interatomic distance $r$ only $v = v(r)$. Now rewrite the system virial in a form independent of the origin of the system, by revising the expression for the internal forces in the virial $\mathbf{f}_i$ in terms of the forces contributed by each individual atom i pulling on atom j, written $\mathbf{f}_{ij}$

$$\sum_i \mathbf{r}_i \bullet \mathbf{f}_i = \sum_i \sum_{j \neq i} \mathbf{r}_i \bullet \mathbf{f}_{ij} = \frac{1}{2} \sum_i \sum_{j \neq i} \mathbf{r}_i \bullet \mathbf{f}_{ij} + \mathbf{r}_j \bullet \mathbf{f}_{ji} \tag{2-14}$$

Every action has an equal and opposite reaction, so $\mathbf{f}_{ij} = -\mathbf{f}_{ji}$, and if $\mathbf{r}_{ij} = \mathbf{r}_i - \mathbf{r}_j$, the force expression becomes

$$\sum_i \mathbf{r}_i \bullet \mathbf{f}_i = \frac{1}{2} \sum_i \sum_{j \neq i} \mathbf{r}_{ij} \bullet \mathbf{f}_{ij} = \sum_i \sum_{j>i} \mathbf{r}_{ij} \bullet \mathbf{f}_{ij} \tag{2-15}$$

The virial in this form is then

$$\mathcal{W} = \frac{1}{3} \sum_i \sum_{j>i} \mathbf{r}_{ij} \bullet \mathbf{f}_{ij} = -\frac{1}{3} \sum_i \sum_{j>i} \mathbf{r}_{ij} \bullet \nabla_{r_i} v(\mathbf{r}_{ij}) = -\frac{1}{3} \sum_i \sum_{j>i} w(\mathbf{r}_{ij}) \tag{2-16}$$

and if it is assumed that $w = w(r)$, with $r$ the scalar distance between two atoms, the gradient becomes simply

$$w(r) = r \frac{dv(r)}{dr} \tag{2-17}$$

Though it may not seem necessary to study the structure of a fluid in order to calculate the phase diagram of a material, it is necessary to evaluate the accuracy of the pair potentials used in the simulations. Structural information about a fluid is generally presented in the form of a radial distribution function, a defined quantity that represents the probabilistic distribution of the distances between pairs of atoms in a fluid. Radial

distribution functions are actually the single most important statistic kept during a Monte Carlo simulation, since the value of all equilibrium thermodynamic properties can be calculated if the structure of the fluid and the interatomic potential of interaction is known. The total internal energy and pressure of an atomistic system can be defined in terms of the radial distribution function $g(r,\rho,T)$ and the system potential energy function $v(r)$ by

$$\frac{E}{Nk_BT} = \frac{3}{2} + \frac{\rho}{2k_BT}\int_0^\infty v(r)g(r)4\pi r^2 dr \tag{2-18}$$

and

$$\frac{P}{k_BT} = \rho - \frac{\rho^2}{6k_BT}\int_0^\infty r\,v'(r)\,g(r)4\pi r^2\,dr \tag{2-19}$$

Similar expressions exist for the calculation of other thermodynamic properties from the radial distribution function and potential energy function.

During the course of a simulation it is more convenient to store the numbers necessary to calculate the radial distribution function, for later Fourier transformation into the static structure factor. The radial distribution function for the canonical ensemble is defined by the integral

$$g(\mathbf{r}_1,\mathbf{r}_2) = \frac{N(N-1)}{\rho^2 Z_{NVT}}\int d\mathbf{r}_3\,d\mathbf{r}_4 \cdots d\mathbf{r}_N \exp\left[-\beta\ V(\mathbf{r}_1,\mathbf{r}_2,\cdots,\mathbf{r}_N)\right] \tag{2-20}$$

which can be transformed to the more computationally useful discrete form

$$g(\mathbf{r}) = \rho^{-2}\left\langle \sum_i \sum_{j\neq i} \delta\left(\mathbf{r}_i\right)\delta\left(\mathbf{r}_j - \mathbf{r}\right)\right\rangle = \frac{V}{N^2}\left\langle \sum_i \sum_{j\neq i} \delta\left(\mathbf{r} - \mathbf{r}_{ij}\right)\right\rangle \tag{2-21}$$

The computational technique used to gather the data for the radial distribution function separates space into discrete segments, with each segment representing a range of distances. A histogram is constructed, with each histogram entry consisting of a counter representing a particular range of distances. The distances between all pairs of atomic

centers are calculated, and the corresponding histogram is incremented. The data can then be stored in histogram form until it is needed to recover an approximation to the continuous radial distribution function. The accuracy of the approximation is a function of the number of configurations generated and the graininess of the histogram used for storage.

While simulating a fluid using atomistic simulation, only the potential energy of interaction with the nearest neighbors of the system is considered to change considerably over the course of the simulation. The remainder of the energy is lumped into a term called the long-range interaction, which is the contribution to energy due to all the other atoms external to the atoms for which forces and energies are actually calculated. In order to calculate these forces, it is assumed that a sphere of radius $r_{cut}$ exists around each atom. Inside the sphere, forces and energies are calculated for each discrete interaction with the contained neighbor atoms. Outside the sphere, the radial distribution function of the fluid is considered uniform and equal to one, an assumption that corresponds to a fluid having the random structure of an ideal gas outside the sphere. The potential energy of a system can then be found by separating the contributions to energy into two terms, one for the atoms within the cutoff radius, for which the previously described statistical mechanical methods are used to describe the average properties of the system, and a term for the region outside the cutoff radius, where a the radial distribution function $g(r)$ is approximated to be one. The expressions for energy and pressure then become

$$E = E_c + E_{LRC} \approx E_c + 2\pi N \rho \int_{r_{cut}}^{\infty} r^2 v(r)\, dr \tag{2-22}$$

$$(PV)_{full} = (PV)_{ig} + (PV)_{LRC} \approx (PV)_{ig} - \frac{2\pi N \rho}{3} \int_{r_{cut}}^{\infty} r^3 v'(r)\, dr \tag{2-23}$$

where $E_{LRC}$ and $(PV)_{LRC}$ are the contributions to the system energy and the pressure-volume product, respectively

The radial distribution function is not the only useful method for representing fluid structure A second quantity can be used to describe the structure of a fluid, the structure factor of a fluid is a representation of fluid structure in Fourier space, given by

$$S(q) = 1 + \rho \int_0^{\infty} 4\pi r^2 \left[g(r) - 1\right] \frac{\sin(qr)}{qr}\, dr \tag{2-24}$$

where $q$ is the wavevector of a radially symmetric system It is the structure factor of an atomic liquid that can be determined from X-ray diffraction studies The intensity of scattered X-rays at any wavevector is directly proportional to the structure factor of a system, the relation given by

$$S(q) = I \Big/ \left\langle N f(q)^2 \right\rangle \tag{2-25}$$

where $N$ is the total number of atoms in a system, $I$ is the intensity of the scattered radiation, and $f(q)$ is the atomic scattering factor The atomic scattering factor for each metal is a tabulated quantity, and can be calculated from first principles The magnitude of the wavevector for the incident radiation is given by

$$q = 4\pi \sin(\theta)/\lambda \tag{2-26}$$

where $\theta$ is twice the scattering angle, and $\lambda$ is the radiation wavelength. The structure factor of a fluid gives the experimental basis necessary to study the structure of atomic fluid for comparison with various theories

An experimental method also exists that allows direct insight into the form of the potential energy function for a system In atomistic simulation, the radial distribution function is determined solely by the choice of the potential energy function of the system It follows then, that if the structure factor or radial distribution function of a liquid system is known, a mean pair potential that defines the system for atomistic simulation should be defined Thus, an experimental method of examining the potential of a system is to determine the potential from X-ray diffraction studies of the liquid phase The static structure factor obtained from X-ray diffraction is inverted through Fourier transform, giving the radial distribution function Then the pair-potential can be obtained by approximation using a complex thermodynamic relation such as the Ornstein-Zernike equation [9] The potential obtained through analysis of experimental data is not unique, for several potentials may yield thermodynamic properties that agree with experiment. This potential may not be the true potential energy function of a system, but is a potential of mean force throughout the system, ignoring local and volume effects Studying the inverted potential can give qualitative insights that are useful in creating an accurate theory for the potential energy of a metal system

In this chapter, a simple thermodynamic system of many atoms was studied. Some of the methods traditionally used in atomistic simulation to calculate average properties, such as energy and the pressure, have been outlined The theory for calculation of a radial distribution function for a single component system has also been presented In addition, average thermodynamic properties have been related to the structure and potential energy function of a single component system, providing a basis for comparison of simulation

results with those results derived from experiment These techniques will be applied in detail in the Gibbs Ensemble Monte Carlo method, discussed in chapter 4 and in the Gibbs-Bogoljubov method, described in chapter 6

## CHAPTER 3
## THE GENERAL MONTE CARLO METHOD

This chapter is devoted to introducing the Monte Carlo method. The necessity of the Monte Carlo method will be outlined, and a simple method for integral evaluation will be summarized and applied to a model that is simply defined mathematically, but extremely difficult to examine numerically. Monte Carlo integration will then be discussed as a tool for evaluating the integrals that arise in statistical mechanics. The theory of branching processes and Markov chains will be reviewed, and the Metropolis algorithm for increasing the efficiency of Monte Carlo integration will be discussed. Finally, methods previously developed for statistical analysis of Monte Carlo results will be outlined.

### The Necessity of the Monte Carlo Method

The Monte Carlo method is a means of integration employed for integrals which cannot be solved reasonably either by numeric quadrature or analytic means. In general, the Monte Carlo integration method is applied to integrate volumes of more than three dimensions. The results, as will be shown, are statistical in nature and demand an error analysis similar to the analysis applied to experimental results.

As an example of the difficulties involved in the integration of a function of more than one variable, consider a volume contained in a unit "cube" in twenty dimensional

space described by the set $\{x_0, x_1, \cdots, x_{19}, x_{20} \in [0,1]\}$ Assume that the volume is defined by the twenty bounding inequalities given by

$$\begin{aligned} f_0(x_1, x_1, \cdots, x_{19}) &\le x_0 \le g_0(x_1, x_1, \cdots, x_{19}) \\ f_1(x_0, x_1, \cdots, x_{19}) &\le x_1 \le g_1(x_0, x_1, \cdots, x_{19}) \\ &\cdots \\ f_{19}(x_0, x_1, \cdots, x_{19}) &\le x_{19} \le g_{19}(x_0, x_1, \cdots, x_{19}) \end{aligned} \qquad (3\text{-}1)$$

where each function $f$ and $g$ is slowly varying and continuous, have values for all $x_n$ within the interval (0 1), and show no strong peaks The volume is defined on all sides, the integral of interest is simply the calculation of the volume within the bounding functions

Assume that simple quadrature is to be used to find the volume of the twenty dimensional object The problem for such a system now becomes the identification of the surface of the volume, fitting a functional representation of the surface between each equally spaced point in the grid, and evaluating the integral using a simple algorithm such as Simpson's rule over all twenty dimensions. Simpson's rule demands equally spaced abscissas, and for a ten point evaluation over each dimension, the integral, at minimum, will require the availability of points at $10^{20}$ equally spaced sites on the surface of the defined volume. The surfaces must be identified computationally, a proper function must be fit for quadrature, and the appropriate quadrature formulas must be evaluated For more than the simplest of functions this approach is intractable

A simpler brute force algorithm constructs an equally spaced grid throughout the twenty dimensional space within the unit cube and counts the $n$ points that lie within the volume. Each point in the grid is tested to see if it is within the volume, and a ratio of points within the volume to the $n^{20}$ points tested gives an estimate to the volume of the

defined area, which increases in accuracy as $n \to \infty$. For a relatively simple evaluation, using a grid consisting only of ten points in each dimension, a volume estimation will use $10^{20}$ evaluations of each of the inequalities, again an intractable calculation on the fastest of machines. Results can also be inaccurate if the volume makes its way through the unsampled space: a twenty dimensional torus with small minor radii will show the weaknesses with this algorithm.

Monte Carlo integration of the volume does not construct a grid. It merely takes points at random throughout twenty-dimensional space, and tabulates whether or not the point lies within the volume, and again the volume of the cube is determined by a ratio of points found to lie within the cube to the total points sampled. In this manner, only a few thousand points may give an idea of the surface volume, with the estimate statistically refined as the number of samples increases.

The Metropolis Algorithm - Weighted Sampling

The Monte Carlo method as used in statistical mechanics was first proposed by Nicholas Metropolis *et al.* [10] and modifies the true Monte Carlo scheme by eliminating samples from regions of space known to make little contribution to the integral. The Metropolis scheme is based on an interpretation of the equipartition of energies from statistical mechanics, and is used to evaluate the integral found in equation (2.2) to determine average properties. If the potential energy of the system is dependent only on the relative positions of the particles in the system, as is the case when considering only volume and pair interactions within the system, then an average property of a system can be calculated by evaluating this integral over $3N$-dimensional space. Metropolis decided

that a random sampling of all possible energy states in thermodynamic system would be inefficient. The computation of integrals for statistical mechanics could be made more efficient without a loss in accuracy if the system were sampled only near regions that made major contributions to the value of the average property integral. For thermodynamic properties, this region is known to lie at states near the system's lowest energy configuration.

An initial configuration of a thermodynamic system would be allowed to start at a high energy, high entropy, low probability configuration, and by the application of a suitable chain of processes, the system could be moved to the low energy states that define the equilibrium values for a system. Sampling in a suitable distribution around the minimum energy would ensure that all the major contributions to the average property integrals are tabulated for the integral. Thus, the problem of Monte Carlo integration in a statistical mechanical system becomes two-fold: first, a means by which the system can be driven to its low energy configuration must be characterized, and second, a suitable probability distribution that allows efficient sampling of the parameter (phase) space that contributes most to the integral to be evaluated must be defined.

As an example, consider the canonical ensemble. For this system, any average value $\mathcal{A}$ of a system of atoms can be evaluated by converting (2.2) to the integral

$$\langle \mathcal{A} \rangle_{NVT} = \int d\Gamma \rho_{NVT}(\Gamma) \mathcal{A}(\Gamma) \qquad (3\text{-}2)$$

where $\rho(\Gamma)$ is the distribution within the state space $\Gamma$ and $\mathcal{A}$ is the property to be averaged. This average also contains a normalizing factor, which is the partition function of the canonical ensemble, but this factor drops from calculation and is included implicitly

in this equation The properties of the system can be approximated over many discrete samples chosen from a probability distribution $\rho$ by approximating the average integral by

$$\langle A \rangle_{NVT} = \left\langle \frac{A\rho_{NVT}}{\rho} \right\rangle_{trials} \tag{3-3}$$

If the thermodynamic energies of a system are continuous functions of the state space variables, and the potential energy of the canonical ensemble is typically defined in terms of the position vectors of the atoms in the system, the average properties of the system can be further approximated by sampling the system near the mean energy with the Boltzmann distribution $\rho = \rho_{NVT}$, since this region makes the most significant contribution to the integral (3-2) By choosing this distribution, the average properties of a system will become the average properties of the trial configurations, turning the continuous integral into a discretely defined sampling given by

$$\langle A \rangle_{NVT} = \langle A \rangle_{trials} \tag{3-4}$$

Discrete sampling also allows the calculation of a standard deviation and fluctuation values for the collected average, and thus error estimates and estimates to other static thermodynamic quantities, such as heat capacity, can also be made

A path to the mean value for the energy of the system must now be outlined A mathematical construct that allows any system configuration with an asymptotic limiting distribution (in this case, the system at equilibrium) to reach this limiting distribution is the Markov chain. A Markov chain of processes is defined to have two properties

i) There exists a finite set of outcomes for each trial, defined by the set $\{\Gamma_1, \Gamma_2, \cdots, \Gamma_n, \Gamma_{n+1} \cdots\}$, and this set of outcomes is called state space.

**ii)** The outcome of each trial depends only on the preceding trial

The probability of a state $\Gamma_m$ going to an adjacent state $\Gamma_n$ is given by a matrix element $\pi_{mn}$. Matrices of these probabilities can be set up that exhibit the properties of Markov chains, and exactly define the limiting distribution of a system. Let $\rho_1$ be the initial probability distribution of a system, and let the matrix $\pi$ define the probabilities for an initial state to an intermediate state. Each row in the matrix $\pi$, called the stochastic matrix, should add to one, since each row defines all the transition probabilities for a system

$$\sum_n \pi_{mn} = 1 \tag{3-5}$$

Define each transition by the subscript $\tau$, that is, the stochastic matrix for the first transition is $\pi_1$, that of the $\tau$th transition is $\pi_\tau$, then the limiting distribution $\rho$ of a Markov chain of states is given by

$$\rho = \rho_1 \prod_{\tau=1}^{\infty} \pi_\tau \tag{3-6}$$

The limiting distribution must also satisfy the eigenvalue equation given by

$$\rho \pi = \rho \tag{3-7}$$

which is not a function of the starting condition of the system, and therefore the limiting distribution does not depend on the initial probability distribution of the system, but the rate of convergence to the limiting distribution does

Markov chains for the evaluation of statistical mechanical integrals are easily defined. Most systems considered in Metropolis sampling are functions of the position vectors of the system, or any $\Gamma_m = \{\mathbf{r}_1, \mathbf{r}_2, \ldots, \mathbf{r}_n \mid \mathbf{r} \in (x, y, z), x, y, z \in \Re\}$, where $n$ is the number of particles in the system. The stochastic matrix can then be defined as the

probability that the system will move to a different configuration of position vectors, either through a change in the position vectors of the atoms, the insertion or deletion of a position vector (atom) from the set, or a change in volume that affects all the position vectors of the set. It has been proven [11] that the thermodynamically defined probability for a reversible fluctuation away from a given system configuration is given by

$$\mathcal{P} \propto \exp\left(\frac{\Delta S}{k_B}\right) = \exp\left(\frac{-\Delta E_{rem}}{k_B T}\right), \tag{3-8}$$

and it is this equation that defines the transition probability matrix, $\pi$. The transition probability matrix for a liquid is very large, and if it were not for the finite states represented by a finite representation of real numbers in computing machines, and the limitation of the size of the reversible energy fluctuations by parameters in the simulation, the matrix would be infinitely large. Fortunately the Metropolis scheme does not need knowledge of the entire matrix, but calculates the needed values for the stochastic matrix as the calculation progresses, allowing the application of the Markov chain without knowing the structure of the entire transition probability matrix. Further, to simulate the concept of thermodynamic equilibrium as the system approaches its mean value, the condition of microscopic reversibility is imposed on the matrix elements of $\pi$, or

$$\rho_m \pi_{mn} = \rho_n \pi_{nm} \tag{3-9}$$

which states that the likelihood that a system will move from a state $m$ to $n$ is the same as the probability that a system will move from state $n$ to $m$. This criterion also satisfies the eigenvalue relation given by (3-7), since

$$\sum_m \rho_m \pi_{mn} = \sum_m \rho_n \pi_{nm} = \rho_n \sum_m \pi_{nm} = \rho_n. \tag{3-10}$$

Metropolis proposed that if the states $m$ and $n$ are distinct, a trajectory in the parameter space of the canonical ensemble can be constructed by introducing the symmetric matrix $\alpha$ such that

$$\begin{aligned} \pi_{mn} &= \alpha_{mn} & \rho_n \geq \rho_m \qquad & m \neq n \\ \pi_{mn} &= \alpha_{mn}(\rho_n / \rho_m) & \rho_n < \rho_m \qquad & m \neq n \end{aligned} \tag{3-11}$$

which simply states that if the probability that a system lies in a new configuration $n$ is greater than or equal to the probability that it lies in the old configuration $m$ the transition probability is merely the calculated stochastic matrix element The condition of microscopic reversibility is introduced when the probability that the system lies in the initial state is greater than in the final state. There is also a probability that the liquid will remain in the same state, and this probability is defined by the relation

$$\pi_{mm} = 1 - \sum_{m \neq n} \pi_{mn} \tag{3-12}$$

These equations are applied in various ways to the stochastic matrices defined for reversible transitions in the NVT, NPT and μVT statistical mechanical ensembles, and in each case, the equations for microscopic reversibility (3-9) and the equation describing the sum of probabilities (3-8) are satisfied for each probability $\rho$

The accuracy of this method is determined by the number of trials used in the calculation If the average $\langle \mathscr{A} \rangle_{run}$ is found after $\tau_{run}$ trials, the calculated average is related to the true average of the system by the relation

$$\langle \mathscr{A} \rangle_{NVT} = \langle \mathscr{A} \rangle_{run} + O\left(\frac{1}{\sqrt{\tau_{run}}}\right) \tag{3-13}$$

where $O$ is an operator describing the rate of growth of a function. This relation ensures 2% accuracy with a 99% certainty at $10^6$ iterations, but in practice results may be more accurate statistically. To decrease the statistical error by one-tenth at this point, however, slightly less than $10^6$ more calculations must be performed. Because of the nature of the calculation, the process can be stopped and resumed at any time, allowing for other work to be performed on the same computer. The accuracy of the calculation also depends on the reliability of the chosen computing platform's random number generator. A true trajectory of the simulated system depends on the "randomness" of the numbers, and if periodicities manifest themselves over the $10^6$ iterations of a typical simulation, a more complicated harmonic analysis of the "artificial forces" on the system must be considered to remove artificial contributions to the computed averages.

Metropolis calculations are parallelizable. A single state subject to one initial transition will eventually deviate from the same initial state subjected to any other arbitrarily chosen initial transition. If a computer with multiple processors, each capable of maintaining its own system configurations, is assumed, a procedure can be outlined to increase the efficiency of statistical calculation. Uncorrelated system configurations can be passed to separate processors, each capable of generating its own set of statistics. The statistics can then be collected from each processor after the generation of a finite number of configurations, with the standard deviation of the new averages improving with the number of configurations generated at each processor.

## Monte Carlo Error Analysis

Interpreting Monte Carlo data can be as complicated as interpreting the data generated by experimental systems. Raw data is subject to statistical errors, and trends can be artificially induced by pseudo-random numbers, biases in the methods of integration, or even incorrect simulation techniques. Simulations also generate a finite number of system configurations representing a very small number of the actual configurations that describes a complete thermodynamic system. Previously suggested methods for calculating the error associated with calculating average values through the Monte Carlo method are outlined here. These techniques were used to analyze the data generated for this thesis.

In order to conduct an error analysis on experimental data, a distribution about the mean value must be assumed. In the case of Monte Carlo simulation, this distribution is assumed to be Gaussian in shape. Analysis of a system with error distributed in a Gaussian fashion is complete when the mean value and the variance of a studied parameter is calculated. Not only can the entire simulation length be analyzed as a Gaussian distribution, but large subdivisions of the simulation data can also be analyzed as smaller, less perfect representations of the Gaussian distribution. Analysis of the subdivisions of data reveals information on the efficiency of the simulation, and data collected on the subdivisions will also give variance estimates that are more informative than estimates considering the entire data set at once.

The variance, and thus the standard deviation of the mean, may be calculated from data collected from each system configuration. As an example, assume that a simulation

has generated $\tau_{run}$ time steps or configurations As discussed before, the average value of the property $\mathcal{A}$ calculated from discrete configurations is given by

$$\langle \mathcal{A} \rangle_{run} = \frac{1}{\tau_{run}} \sum_{\tau=1}^{\tau_{run}} \mathcal{A}(\tau) \tag{3-14}$$

It is assumed also that the samples of $\mathcal{A}$ gathered are statistically independent. so that the variance in the mean is given by

$$\sigma^2\left(\langle \mathcal{A} \rangle_{run}\right) = \frac{\sigma^2(\mathcal{A})}{\tau_{run}} \tag{3-15}$$

where

$$\sigma^2(\mathcal{A}) = \left\langle \delta \mathcal{A}^2 \right\rangle_{run} = \frac{1}{\tau_{run}} \sum_{\tau=1}^{\tau_{run}} \left(\mathcal{A}(\tau) - \langle \mathcal{A} \rangle_{run}\right)^2 \tag{3-16}$$

Once the variance is calculated, the standard deviation of the mean $\sigma\left(\langle \mathcal{A} \rangle_{run}\right)$ gives the estimated error for $\mathcal{A}$ In practice, however the samples examined are not statistically independent In the case of Monte Carlo methods the samples are highly correlated to a few surrounding iterations To remedy this fault in the collected data, assume again that the $\tau_{run}$ generated configurations are partitioned into blocks of $2\tau_{\mathcal{A}}$ identical configurations If $\tau_{\mathcal{A}}$ is large, then the variance is increased by a constant of proportionality with the new expression given by [12]

$$\sigma^2\left(\langle \mathcal{A} \rangle_{run}\right) = \frac{2\tau_{\mathcal{A}}\sigma^2(\mathcal{A})}{\tau_{run}} \tag{3-17}$$

The increased variance reflects the lowered efficiency and accuracy of a given simulation length

In order to combat this problem, the stored configurations are split into sections of length $\tau_b$, with $n_b$ blocks such that $n_b \tau_b = \tau_{run}$. The mean of each of these blocks is then simply defined as

$$\langle \mathscr{A} \rangle_b = \frac{1}{\tau_b} \sum_{\tau=1}^{\tau_b} \mathscr{A}(\tau) \tag{3-18}$$

which considers only the configurations in the block $b$. The new set of averages for all the blocks $b$ can then be used to calculate the variance

$$\sigma^2\left(\langle \mathscr{A} \rangle_b\right) = \frac{1}{n_b} \sum_{b=1}^{n_b} \left(\langle \mathscr{A} \rangle_b - \langle \mathscr{A} \rangle_{run}\right)^2 \tag{3-19}$$

As $\tau_b$ increases the blocks will become large enough to be statistically uncorrelated. It is expected that a constant of proportionality exists that will allow an estimate of the variance as the block size approaches $\tau_{run}$ in length. Defining this measure of statistical inefficiency [13]

$$s = \lim_{\tau_b \to \infty} \frac{\tau_b \sigma^2\left(\langle \mathscr{A} \rangle_b\right)}{\sigma^2\langle \mathscr{A} \rangle} \tag{3-20}$$

which represents a ratio of the observed variance to the variance defined by the assumption of uncorrelated Gaussian statistics, certain techniques can be used to reduce $s$, increasing the information gained in simulation, and thus increasing the efficiency in gathering statistics.

As a simple example of an increase in calculation efficiency, the chemical potential calculation in a molecular liquid can be approached using two valid methods. The first method is to insert particles on a defined lattice using pre-defined orientations. In a study done by Fincham *et al* [14], a statistical efficiency of $s \approx 20$ was claimed using the lattice

method. A second method uses a random number generator to arbitrarily pick an orientation and location for the inserted molecules during simulation, reducing the statistical inefficiency to $s \approx 10$. About twice the statistical information is accumulated using the random technique over the lattice approach, and such a random approach to the chemical potential calculation is used throughout the simulations in this thesis.

Radial distribution functions and structure factor calculations are non-linear calculations that depend on histograms. These histograms consist of counters, called bins, that are incremented when two atoms be within a certain range of interatomic distances. Each bin, then, represents the count of atoms that lie within concentric spheres centered upon a hypothetical central atom. For a large number of samples, the average quantity of particle counts in each bin begins to obey the central limit theorem of statistics, and again the approximation of Gaussian statistics can be used to look at the inherent error. The average count in each bin per configuration generated can be analyzed using the methods described earlier to calculate the average properties of the system. Eventual calculation of the variance for the system will allow limits for the error in the final radial distribution function $g(r)$ to be calculated by first adding the variance to the bin average and calculating the function, then subtracting the variance from the average and recalculating, yielding the upper and lower bounds for the radial distribution function. As $r$ increases, the function $g(r)$ should grow statistically more accurate, since the volume of the shell for which the function is being calculated will increase. Since the structural quantities are not crucial in the calculation of the vapor-liquid envelope, the large amount of information necessary for this sort of analysis was not kept. Even in the most rigorous of analysis, the

information on bin average must be kept only for a few points scattered throughout $g(r)$ For further discussion on the methods used to calculate radial distribution functions, refer to Appendix C

This chapter summarizes the necessity of finding an efficient means for evaluating multi-dimensional integrals A simple test case in twenty-dimensional space shows the increased efficiency of a Monte Carlo approach to integral evaluation when compared to the approaches of traditional numerical quadrature The Monte Carlo technique is applied to the calculation of average properties from statistical mechanical ensembles, and the pertinent conditions for integral evaluations are outlined Finally, the error associated with Monte Carlo technique is evaluated. Monte Carlo methods will allow direct calculation of liquid-vapor equilibrium, as will be outlined in the next chapter

# CHAPTER 4
# THE MONTE CARLO METHOD IN TWO-PHASE CALCULATIONS

The Monte Carlo method has been used in various forms to evaluate phase coexistence in the Lennard-Jones fluid. Calculations in the constant NVT (canonical) ensemble allow for the calculation of the pressure-volume equation of state for a system. Once the equation of state is established, stability criteria derived from macroscopic thermodynamics and chemical potential calculations based on integration of the pressure-volume curve at a given temperature allow for calculation of coexistence properties for a single component system [15,16]. The basic methods used to calculate thermodynamic quantities in the canonical ensemble can be extended to calculate properties using the constant pressure (NPT) ensemble [17,18] or the constant chemical potential ($\mu$VT) ensemble [19,20,21]. Constant chemical potential simulations are particularly suited to examine phase coexistence, but studies using these ensembles are computationally expensive, and the number of simulations necessary increases quickly with the introduction of multiple components. The Widom potential distribution theorem [22] has allowed for the determination of chemical potentials within the constraints of constant NVT [23], constant NPT, and molecular dynamic systems [24,25], and, as a result, parameter space searches have been conducted to calculate vapor-liquid phase equilibria for binary systems. Some prior knowledge of pertinent parameters is necessary for an efficient search using

the Widom technique, so these methods prove inefficient for examining the liquid-vapor coexistence properties of systems with complicated potential energy functions

The Gibbs ensemble method is based on a combination of the probability distributions defined in the NVT, NPT, and μVT [1,26] This method divides a system into two bulk regions in coexistence Both these regions are cubic, have periodic boundary conditions, and are not connected by a common surface The technique has proven successful in describing the Lennard Jones single component and binary phase equilibria, but has not been used to calculate the phase-equilibria for systems with more realistic potentials. The macroscopic thermodynamic properties of a system obtained using the Gibbs ensemble method have been proven equivalent to those found by the more computationally intensive method of constructing an equation of state using the canonical ensemble [27] The Gibbs ensemble is the Monte Carlo method chosen here for the study of pure metal systems.

Theory

Take two subsets of two bulk systems in coexistence, phase I, with $N^I$ particles, at temperature $T^I$, pressure $P^I$, and volume $V^I$, and phase II, with $N^{II}$ particles, temperature $T^{II} = T^I$, pressure $P^{II}$, and volume $V^{II}$ For simulation purposes, both phases are fluid phases, are cubic in shape, and have bulk properties that are approximated by enforcing periodic boundary conditions The total volume of the system is constant, so that a volume change of $\Delta V$ in one phase prescribes a corresponding volume change $-\Delta V$ in the other phase. The total number of particles $N = N^I + N^{II}$ is also constant Three transition moves will be defined that allow modifications to the Gibbs system one move

that maintains constant temperature, total particle number, and volume (the NVT step), one move that maintains constant temperature, total particle number, and pressure (the NPT step), and a final move that maintains constant temperature, volume, and chemical potential (the μVT step). Through these three steps a Markov chain will be constructed that will allow a high energy initial configuration to find a lower energy region, and the mean energy of this lower energy region will yield thermodynamic parameters corresponding to the average properties of the system.

The first transition move is the displacement step as defined by Metropolis for a constant NVT system. This step is chosen by examining the partition function derived for the canonical ensemble, and the conditions for which it is derived. For a system with a number of particles $N$ contained in a volume $V$ immersed in a "infinite" heat bath of temperature $T$, the partition function is

$$Q(N,V,T) = \sum_{E} \Omega(N,V,E) \exp\left(-\frac{E(N,V)}{k_B T}\right) \tag{4-1}$$

with $\Omega(N, V, E)$ representing the degeneracy of energy levels for a given energy. The average value for any property $\mathscr{A}$ is given by

$$\langle \mathscr{A} \rangle_{NVT} = \frac{\sum_{E} \Omega(N,V,E) \mathscr{A}(N,V,E) \exp\left(-\frac{E(N,V)}{k_B T}\right)}{Q(N,V,T)}. \tag{4-2}$$

In systems with closely spaced energy levels, both summations can be approximated by integrals, yielding a new expression for the average property of a system

$$\langle \mathscr{A} \rangle_{NVT} \approx \frac{\int_E \Omega(N,V,E)\mathscr{A}(N,V,E)\exp\left(-\frac{E(N,V)}{k_B T}\right)dE}{\int_E \Omega(N,V,E)\exp\left(-\frac{E(N,V)}{k_B T}\right)dE} \tag{4-3}$$

This integral formulation can be evaluated by Monte Carlo integration, and the needed properties found by Monte Carlo averaging. In order to evaluate the given integrals, a means of stepping through the possible energies of the system must be found. Since the classical potential energy of the system is a function of position only, changing the potential energy by moving the particles contained in the NVT system is a simple means of varying the system energy.

The fluctuation equation gives the probability $\mathscr{P}$ that any given fluctuation can occur in a system

$$\mathscr{P} = \exp(\Delta S_t / k_B) = \exp(-\Delta E_{min} / k_B T) \tag{4-4}$$

with $\Delta S_t$ the change in entropy of the system, including the change in entropy due to long-range interaction outside the system's cube, and $\Delta E_{min}$ the minimum reversible difference in energy needed to create a fluctuation from an equilibrium state. In the NVT system, the fluctuations are defined as a displacement of an atom at position $\mathbf{r}$ by a small random vector $\delta\mathbf{r}$, which is produced by randomly generating a vector with a magnitude between zero and one, and multiplying this vector by a scalar defining the largest possible displacement within an atomic system. The transition probability from a state $x$ to a state $x'$ is then defined by

$$\frac{\mathscr{P}(x \to x')}{\mathscr{P}(x' \to x)} = \exp(-\Delta E_{min} / k_B T) \tag{4-5}$$

where $\Delta E_{min}$ is now defined as the minimum work needed to move a system from a state $x$ to the state $x'$. As in Metropolis scheme, the transition probability must be chosen so that a Markov chain of states ensures that the statistical sampling of thermodynamic averages is done in a Boltzmann distribution about the equilibrium average of the system. This is accomplished by choosing the transition probability of the system to be

$$\mathcal{P} = \min\left(1, \exp\left[-\Delta E_{min} / k_B T\right]\right) \tag{4-6}$$

which in the sense of a Markov chain drives a system to its lowest energy configuration, but also samples around the energy in a Boltzmann distribution.

The change in the total energy of the system for a particle displacement step corresponds to the difference between the total energy of the system after displacement and the energy of the system before the step. For multiple displacements in both phases, the energy change would be the summation of the small changes, given by

$$\Delta E_{min} \approx \Delta E' + \Delta E'' \tag{4-7}$$

Since the two systems I and II are modeled as bulk systems, the displacement in phase I can be calculated individually from displacement in phase II. In fact, each individual displacement has a transition probability defined in (4-6) and thus as each displacement is attempted, the probability for its acceptance can be calculated.

Thus, a particle displacement step can be implemented by displacing a particle a random distance to a new position, with the maximum distance defined by a multiplier. The energy of the new configuration is calculated, and the energy of the old configuration is subtracted to calculate the change in system energy. The transition probability follows immediately. A random number between zero and one is generated, if the generated

number is less than the probability for transition, the particle displacement is accepted and recorded, otherwise the configuration of the system remains in its original state. The convergence of this step to the equilibrium properties of the system is influenced by the multiplier that represents the maximum distance that an atom can be displaced from its original position.

The second transition move corresponds to determining an equilibrium volume in the constant NPT ensemble. For the NPT ensemble, an average property is given by

$$\langle \mathcal{M} \rangle_{NPT} \approx \frac{\iint_V \Omega(N,V,E)\mathcal{M}(N,V,E)\exp\left(-\frac{E}{k_B T}\right)\exp\left(-\frac{PV}{k_B T}\right)}{\iint_V \Omega(N,V,E)\exp\left(-\frac{E}{k_B T}\right)\exp\left(-\frac{PV}{k_B T}\right)} \tag{4-8}$$

The energy for a reversible volume change within the system can be most easily calculated by examining the system from the perspective of the system enthalpy. The energy of the system for the old configuration $x$ is given by

$$\Delta E^{I}_{trans,old} = PV^{I} + E^{I}_{old} + Nk_B T \ln\left(V^{I}\right) \tag{4-9}$$

For a new state $x'$ with a volume change $\Delta V$ the energy of the system is given by

$$\Delta E^{I}_{trans,new} = P\left(V^{I} + \Delta V\right) + E^{I}_{new} + Nk_B T \ln\left(V^{I} + \Delta V\right) \tag{4-10}$$

The probability of transition from the new state to the old state is then

$$\wp^{I}_{vol} = \frac{\exp\left(-\frac{P\left(V^{I} + \Delta V\right)}{k_B T} - \frac{E^{I}_{new}}{k_B T} + N^{I}\ln\left(V^{I} + \Delta V\right)\right)}{\exp\left(-\frac{PV^{I}}{k_B T} - \frac{E^{I}_{old}}{k_B T} + N^{I}\ln\left(V^{I}\right)\right)} \tag{4-11}$$

which simplifies to

$$\mathcal{P}_{vol}^{I} = \exp\left(-\frac{\left(P\Delta V + \Delta E^{I}\right)}{k_B T} + N^{I}\ln\left(V^{I} + \Delta V\right) - N^{I}\ln\left(V^{I}\right)\right) \tag{4-12}$$

Since the total volume of the two boxes is constant , there will be a corresponding volume change $-\Delta V$ in phase II The move corresponds to the NPT ensemble, and by definition the pressure in phase II is the same as in phase I The probability for transition from the old state to the new state is then given by

$$\mathcal{P}_{vol}^{II} = \exp\left(\frac{\left(P\Delta V - \Delta E^{II}\right)}{k_B T} + N^{II}\ln\left(V^{I} - \Delta V\right) - N^{II}\ln\left(V^{II}\right)\right) \tag{4-13}$$

The overall probability for both transitions is found by multiplying the probability of the volume change in phase I by the probability for volume change in phase II giving

$$\mathcal{P}_{vol} = \mathcal{P}_{vol}^{I} \times \mathcal{P}_{vol}^{II} \tag{4-14}$$

$$\mathcal{P}_{vol} = \exp\left(-\left[\Delta E^{I} + \Delta E^{II} - N^{I}k_B T\ln\left(\frac{V^{I} + \Delta V}{V^{I}}\right) - N^{II}k_B T\ln\left(\frac{V^{II} - \Delta V}{V^{II}}\right)\right]\Big/\left(k_B T\right)\right) \tag{4-15}$$

Again using the Metropolis algorithm as an example, the Markov chain and integral are established by accepting the volume exchange between systems with the probability min(1, $\mathcal{P}_{vol}$) A volume interchange is accepted in simulation if a random number generated between zero and one is less than the probability for interchange

The third possible system transition is the exchange of particles between the two systems This transition represents the contributions to the phase equilibria represented by the average integral defined for the grand canonical ensemble Assume a particle is to be

created in system I, at a random position In moving from the old state to the new state, the transition probability is defined by

$$\mathcal{P}_{int}^{I} = \frac{\exp\left[-\frac{E_{new}^{I} - (N^{I}+1)\mu}{k_B T} - \ln\left((N^{I}+1)!\right) - 3(N^{I}+1)\ln\lambda + (N^{I}+1)\ln V^{I}\right]}{\exp\left[-\frac{E_{old}^{I} - N\mu}{k_B T} - \ln(N^{I}!) - 3N^{I}\ln\lambda + N^{I}\ln V^{I}\right]} \tag{4-16}$$

$$\mathcal{P}_{int}^{I} = \exp\left[-\frac{\Delta E^{I}}{k_B T} + \ln\left(\frac{zV^{I}}{(N^{I}+1)}\right)\right] \tag{4-17}$$

with the activity coefficient $z = \exp(\mu/k_B T)/\lambda^3$ , and $\lambda$ is the de Broglie wavelength of the atoms. Since a creation was attempted in phase I, and the total number of particles between phase I and phase II are conserved, a simultaneous destruction move must be attempted in phase II The overall probability for particle interchange is found by multiplying the probability for particle creation in phase I by the probability for particle destruction in phase II. For a particle destruction in phase II, a random particle in phase II is chosen for deletion, and arguments similar to those for particle creation in phase I give

$$\mathcal{P}_{int}^{II} = \exp\left[\frac{\Delta E^{II}}{k_B T} + \ln\left(\frac{N^{II}}{zV^{II}}\right)\right] \tag{4-18}$$

The overall probability for particle exchange is

$$\mathcal{P}_{int} = \mathcal{P}_{int}^{I} \times \mathcal{P}_{int}^{II} \tag{4-19}$$

or

$$\mathcal{P}_{acc} = \exp\left(-\frac{\left[\Delta E^{I} + \Delta E^{II} + k_B T \ln\left(\frac{V^{II}(N^{I}+1)}{V^{I}N^{II}}\right)\right]}{k_B T}\right) \tag{4-20}$$

To create the Markov chain, the trial exchange is accepted with the probability min{1, $\mathcal{P}_{acc}$}. If a move is rejected, the properties of the old system configuration are recounted in the overall system statistics. Since this is a model with microscopic reversibility, the same number of particle deletions and insertions must be attempted in a single phase over the course of the simulation. This condition can be met in one of two ways: i) over each program iteration, a fixed number of insertions and the same fixed number of atom deletions are attempted, or ii) the likelihood of insertion and creation in phase I are equal, so either step is chosen with equal probability, and attempted. Over the course of the simulation, both approaches will yield the same result. Statistics can be kept on the number of particle exchanges attempted. Near equilibrium, the number of creations in phase I should be very close to the number of particle deletions in phase I. To modify the equations for particle creation in phase II and particle deletion in phase I, the I and II superscripts in the previous equations must be switched.

Now that all of the Monte Carlo steps have been delineated, a technique for simulation can now be outlined. Two initial systems must be generated. The $N^{I}$ atoms initially in system I are randomly put on a body-centered cubic lattice generated over the volume $V^{I}$ such that the largest interatomic spacing is achieved. The same is done for system II, but a slightly smaller system density $N^{II}/V^{II}$ is chosen for system II so that the

system has a small initial perturbation from overall system homogeneity This difference in system configuration allows for quicker separation of phases, and is necessary when the two phases have qualitatively different potential representations not valid over the entire range of simulation. The Monte Carlo steps can then be taken several thousand times, and these initial steps are performed to drive the system to equilibrium. Particle displacement steps are independently performed for each particle in phase I and phase II, then a correlated volume displacement from one phase to the other is attempted A set number of particle interchange steps between phases is then tried, with a random number generator determining whether the particle is created or destroyed in phase I After each set of Monte Carlo steps, statistics are gathered on the system energy the system virial, the system density, and the structure of the system. During the initial equilibration phase these numbers are studied until each system reaches a point where the numbers change slowly over several iterations (The initial equilibration is quite rapid) The statistics are then discarded, and a new simulation is begun on the equilibrated system configurations Statistics are kept after each suite of steps - one suite consisting of the particle displacements, volume displacements, and particle interchanges - is performed A predetermined number of calculation steps are performed

After simulation the data are analyzed, and if the calculated average values did not vary significantly, the point is considered a member of the phase diagram If they were not, two possibilities can lead to spurious results The first possibility is that the system was not equilibrated long enough, so the average values obtained through simulation are not equilibrium values The second possibility is that the statistics are poor because of

large fluctuations during the calculation phase, and that more calculation steps are needed to lower the standard deviation associated with the average values calculated.

It has been established that the long range corrections to the pressure and energy of a system are a function of the potential cut-off radius, the density of the fluid, and the potential function assigned to the system. Any adjustment to the system that modifies any of these parameters must calculate the corresponding change in the long range corrections for the system. The displacement moves do not modify these quantities, but the volume displacement and particle displacement steps both modify the system density, and the volume displacement step will also alter the cut-off radius. Changes in density can also change the potential energy function of the system. The $\Delta E$ term must include these modifications for simulations in which the long-range terms are considered.

The Monte Carlo steps outlined above can be generalized to mixtures. The displacement and volume change steps in a mixture should remain the same, but there are new rules for the particle exchange step that must be incorporated into the simulations in order to preserve microscopic reversibility. Again, either system I or system II must be chosen for particle creation with equal probability. Since there are numerous species in the system, one of the species must be picked with a fixed probability. To ensure reversibility it is not necessary to assign an equal probability for interchange for each species, and different probability assignments will allow for different rates of convergence of the Markov chain. As with all probabilities, the sum of the probabilities must be one. Thus, a two species system will add one parameter that determines the rate of convergence for the system, a three component system adds two independent parameters, *ad infinitum*. Since

the number of particles in a system is discrete, there is no criterion established that does not allow a species to completely disappear from one of the phases. The calculations are continued in this case, since the practical interest lies only in the average values for particle concentration and its fluctuation.

The consideration of mixtures also allows for another type of simulation step that can be very useful for approximating the two-phase simulation volumes for single-component simulations. The addition of a single component to a system with a fixed number of phases adds an additional degree of freedom according to the Gibbs Phase rule, and in the case of the binary mixture, one of the additional specified degrees of freedom can be the pressure of the system. Each system (I and II) can be modeled as an isothermal-isobaric ensemble, where a pressure P has been chosen as a fixed simulation parameter. The total volume of the system is no longer constant, and the probability for rearrangement is given by the expression

$$\mathcal{P}_{acc} = \exp\left\{-\beta\left[\Delta E^{I} + \Delta E^{II} - N^{I}kT\ln\left(\frac{V^{I}+\Delta V^{I}}{V^{I}}\right) - N^{II}kT\ln\left(\frac{V^{II}+\Delta V^{II}}{V^{II}}\right) + P\left(\Delta V^{I}+\Delta V^{II}\right)\right]\right\} \qquad (4\text{-}21)$$

where $\Delta V^{I}$ and $\Delta V^{II}$ are independently chosen displacements chosen for each phase. The Markov chain is established by choosing the probability for transition as $\min(1, \mathcal{P}_{acc})$. Convergence using this criterion can be hastened by attempting a volume change in only one of the regions at a time.

In order to check the consistency of the calculation, the average pressures and the chemical potentials of each system are kept for comparison purposes. The pressure is a basic ensemble average, calculated from the instantaneous system virial. The chemical potential is calculated by a method first proposed by Widom [28] for the constant NVT

ensemble, then modified to include ensembles in which the volume of the system is allowed to change. The method is based on the insertion of an imaginary particle at a random position in the system, the calculation of the energy change in the system, then the application of transformations necessary to keep track of the average chemical potential. For a constant volume system, such as the NVT ensemble, the potential distribution theorem states that the chemical potential of component i can be calculated in its residual form $\mu_i^{res} = \mu_i - \mu_i^{ideal}$, where $\mu_i$ is the true chemical potential of the system. The residual chemical potential is an ensemble average, given by the expression

$$\mu_i^{res} = -k_B T \ln\left\langle \exp\left(-\frac{\psi_i}{k_B T}\right)\right\rangle_{N_1,\ldots N_n,V,T} \tag{4-22}$$

with the temperature given by $T$, $k_B$ denoting Boltzmann's constant, and $\psi_i$ denoting the additional energy added to a system by the particle insertion. The ideal chemical potential is given by

$$\mu_i^{ideal} = k_B T \ln\left(\frac{(N_i+1)\Lambda^3}{V q_i}\right) \tag{4-23}$$

where $V$ is the total system volume, $N_i$ is the number of particles in the system, and $q_i$ the product of the partition function contributions due to vibrational, rotational and electronic modes. The thermal de Broglie wavelength of the system $\Lambda$ is given by

$$\Lambda = \left(h^2/\left(2\pi m k_B T\right)\right)^{1/2} \tag{4-24}$$

The calculation of the potential for a single particle insertion is an expensive operation involving $N$ evaluations of the system potential, potential recalculation if the potential is density dependent, and calculation of the new long range potential. Fortunately, particle

insertions and deletions in the system are part of the Gibbs ensemble algorithm, and when these steps are performed the necessary data is stored within the simulation, and an explicit insertion step for the calculation of the chemical potential is not necessary

Evaluation of the chemical potential is slightly different in a system in which the volume is allowed to change The residual chemical potential is given by

$$\mu_i^{res} = -k_B T \ln\left[\frac{\langle V \exp(-\beta\varphi_i)\rangle}{\langle V\rangle}\right] \tag{4-25}$$

and the ideal gas potential takes the form

$$\mu_i^{ideal} = k_B T \ln\left(\frac{(N_i+1)\Lambda_i^3}{\langle V\rangle q_i}\right) \tag{4-26}$$

where $\langle V\rangle$ is the ensemble average volume These volume corrected expressions are used throughout Gibbs ensemble calculations

Systems Previously Studied with the Gibbs Ensemble Simulation Method

Besides the Lennard-Jones system, several atomic systems have been studied using various pair-potential functions and the Gibbs ensemble technique Studies have been conducted on the square-well potential, fluids that have strong dipole-dipole interactions (Stockmayer fluids) [29] and fluids with quadrupole-quadrupole interactions [30] Ionic fluids have been simulated using the restricted primitive model A simple model for screened Coulombic interactions, the Yukawa potential has been analyzed using the Gibbs ensemble [31] Gay-Berne fluids that incorporate parameters to model potentials with anisotropic interactions have also been simulated [32] as has the water system using the

TIP4P potential [33] With the exception of the last model, these simulations proved to be interesting assessments of the coexistence behavior for some familiar potential models, but no predictions were made for actual systems.

A study of the phase equilibrium of an eight-bead Lennard Jones molecule has been performed by Mooij *et al* [34] Each bead on the molecule is treated as a separate Lennard-Jones site A similar simulation by de Pablo *et al* [35] modeled mixtures of methane and other chain hydrocarbons The pair potential for long-chain hydrocarbons was approximated by using a site-dependent potential [36], with the Lennard-Jones parameter ε modeled as a linear function of site density Site-site interactions were shown to be the microscopic analog to group contribution methods for estimation of thermodynamic properties Estimation of the heat of vaporization for pure hydrocarbon systems, including systems as complex as cyclohexane and neopentane, compared very well to experimental systems. Binary mixtures were also modeled, with the Gibbs method results comparing well with low pressure results, but deviations from experimental values increased with increasing temperature and pressure. Calculations began to deviate from experiment at temperatures slightly above the normal melting temperature Both authors report very promising results for the prediction of thermodynamic properties of phases in equilibrium using the Gibbs method

Apparent Weaknesses of the Gibbs Ensemble Simulation Method

It has been shown [37] that the results obtained using the Gibbs ensemble method are equivalent to those obtained by simulating the canonical ensemble in the thermodynamic limit, as the number of particles approaches infinity It has also been

shown, both through statistical analysis and theoretical evidence, that as the simulation conditions of a *finite* system approach the critical point of the system, vapor liquid coexistence cannot be simulated. At points very near the critical point, the average density of the system should be observed, rather than two separate densities corresponding to a liquid and a vapor phase. A simple explanation has been set forth. At low temperatures, surface tension is large, and because it is large, it is unlikely that the liquid and vapor phases will be able to coexist in the same sub-volume. As temperature increases, the surface tension of the system drops, until there is no surface tension between phases at the critical point. Energy contributions to the Gibbs energy due to surface tension at high temperature become comparable in magnitude to the entropic contribution attributed to the formation of an interface, and the difference in Gibbs energy needed for the formation of two distinct phases vanishes. The measured thermodynamic quantities in each subsystem will be a measure of the properties of a schizophrenic phase, defined as a system that cannot decide whether it should become a liquid or a vapor, and so becomes both. As a result, the average properties for both phases in the simulation are the same, and the calculated critical temperature will be too low for the simulated system.

Extension of Parameter Space in the Simulation

Several parameters unique to the Gibbs method of Monte Carlo simulation were introduced to further limit the regions of the average property integral sampled. During simulation, it was noticed that the algorithmic step with the largest energy changes using a continuous potential was the simultaneous particle insertion/particle deletion step. Often when this step was successful, the total energy of the system changed considerably, and

since the magnitude of the system virial was closely related to the magnitude of the potential, sampled values such as pressure and total energy deviated from the mean value In order to gather more accurate statistics over a shorter calculation period it was ascertained that if the statistics recorded could somehow be limited more to the region near the average value of the system, while again maintaining the appropriate distributions in parameter space, both the fluctuations in the system and the standard deviations in the calculations could be held to a minimum The order of the simulation steps could be changed and even repeated, in order to sample statistics at values nearer to the mean values. Thus the particle displacement, volume change and particle insertion/deletion steps were interchanged, with the sampleg taking place after one or more displacement steps By "re-equilibrating" the system in this manner, it was assumed that the statistics taken were closer to the average, and fewer steps were needed to approximate equilibrium values.

Such a change to the Panagiotopoulos algorithm [1] added parameters of convergence to the system Since each particle displacement, volume change, or particle interchange is essentially the application of a different stochastic matrix to the original system, the rate of convergence to equilibrium and the shape of the sampled distribution can now be controlled by the number of attempts to modify the current configuration assigned to each step configuration, and the order in which these steps were applied Since a major goal in extending the simulation technique was to increase the rate of convergence to equilibrium values, the addition of these parameters to the simulations provided a means

to accomplish both, allowing different combinations of stochastic matrices to be applied during system equilibration and calculation

The Gibbs Ensemble Monte Carlo method for a single component system has two inputs the initial conditions of the system, and the potential energy function of the atoms within a phase Cycles of three independent steps are performed to calculate the average saturated properties of the two bulk phases simulated The particle displacement, correlated volume change, and particle interchange steps allow the two systems to be linked, without the problems associated with simulating an interface The Gibbs Ensemble Monte Carlo method has been applied to many systems, with varying degrees of success Simulations near the liquid-vapor critical point of the system do not show two distinct phases, and the equilibrium values for simulations with high-density liquid phases can be inaccurate, since particle interchange steps become more unlikely with increasing liquid density Various techniques can be applied to speed the calculation of equilibrium properties

# CHAPTER 5
# ASSESSMENT OF FLUID MODEL POTENTIALS

## Introduction

Potential energy functions derived from experiment for liquid metals have many complex features, and though equations may have been written that can eventually lead to the theoretical calculation of these potentials exactly, today's models of many-body systems can only approximate the interatomic forces in metal systems. This chapter will look at two empirical potentials that have been extensively studied, both of which are capable of modeling coexistence for different classes of one-component systems. The first of these, the Lennard-Jones potential, is included in both the 6-12 and n generalized form. Liquid-vapor phase coexistence properties for single component systems have already been calculated for the 6-12 potentials. The second potential model discussed is a potential energy function derived to describe crystalline metals from linear response theory. This potential is derived from a simple pseudopotential model for the ion cores within a metal melt, and is called the empty-core pseudopotential model. Few phase-coexistence studies have been conducted using the empty-core pseudopotential, but preliminary studies have shown this potential to be a promising starting point for examining liquid metal behavior.

The Lennard-Jones Potential

A simple interatomic potential that shows two-phase behavior when used to describe an atomic system is the Lennard-Jones 6-12 potential, given by

$$v(r) = 4\varepsilon\left[\left(\frac{\sigma}{r}\right)^{12} - \left(\frac{\sigma}{r}\right)^{6}\right] \tag{5-1}$$

where $r$ is the scalar distance between two atoms, $\varepsilon$ represents the potential well depth, and $\sigma$ determines the distance from the center of an atom to the minimum well depth, and thus the effective collision diameter of the system. The values of the parameters are empirical, and found by forcing agreement between a measured physical property, often the second virial coefficient or the viscosity, to a model containing the Lennard-Jones potential as an argument. The valence electrons in systems that are accurately modeled by this potential are tightly bound. Thus, the noble gases are modeled extremely well, and even molecular systems such as the tightly bound diatomics (nitrogen) and methane exhibit behavior close to that of a Lennard-Jones fluid. Evaluation of the potential involves only simple arithmetic, so calculations are performed without the aid of a table for interpolation. The simple analytic formulation lends itself to quick calculation of the virial and long-range energy and pressure corrections to the system.

The Lennard Jones model works very well for single component simulations, and mixing rules can be defined to approximate binary interactions in a system, allowing for simulation of binary systems. It is in reactive systems that the Lennard Jones model begins to show weakness. Parameters must be defined for every possible interaction between components in a phase. This is difficult, since there is no experimental basis for measuring

Lennard-Jones parameters for interactions between different kinds of atoms or molecules coexisting in the same phase In a vapor phase consisting of monomers and dimers, unique Lennard-Jones parameters must be incorporated for the monomer-monomer interaction, the monomer-dimer interaction, and the dimer-dimer interaction If the experimentalist is fortunate, the interaction parameters for pure monomer can be measured in the liquid or dilute vapor phase. The interaction between dimers must be approximated, either from other fluid theories, or by fitting simulation to the experimental properties. Further approximation in the form of mixing rules is necessary to approximate the monomer-dimer interaction The volume of experimental data necessary eliminates the possibility of using a Lennard-Jones potential energy function as a predictive tool for all but the simplest of physical systems

Many other variations on the empirical Lennard Jones potential exist The generalized Lennard-Jones form,

$$v(r) = \varepsilon \left\{ \frac{m}{n-m} \left( \frac{r}{r_0} \right)^n - \frac{n}{n-m} \left( \frac{r}{r_0} \right)^m \right\} \qquad (5\text{-}2)$$

for $n > m$, is an attempt to improve the Lennard-Jones model by increasing the number of parameters from two to four The cohesive energy, zero-point volume, and zero-point compressibility of metallic systems have been used to establish nearly optimal parameters for systems that have crystals with hexagonal close packed, body-centered cubic, or face-centered cubic structure [38] The Lennard-Jones 6-12 potential does not describe solid metallic systems well, since the compressibility predicted by this potential for parameters optimized to solid state properties deviates by a factor of 5-10 from experimental values.

The generalized Lennard-Jones model improves this agreement considerably, giving values of compressibility within 5% of the experimental value. The process of calculating the parameters using solid phase lattice properties can destroy the usefulness of the potential in both the liquid and vapor regime, where electron behavior is qualitatively different. This potential form has not been used to model liquids and vapors extensively, and the form of the phase diagram for different values of the four parameters is not known.

In this dissertation, the 6-12 Lennard-Jones model was used as a test of the computer code to determine if the system could reproduce the thermodynamic properties of the Lennard-Jones fluid previously tabulated in literature.

The Empty-Core Pseudopotential

The calculation of the actual potential energy of an atomic system is based on the solution of the time-independent Schroedinger equation for the system. Calculating exact solutions to the Schroedinger equation for all but the simplest of atomic systems is an open problem, and little progress has been made for metal systems. To approach metal systems, simplifications must be introduced that allow the calculation of the potential energy.

All solid and liquid metal systems can be represented by tightly bound spherical ions sitting within an electron gas consisting of valence electrons. Most of the macroscopic physical and chemical behaviors of a metal system are a result of the interactions between valence electrons and other valence electrons and inner core ions. As a result, many models have been proposed that simulate the interaction of a single valence electron with other valence electrons and inner core ions. One approach that has enjoyed

modest success in modeling solid state properties of a metal system is the pseudopotential description

Quantum mechanical methods, such as the Hartree-Fock self consistent field calculation, will allow for the approximation of the potential energy of a metal system. These calculations use a basis set of orthogonal functions to iteratively refine the wavefunction of a system, and the corresponding potential energy. Once the wavefunction of the system is known, postulates from quantum mechanics allow the calculation of the average properties. This problem can always be solved in theory with the proper choice of basis functions, given enough time to refine the estimates for the wavefunction and potential energy. In practice, however, this method can be inaccurate and converge too slowly for practical use.

In a metal system, where some electrons are tightly bound to the ionic cores and others, the valence electrons, are loosely bound to the same cores, the calculation of a wavefunction describing the atomic system is difficult. One wavefunction basis set must be chosen that can model localized electron behavior near the ion core, while another, qualitatively different set must be chosen to model delocalized valence electron behavior. Since each electron is capable of being a core electron or a valence electron, a very large basis set describing both localized and delocalized electron behavior must be incorporated into the calculation of the potential energy of the system. The Hartree-Fock calculation is made larger still by the sheer number of electrons and nuclei for which a wavefunction must be calculated in a metal system.

Rather than trying to calculate the wavefunction of the metal system, the problem can be simplified somewhat by identifying the quantities that make major contributions to the total potential energy of the system. The pseudopotential is just such a simplification. By definition, the pseudopotential is a potential energy function for the ionic cores that can reproduce the band structure energy of a metal outside the ionic core. Coupled with the Schroedinger equation, the pseudopotential can also reproduce the wavefunction of the metal valence electrons, subject to the boundary condition that the logarithmic derivative of the radial wave function of an electron inside the core matches the logarithmic derivative of the wave function of the same electron outside the core, regardless of its symmetry. Expanding the core radius to cover all the atomic-like oscillations in the wavefunction eliminates one of the length scales needed in the basis set chosen for calculation, and coincidentally this is the length scale that demands the finest resolution in the wave function. Thus, local effects are nearly eliminated, and the basis set describing the wavefunction of electrons is simplified to model only delocalized electron behavior.

Another approach to calculating an effective pseudopotential for a metal system is popular due to its simplicity and its successes. A simple model can be assumed for the interaction potential of ionic cores with valence electrons. The corresponding metal theory, taking into account fluctuations in electronic configuration, can be subsequently derived, and the model parameters fit to reproduce the band structure and scattering characteristics of the metal. The models chosen for the core-electron interaction are very simple, one potential interaction is assumed for electrons within a core radius, and outside

the core radius, the potential energy interaction has a different form. Inside the core, energy dependent contributions due to each angular momentum quantum number are present, so an energy dependent function that can be fit to spectroscopic data giving the energy levels of one electron is used to describe the potential inside the core. The potential contribution inside the core is often assumed to be a constant, simplifying the process of fitting theory to experimental data. Outside the core a simple Coulombic interaction between cores is assumed. This is the approach taken for this dissertation. Creating a semi-empirical model for the core-electron interaction circumvents the problem of wavefunction calculation altogether, but inaccuracy is introduced again by the model dependent assumptions.

The simplest of the model pseudopotentials is the empty core pseudopotential [5]. In this model, the potential ion-electron interaction is represented by a Coulombic term outside a certain model core radius, and the potential value drops to zero within the model core radius. This model can be explained quantitatively in the language of quantum mechanics from empirical evidence [39] and theoretical [40] arguments referred to as the *cancellation theorem*, which states that if for a given angular momentum quantum number the wavefunction has core states, the potential energy function is almost zero within the core. Thus the potential of interaction between cores and single electrons in atomic units can be written

$$v_{ion}(r) = \begin{cases} 0 & r \le R_c \\ -\dfrac{Z}{r} & r > R_c \end{cases} \qquad (5\text{-}3)$$

where $r$ is the scalar distance form the center of the atom core, $R_c$ is the ion core radius, and $Z$ is the metal valence. The Fourier transform of the pseudopotential, which is useful in formulating the actual calculation of the potential energy function, is

$$v_{ion}(q) = -\frac{4\pi Z^2}{q^2}\cos(q R_c) \tag{5-4}$$

where $q$ is the transform variable in reciprocal lattice space. This energy of interaction is a local interaction term only. Electrons are not modeled in a classical manner, but are modeled as a Fermi gas, and the model for the potential energy of the system will reflect this assumption.

Once a model is assumed for the ion core-electron interaction, a framework can be constructed to approximate the contributions to potential energy from the electron gas, assumed to lie in the interstitial region between cores and the core interaction and screening due to the dielectric function of the electron gas. Linear response theory allows for the conversion of a core interaction model into a potential energy function describing a model metal system. In this theory, a homogeneous electron gas is considered to be perturbed by an arrangement of compensating positive charges. Perturbation theory treatments allow the calculation of approximations to the screening charge density of an electron gas. The free-energy of the electronic system is calculated by using an integral variant of the Hellman-Feynman theorem [41]. Once the relevant expressions are substituted into the system's adiabatic Hamiltonian, the terms contributing to the potential energy function of the metal system can be identified. Because electron density is calculated using a perturbation scheme, it is necessary to assume for this dissertation that

third and higher order effects from the perturbation series for electron density do not contribute significantly to the potential energy of the system

Linear response theory gives a characteristic general form of the volume dependent potential energy function, found by subtracting the appropriate terms from the free-energy

$$v(\mathbf{r}_1, \ldots, \mathbf{r}_N) = E_v(n_e) + \sum_{i<j} v_2(r_{ij}, n_e) + \sum_{i<j<k} v_3(r_{ij}, r_{jk}, r_{ki}, n_e) \qquad (5\text{-}5)$$

with the electron concentration represented by $n_e$, the volume energy contributions to the potential given by $E_v(n_e)$, the pair potential contributions given by the sum of $v_2(r_{ij}, n_e)$, and the triplet contributions given by the three-body summation of $v_2(r_{ij}, r_{jk}, r_{ki}, n_e)$. This equation includes a third order contribution to potential, a rigorous derivation for the potential energy function of a metal system would also include fourth order and higher terms. The electron density term $n_e$, which is the metal valence multiplied by the density of ionic cores in the system, is essentially a representation of local configuration

It is characteristic of such semi-empirical volume dependent potentials that only metallic elements with low electron densities will have a potential minimum that corresponds to the nearest-neighbor distance for close packing. As the density of electrons increases, this minimum is masked by screened interionic repulsions. Systems like germanium and silicon exhibit a pair potential that is actually repulsive near the nearest neighbor distance, and at shorter distances has a small inflection point. The nearest neighbor shell is modified so that some of the twelve nearest neighbor atoms are moved inward toward the potential depression, and others are pushed outward toward the potential global minimum, lowering the coordination number of the system

Most of the contribution to coordination number in both the liquid [42] and solid phases are due to pair and volume forces, though three-body forces have been found to play an important role in influencing triplet correlations, and in the stabilization of the transverse acoustic branches of the phonon spectra in solid group IV elements exhibiting the diamond structure. It can also be true that complex bond hybridization and thus three-body forces may be important in the description of liquid metals these effects are not considered in this dissertation

After the perturbation theory calculation for electron density and the subsequent conversion to an expression for the free energy of the system is performed, the volume energy term listed in (5-5) can be broken into two terms,

$$E_v(n_e) = E_{eg}(n_e) + E_{ion}(n_e) \tag{5-6}$$

where $E_{eg}(n_e)$ is the contribution to the potential energy by the electron gas, and $E_{ion}(n_e)$ is the potential contribution due to Coulombic interactions between the ionic cores and the electron gas An explicit expression for the energy of the electron gas is available [43], and it is given by

$$E_{eg}(n_e) = Z\left(\frac{1105}{r_s(n_e)^2} - \frac{0.458}{r_s(n_e)} + 0.031\ln r_s - 0.115\right) \tag{5-7}$$

where $r_s$ is the electron density dependent radius of a sphere containing on average one electron, and $Z$ is the valence of the modeled metal This expression accounts for the self-energy of the gas resulting from electrostatic repulsion of electrons, and approximations to the quantum mechanical exchange and correlation effects present in the electron gas

Perturbation theory leads to the expression for the interaction between the electron gas and the atomic cores,

$$E_{ion}(n_e) = 8Z^2 \int_0^\infty \frac{\chi(q,n_e)}{\varepsilon(q,n_e)} \cos^2(qR_c)\, q^2\, dq \tag{5-8}$$

where $R_c$ is the pseudopotential core radius, $\chi(q)$ is the static polarizability, and $\varepsilon(q)$ is the static dielectric function of the electron gas. The polarizability and the dielectric function of the electron gas are modeled using the Ichimaru-Utsumi approximation [44,45], while the core radius is chosen to fit electronic band calculations [41,46 47] In all metallic and semiconductor systems, the largest contribution to the total energy is from the ground state term $E_{ion}(n_e)$ [41,48]. Core-core exchange and correlation effects are not considered in the empty-core pseudopotential model, and are assumed negligible in energy with respect to the energy contributions from other phenomena.

For the empty core model, the pair potential is represented by the integral

$$v_2(r,n_e) = \frac{Z^2}{r}\left(1 + 16\int_0^\infty \frac{\chi(q,n_e)}{\varepsilon(q,n_e)} \cos(qR_c)\sin(qr)\, q^2\, dq\right) \tag{5-9}$$

where $r$ is the interatomic distance between core centers. The perturbation approach is clear in this expression, the pair interaction between atomic cores has a functional form resembling a pure Coulombic potential, which is the interaction expected between charged hard spheres in a vacuum. The perturbation term represents the mediation of charge interaction by the surrounding electronic gas, this term is responsible for Friedel oscillations, the oscillatory pair potential tail characteristic of metals

In order to calculate the dielectric function and the polarizability of an electron gas, another model must be constructed. The electrons present in a molten metal are modeled by the Hamiltonian of a one-component plasma (OCP) and by using this representation the screening effect between metal nuclei can be approximated. It must be noted that the models are for systems in which there exists a homogeneous background of neutralizing charges, and this background does not strictly exist in the liquid metal system, especially when the liquid structure represented by the radial distribution function is distorted in dissimilar pair interactions such as those in a binary semiconductor system. Since this project is the first to assess the validity of the model pseudopotential in such systems, the current OCP theory will be tested for approximation of experimental equilibrium values.

Systems that obey Fermi statistics have an analog to kinetic energy represented by the Fermi energy, found through the expression

$$E_F = \frac{\hbar^2}{2m}\left(3\pi^2 n\right)^{2/3}, \tag{5-10}$$

where $m$ is the mass of an electron, and $n$ is the density of electrons in the system. The definition of the coupling constant of a plasma system obeying Fermi statistics is based on the Fermi energy and given by the expression

$$\frac{e^2/a}{E_F} = 0.543 r_s \tag{5-11}$$

where $e$ is the charge of an electron, $a$ is the Bohr radius, and $r_s$ is the Wigner-Seitz radius of the homogeneous electron system in units of the Bohr radius, this quantity being given by

$$r_s = \left[\frac{3}{4\pi n}\right]^{\frac{1}{3}} \tag{5-12}$$

where the density of electrons $n$ is given in atomic units. Solid metal systems typically have a value of $r_s$ between two and six, with liquid metals having values slightly larger The coupling constant in these systems is greater than one, and this property is used as a measure to define this system as possessing the properties of a degenerate, strongly coupled plasma.

Treating the electron gas as a plasma allows the use of conventional plasma models when representing the quantities $\varepsilon(q\ \omega)$ and $\chi(q\ \omega)$, with both quantities not just a function of electron wavevector/energy but also a function of a characteristic frequency $\omega$ of the plasma system The polarizability of the electron system can be written in its discrete form as

$$\chi_0(q,\omega) = \frac{2}{\hbar V}\sum_{p}\frac{f_0(p) - f_0(|\mathbf{p}+\mathbf{q}|)}{\omega - \omega_{pq} + i0} \tag{5-13}$$

where $q$ and $p$ are wavevectors, the positive infinitesimal in the denominator indicates the summation is evaluated over retarded boundary conditions, and the Fermi distribution at zero temperature $f_0(q)$ is given by

$$f_0(q) = \begin{cases} 1, & q \le q_F \\ 0 & q > q_F \end{cases} \tag{5-14}$$

with

$$\omega_{pq} = \left(\frac{\hbar}{2m}\right)\left(2\mathbf{p}\bullet\mathbf{q} + q^2\right) \tag{5-15}$$

The traditional model used to evaluate the polarizability of the electron gas is the random phase approximation, an approximation that assumes the long range part of the Coulombic field can be treated as an external field to an electron in a plasma. The main contribution to the electron polarizability comes from its static value, when the plasma frequency is zero Assuming a continuum throughout reciprocal space and a corresponding density of states function allows for a functional evaluation of (5-13), and the static polarizability computed is the Lindhard [49] function

$$\chi(q,0) = -\frac{3n}{2E_F}\left[\frac{1}{2} + \frac{q_F}{2q}\left(1 - \frac{q^2}{4q_F^2}\right)\ln\left|\frac{q+2q_F}{q-2q_F}\right|\right] \tag{5-16}$$

The static dielectric function $\varepsilon(q\ 0)$ is related to the static polarizability and can be calculated using the expression [50]

$$\varepsilon(q,0) = 1 - \frac{v(q)\chi_o(q,0)}{1+v(q)G(q,0)\chi_o(q,0)} \tag{5-17}$$

with $G(q, 0)$ defined as the static local field correction and $v(q)$ given by

$$v(q) = \frac{4\pi e^2}{q^2} \tag{5-18}$$

In the random phase approximation, the local field correction is zero, and the static dielectric function is reduced to

$$\varepsilon(q\,0) = 1 - v(q)\chi_o(q,0) \tag{5-19}$$

This computationally simple form breaks down at lower electron densities ($r_s$>1), and the more complicated local-field correction must be included for greater accuracy at the metal densities of interest

The local-field correction has been through many theoretical iterations A form that compromises accuracy with computational simplicity was first proposed by Ichimaru and Utsumi [51], and is given by

$$G(q)=A\left[\frac{q}{q_r}\right]^4+B\left[\frac{q}{q_r}\right]^2+C+\left[A\left[\frac{q}{q_r}\right]^4+\left(B+\frac{8}{3}A\right)\left[\frac{q}{q_r}\right]^2-C\right]\left[\frac{4q_r^2-q^2}{4q_rq}\ln\left|\frac{2q_r+q}{2q_r-q}\right|\right] \tag{5-20}$$

with the parameters

$$\begin{aligned} A &= 0.029 \quad (0\le r_s\le 15) \\ B &= \frac{9}{16}\gamma_0(r_s)-\frac{3}{64}\left[1-g(0)\right]-\frac{16}{15}A \\ C &= -\frac{3}{4}\gamma_0(r_s)+\frac{9}{16}\left[1-g(0)\right]-\frac{16}{5}A \end{aligned} \tag{5-21}$$

given that

$$\gamma_0(r_s)=\frac{1}{4}-\frac{\pi\lambda}{24}\left[r_s^3\frac{d^2E_c(r_s)}{dr_s^2}-2r_s^2\frac{dE_c(r_s)}{dr_s}\right] \tag{5-22}$$

and the derivative of the correlation energy of an electron gas $E_c(r_s)$

$$r_s\frac{dE_c(r_s)}{dr_s}=-b_0\frac{1+b_1x}{1+b_1x+b_2x^2+b_3x^3} \tag{5-23}$$

with $x=\sqrt{r_s}$, $b_0=0.0621814$, $b_1=9.81379$, $b_2=2.82224$, and $b_3=0.736411$ The radial distribution function at $r=0$ is given by

$$g(0)=\left[\frac{z}{\mathbf{I}_1(z)}\right]^2, \tag{5-24}$$

with the parameters $z = 4(\lambda r_s / \pi)^{1/2}$, $\lambda = (4/9\pi)^{1/3}$, and $I_1(z)$ is the modified Bessel function of the first kind. The parameters A, B, and C are determined through Monte Carlo calculation, ladder diagram calculation of the value of the radial distribution function $g(0)$, and the dielectric formulation proposed also by Ichimaru and Utsumi.

The parameterized dielectric function with this local-density correction satisfies two major tests of thermodynamic consistency. The compressibility sum rule states that at the long plasma wavelength limit, the local field correction can be calculated through

$$\lim_{q \to 0} G(q) = \gamma_0(r_s)(q/q_F)^2 \tag{5-25}$$

with the coefficient $\gamma_0(r_s)$ determined by the system compressibility

$$\kappa = -\left[V \frac{\partial P}{\partial V}\right]^{-1} \tag{5-26}$$

and the relation

$$\frac{\kappa_0}{\kappa} = 1 - \left[\frac{4\lambda r_s}{\pi}\right] \gamma_0(r_s) \tag{5-27}$$

given the relation $\kappa_0 = 3/2 E_F n$. The second rule by which local-field corrections are gauged is the short-range correlation condition, given by

$$\lim_{q \to \infty} G(q) = 1 - g(0) \tag{5-28}$$

Both the compressibility sum rule and the short-range correlation condition are satisfied to a good degree of accuracy by the Ichimaru-Utsumi approximation, justifying its choice as the model for local-field correction in an electron gas.

The Ichimaru-Utsumi model for the local-field correction is valid for values of $R_s$ between 1 and 15. It is quite possible during the simulation of these materials that the

density of the liquid or vapor phase can render the model invalid. In fact, as density decreases, as in the vapor phase, there is no longer the long-range periodic ordering and screened Coulombic interaction that the model pseudopotential strives to capture in simulation. If the valence electrons of the studied systems were tightly bound, lower density vapor-phase behavior should approach that of the noble gases, allowing for the use of a simpler, Lennard-Jones like potential.

The calculation of the pair-potential for the empty-core pseudopotential model is the most time consuming portion of a coexistence calculation. To expedite calculation, the pair potential is calculated for a few hundred distances and these numbers are placed in a lookup table that approximates pair-potential values using a basic central difference method. If the integral formulation of the real space pair potential is used, each point in the lookup table involves the integration of a slowly convergent oscillatory integrand, which can involve the evaluation of several thousand points on the integrand curve. Integration of the pair-potential integrand in the complex plane overcomes this problem, by providing an easily evaluated real-space representation of the potential. When the expressions for electron-gas polarizability and the Itamaru-Utsumi form of the local field corrections are represented by a rational polynomial fit, it is found that the potential can be evaluated for all $r$ with a simple trigonometric expression that depends only on the polynomial roots of the denominator of the integrand. Further, this form can be integrated to give the long-range corrections to the potential. The method developed to calculate the pair-potential and its long-range corrections by integration in the complex plane is included in Appendix B.

Linear response theory also allows the formulation of a reciprocal space representation of the empty-core pseudopotential model This formulation relies not only on the form of the pseudopotential chosen but also on liquid structure. These are the two representations standard to a Gibbs-Bogoljubov calculation Discussion of the terms derived from response theory in reciprocal space will be postponed until the next chapter which details the Gibbs-Bogoljubov method

The parameters in pseudopotentials are usually calculated to fit a property of the solid phase, and thus the distortions in the free electron structure modeled are often distortions that rely on the periodicities of surrounding solid crystal structure during calculation. One of the assumptions implicit in previous liquid phase simulations [6] is that the calculated potentials are preserved in a global sense during a dynamic simulation, that is, the density of ion cores and electrons is assumed to be homogeneous throughout the simulation cube It is known that distortions in a crystal lattice will change the energy of the lattice appreciably, and these energy changes can qualitatively change the shape of the true potential of the metal system as the metal shifts from a solid system to a liquid. Pseudopotentials are sensitive to local-effects, such as fluctuations in electron density near an atomic core Configurations of atoms in a simulated liquid system are more prone to distortion than the rigid lattices of solid systems, and the pseudopotential calculated for a solid system may be only a first approximation to a mean potential that better describes a liquid system

Two potential energy functions have been described that have been used to represent real systems The empirical Lennard-Jones potential is used to represent the

noble gases and inert fluids The Lennard-Jones 6-12 potential is well studied, but a generalized form of the Leanard Jones potential has been proposed that has not been examined in detail theoretically The second potential, the empty core pseudopotential model is a potential energy function used to describe solid metals Its fitted paramaters, the core radius and the valence, are usually chosen so that the potential energy function reproduces bulk compressibility and band structure for a solid metal The empty core pseudopotential model is broken into two parts in its traditional real space formulation, one part represents the energy contribution due to the density of the system, and the second contribution is due to the pair-potential interaction within the system The empty core pseudopotential has not been tested in liquid metal simulations with free boundaries.

# CHAPTER 5
# THE GIBBS-BOGOLJUBOV METHOD

Since the calculation of liquid-vapor equilibrium ultimately becomes the problem of determining two distinct phases with the same temperature, pressure, and chemical potential, any method that allows calculation of the pressure and chemical potential for a fixed temperature will find phase-equilibrium. Traditionally, physicists have not been concerned with the macroscopic thermodynamic properties of a system, but have extensively studied the two classical properties of the system that allow for approximation of thermodynamic properties. The first of these, the radial distribution function, represents the structure of the system, while the second, the potential energy function of the system, represents the interaction between atoms. Potential energy functions, as discussed in Chapter 5, have been formulated for solid metals and liquid metals near their melting temperature from pseudopotential theory, but the theoretical description for radial distributions for liquid metals is still in its infancy. This chapter outlines two methods for the calculation of the macroscopic properties of a coupled liquid-vapor system from known theoretical descriptions of the radial distribution function using the empty-core pseudopotential formulated in reciprocal space. The first method described uses an ideal monatomic gas vapor phase model. The second model simulates polyatomic constituents

in the vapor phase by using the canonical ensemble partition function to calculate the Gibbs free-energy of the vapor system.

Theoretical Outline of the Gibbs-Bogoljubov Method

Perturbation theories allow the use of a well-studied reference system to approximate the properties of the less ideal systems of interest to the engineer. One of these perturbation theories, the Gibbs-Bogoljubov inequality [52], is a variational method that allows for the calculation of an upper bound to the Helmholtz energy of a system. The upper-bound estimate is found by evaluating the free energy $F_0$ of a reference system and adding a perturbation term $\langle V \rangle_0$ that amounts to the calculation of the difference between the real and reference system Hamiltonians averaged by integration over the structure of the reference system

$$F \leq F_0 + \langle V \rangle_0 \tag{6-1}$$

The best estimate to the Helmholtz energy of a system is obtained when the right-hand side of equation (6-1) is minimized with respect to the parameters that characterize the structure model of the reference fluid. Once the Helmholtz energy is known, the Gibbs-energy, which is the chemical potential of a single-component system, can be found by making an a pressure-volume correction to the approximated Helmholtz energy

$$\mu - G = F + PV \tag{6-2}$$

The pressure of the system can be approximated using the same model by the partial differentiation of the right hand side of the model with respect to the specific volume of the system $\Omega$

$$P = -\left(\frac{\partial\left(F_0 + \langle V\rangle_0\right)}{\partial\,\Omega}\right)_T \qquad (6\text{-}3)$$

The coupling of these two condition with a vapor-phase model allows the direct calculation of the saturated equilibrium conditions

Calculation of liquid phase thermodynamic properties requires knowledge of the radial distribution function or structure factor of a liquid In most cases for liquid metals, however, this radial distribution function has to be determined experimentally, and few accurate results are available for even low-melting temperature metal systems. Fortunately, the determination of liquid structure through diffraction experiments has shown that the distribution functions of the simple sp-bonded metals are similar to the structures defined by simple physical models

One model that closely represents experimental diffraction results is the hard-sphere fluid [53], a model that simply approximates each atom in a fluid as a simple sphere that does not interact with its neighbors Analytic approximations to the structure factor and thus the pair-distribution function are available for the hard-sphere model based on a solution of the Percus-Yevick equation The Percus-Yevick solution has been extended to binary systems [54], which can allow the calculation of saturated property curves for binary melts A second model, the one-component plasma model [55], is a more rigorous Monte Carlo calculation for a many particle system of electrons and point positive charges The results for these Monte Carlo calculations are tabulated, and interpolation allows for the approximation of distribution function from the tabulated data Though little modification to existing methods of calculation would be needed to incorporate

distribution functions representing the one-component plasma, the analytic simplicity of the hard-core model lends itself to the theoretical methods to be outlined, so this reference system was chosen as the system for which sample calculations for group I-IV metals would be performed.

The pair-distribution function of the hard-sphere fluid is far more difficult to calculate than the structure factor, so a reciprocal space formulation of the empty-core pseudopotential was chosen for calculation of the Helmholtz energy of the liquid system. Using the conventions of Umar *et al.* [2], the reformulated Helmholtz energy for a pure metal given in the reciprocal space formulation is

$$F_{ps} = F_{eg} + F_1 + F_2 + F_M \tag{6-4}$$

where $F_{eg}$ is the contribution due to the electron gas medium, $F_1$ is the zeroth Fourier component contribution, $F_2$ is the second order (or band structure) energy, and $F_M$ is the Madelung contribution to the energy of the system. Keep in mind that this expression is only a contribution to the total Helmholtz energy of the system, and terms will be added later to describe the ideal contributions and the contributions of the liquid model to the total expression for the Helmholtz energy. A short breakdown will be given to explain what each term represents.

The electron gas energy is the same energy used for the real space calculation of the pseudopotential, but for the purpose of this section was reformulated in terms of the Fermi wavevector of the system.

$$F_{ex} = x\left(\frac{3}{10}k_F^2 - \frac{3}{4\pi}k_F - 0.0474 - 0.0155\ln\left(k_F\right) - \frac{1}{2}\gamma_{ex}T^2\right) \tag{6-5}$$

where $k_F$ is the Fermi wavevector, and $\gamma_{ex}$ is the constant volume heat capacity of the electron gas. The electron gas energy includes the terms for electron-electron repulsion, and the exchange and correlation energy contributions due to Nozieres and Pines [56]. The rigorous expression for the low temperature value of the electron heat capacity normally has exchange and correlation terms [57] but the independent Fermion result

$$\gamma_{ex} = \left(\frac{\pi k_B}{k_F}\right)^2 \tag{6-6}$$

is expected to give accurate results throughout the temperature range of these simulations.

The second term is the zeroth Fourier component of the potential

$$F_1 = nZ\left[\lim_{q\to 0}\left(v(q) + \frac{4\pi Z}{q^2}\right)\right] \tag{6-7}$$

which represents the first order contribution to energy found through perturbation theory. The density of the metal system is represented by $n$. Physically this equation represents the energy contribution of each ion in a uniform electron density. The $v(q)$ term, which is the Fourier transform of the empty-core potential model, is given by

$$v(q) = -\frac{4\pi}{q^2}Z\cos\left(qR_c\right) \tag{6-8}$$

Substitution of (6-8) into (6-7) leads to the analytic result

$$F_1 = 2\pi\, nZ^2R_c^2 \tag{6-9}$$

The second order contribution to the Helmholtz energy of the system includes the electron mediated interaction of ions with other ions, and the interaction between the electron gas and the ions. Structure determines the magnitude of this band energy, represented by

$$F_2 = \frac{1}{16\pi^3}\int_0^\infty \alpha(q,n)\,v(q)^2\left(\frac{1}{\varepsilon(q,n)}-1\right)q^4\,dq \tag{6-10}$$

where $\alpha(q, n)$ is the structure factor of the reference liquid, $q$ is the magnitude of the wavevector of the system, and $\varepsilon(q, n)$ is the dielectric function for an electron gas. The Itsimaru-Utsumi form for the dielectric function is used for all calculations.

The energy of the unmediated interaction of ions is given by the Madelung energy. This energy is also structure dependent, and amounts to averaging a Coulombic interaction between ion centers over the structure of the fluid.

$$F_M = \frac{1}{\pi}\int_0^\infty Z^2\left(\alpha(q,n)-1\right)dq \tag{6-11}$$

The choice of the hard sphere fluid as a reference fluid means that many of the expressions cast as integrals for the evaluation of energy can be replaced with simple analytical results. An exact solution of the Percus-Yevick equation exists for the hard sphere fluid, giving one such approximation to the true structure factor of the fluid [53]. The hard sphere fluid is mathematically defined by the potential

$$v(r) = \begin{cases} \infty & r \le \sigma \\ 0 & r > \sigma \end{cases} \tag{6-12}$$

where $\sigma$ is the radius of the hard-sphere The structure factor for the hard sphere fluid can be found via the Percus-Yevick solution by evaluating the direct correlation function $c(q\sigma)$

$$c(q\sigma) = -4\pi\sigma^3 \int_0^1 ds\, s^2 \frac{\sin(sq\sigma)}{sq\sigma}\left(\alpha + \beta s + \gamma s^2\right) \tag{6-13}$$

where $\alpha$, $\beta$, and $\gamma$ are functions of the packing density parameter $\eta = \pi n \sigma^3/6$ given by

$$\alpha = \frac{\left(1+2\eta^2\right)}{\left(1-\eta\right)^4}, \tag{6-14}$$

$$\beta = \frac{-6\eta\left(1+\frac{\eta}{2}\right)^2}{\left(1-\eta\right)^4}, \text{ and} \tag{6-15}$$

$$\gamma = \frac{\eta\left(1+2\eta\right)^2}{2\left(1-\eta\right)^4} \tag{6-16}$$

The structure factor of the system is calculated from the direct correlation function expressed in terms of a reduced wavevector

$$a(q\sigma) = \frac{1}{\left(1-nc\left(q\sigma\right)\right)} \tag{6-17}$$

The explicit expression for the direct correlation function is given in Appendix A.

Terms that contribute to the Helmholtz energy of the hard sphere reference system are also well defined The Helmholtz energy of the hard sphere system $F_{hs}$ has two terms

$$F_{hs} = \frac{3}{2} k_B T - TS_{hs} \tag{6-18}$$

where

$$S_{hs} = S_{gas} + S_{\eta} \tag{6-19}$$

is composed of the ideal term

$$S_{gas} = \ln\left[\frac{e}{n}\left(\frac{emk_BT}{2\pi\hbar^2}\right)^{\frac{3}{2}}\right] \tag{6-20}$$

where $m$ is the mass of an atom, and the contribution due to the entropy of the ideal hard sphere fluid

$$S_{\eta} = \ln(1-\eta) + \frac{3}{2}\left[1 - \frac{1}{(1-\eta)^2}\right] \tag{6-21}$$

The total Helmholtz energy of the liquid system is

$$F = F_M + F_{pr} \tag{6-22}$$

An analytic expression for the Madelung energy of the hard sphere fluid also exists due to the Percus-Yevick solution, which is

$$F_M = Z^2 \alpha_M \tag{6-23}$$

where

$$\alpha_M = \frac{2\pi n Z^2}{1+2\eta}\left[-\sigma^2 - \frac{1}{5}\left(1 - \frac{\eta}{2}\right)\sigma^2\right] \tag{6-24}$$

Since the contributions to the Helmholtz energy from the empty-core pseudopotential and the hard sphere liquid are now known, an upper bound to the metal system energy can be calculated using the structure factor of the hard sphere system derived from the Percus-Yevick equation to represent the structure of the metallic liquid

The Gibbs-Bogoljubov equation comes from a perturbation scheme, so accurate results can only be expected if the structure of the reference fluid resembles the metal melt structure.

The hard-sphere model has the single variational parameter $\sigma$. Thus, the least upper bound to the Helmholtz energy is calculated by minimizing the right-hand side of equation (6-1) with respect to the hard sphere diameter. A single variational condition defines this minimum

$$\left(\frac{\partial F}{\partial \sigma}\right)_{\Omega,T} = 0 \tag{6-25}$$

This condition also simplifies the expressions for the entropy and the pressure of the system written in terms of the total Helmholtz energy of the system, which can now be given by the partial derivatives

$$S = -\left(\frac{\partial F}{\partial T}\right)_{\Omega,\sigma} \tag{6-26}$$

and

$$P - n^2\left(\frac{\partial F}{\partial n}\right)_{T,\sigma} = -\left(\frac{\partial F}{\partial \Omega}\right)_{T,\sigma} \tag{6-27}$$

The Ideal Gas Vapor Phase

Once an expression for the liquid Gibbs energy is available, an assumption must be made about the vapor phase of the system to complete the calculation of saturated properties. The ideal gas is the simplest possible representation of the vapor phase. For a

pure metal system, the Gibbs free energies of the vapor and liquid phase can be equated, giving

$$F_l + P\Omega_l = F_v + P\Omega_v \tag{6-28}$$

where the subscripts $l$ and $v$ denote the liquid and the vapor phase respectively. The kinetic contributions to energy are the same in both phases, as is the de Broglie wavelength contribution to the ideal entropy. These terms are not included in the redefinition of a function $\Phi$ which includes all terms in the liquid Helmholtz energy not representing the ideal state, abbreviating the liquid Helmholtz energy to

$$F_l = \frac{3}{2}k_B T - TS_{per}(\Omega_l) + \Phi(\Omega_l) \tag{6-29}$$

with $S_{per}$ as defined in equation (6-20) and

$$\Phi(\Omega_l) = F_{pe} - TS_0 \tag{6-30}$$

The corresponding pressure of the liquid system is found by differentiation to be

$$\frac{P\Omega_l}{k_B T} = 1 - \frac{\Omega_l \Phi'(\Omega_l)}{k_B T} \tag{6-31}$$

The vapor phase is assumed to be an ideal gas of atoms in their ground state. The liquid systems studied with this simulation will be in a regime where energy contributions due to electronic excitations in the vapor phase will be unimportant, and these effects will not be modeled. A correction to ensure the vapor phase has the same zero of energy as the liquid phase will be incorporated into the simulation, and this energy, $-E_{ion}$, will correspond to the energy required to remove all the valence electrons from an atom. The vapor phase free energy is then

$$F_v = \frac{3}{2}k_B T - T S_{gas}(\Omega_v) + E_0 \,, \tag{6-32}$$

and the pressure of the vapor can be described by the ideal gas equation

$$\frac{P\Omega_v}{k_B T} - 1 \tag{6-33}$$

It is now possible to write coexistence equations for the proposed metal system. If the Gibbs energies of the liquid and vapor system are equated, and the corresponding pressure equations substituted into (6-28), an equation that relies only on the specific volume of the liquid phase results

$$1 - \frac{\Phi(\Omega_v)\Omega_v}{k_B T} - \exp\left(\frac{\Phi(\Omega_v) - \Omega_v \Phi'(\Omega_v) + E_0}{k_B T}\right) \tag{6-34}$$

Numerical solution of equation (6-34) with liquid phase specific volume as the single parameter will allow determination of the vapor phase specific volume and the system pressure. Calculation over several different temperatures allows for the construction of the standard liquid specific volume-temperature and pressure-temperature curves.

Several approximations can be used in this calculation procedure to further enhance the accuracy of these calculations. It has been shown that the zeroth Fourier component of the pseudopotential (6-9) can be chosen so that the calculated internal energy of the liquid,

$$U_l = \frac{3}{2}k_B T + F_{ES} + F_{XC} + F_1 + F_2 \tag{6-35}$$

matches the experimental internal energy of the system at the system's melting temperature. This fit is accomplished by changing the coefficient of density in the first Fourier component $F_1$ from the form given in equation (6-9) to a new constant that

reproduces the internal energy of the liquid system at its melting temperature. Fitting the pseudopotential in this manner has an implicit assumption, it is assumed that no terms above second order in the linear response theory contribute significantly to the Helmholtz free-energy of the system. Normal boiling temperature and specific volume data also play a key role in the calculation of $E_{ion}$, which is chosen so that equation (6-34) is satisfied at the boiling temperature. Previous attempts [3] at liquid-vapor equilibrium calculation used melting temperature data calculate $E_{ion}$, but it proved practically impossible in every situation to ensure that sufficient numerical accuracy was available in the calculation to depict the very small energy differences needed to satisfy the equilibrium condition, especially at the low pressures of the melting temperature.

Several sources of error arise in this calculation, adding to the error introduced by the Gibbs-Bogoljubov perturbation theory. The first of these is the assumption of an ideal gas vapor phase. Most metal systems show dimerization [4] in the vapor phase at temperatures above their boiling temperature. Dimerization will lower the vapor phase pressure at a given temperature, which can raise the estimate for the ionization energy of the system, $E_{ion}$. The assumption of a nearly free electron metal in the melt also may prove difficult to justify over all liquid densities, particularly as the metal system approaches its critical point. As the specific volume of an experimental system rises, electron correlation effects will become very strong, and eventually there will be a transition from a nearly free electron conductor to an insulating fluid.

A third error can arise due to the nature of the phase transition itself. Because a liquid metal tends to separate into a low-density constituent and a high-density

constituent, the local fluctuations in system order can contribute significantly to the low-angle portion of the structure factor This behavior has been observed in liquid rubidium at 1400 K (M.P 312 K, B P 961 K) Since this behavior is due to potential interaction between atoms, a structure derived from a non-interactive system such as the hard sphere fluid can describe the liquid metal structure inadequately This behavior does not appear to contribute significantly to phase data between the melting temperature and the boiling temperature of the liquid.

A Simple Model for Dimers

One of the problems particular to the ideal vapor model, the assumption that there is no formation of dimers, trimers, and other n-mers, can be partially remedied by using an associated solution model [7] The Gibbs energy of a system can be calculated from the canonical ensemble partition function of a system, so that if the relevant energy levels of system are known, the population of states is also known, and the Gibbs energy for that system can be calculated Using an ideal gas model for the monomer of the system, and a rigid rotor approximation for the dimer, constants found using vapor phase spectroscopy will yield the information necessary to calculate the Gibbs energy of an ideal gas consisting of a monomer and dimer This method will also be extended to the calculation of n-mers

Assume a vapor system with a constant number of atoms $N$, which is made up of $N_1$ monomers and $N_2$ dimers, so that the conservation of atoms in the phase states that

$$N = N_1 + 2N_2 \tag{6-36}$$

The Helmholtz energy of this system consists of two contributions, both of which are assumed to occupy the total volume of the system $V$

$$F = F_1 + F_2 \tag{6-37}$$

The Helmholtz energy of a system can be expressed in terms of the canonical ensemble partition function $Z_i$, which for each species $i$ in the gas phase can be written

$$F_i = -\frac{N_i k_B T}{N} \ln\left(\frac{e Z_i}{N_i}\right) \tag{6-38}$$

The partition function for the monomer is given by the expression

$$Z_1 = g\left(\frac{M k_B T}{2\pi\hbar^2}\right)^{\frac{3}{2}} V = \zeta_1 V \tag{6-39}$$

where g is the degeneracy due to spin and angular momentum of the system. This partition function assumes the monomer is a non-interacting collection of point masses of mass M.

The dimer is modeled as a rigid rotor, which allows the approximation of the rotational and vibrational contributions to the Helmholtz energy. The partition function for the rigid rotor is

$$Z_2 = \left(\frac{2\pi M k_B T}{2\pi\hbar^2}\right)^{\frac{3}{2}} V \exp\left(\frac{\varepsilon_0}{k_B T}\right)\left(\frac{T k_B M R^2}{2\hbar^2}\right)\left(\frac{k_B T}{\hbar\omega}\right) = \zeta_2 V \tag{6-40}$$

given the diatomic binding energy $\varepsilon_0$, the bond length between atoms in the diatomic $R$, and the angular frequency of vibration $\omega$. The last two terms in (6-40) correspond to the contributions to the partition function due to the rotational and vibrational modes, respectively. It is assumed that the high temperature approximation to this partition

function is valid, and experimental values for metals in their vapor state confirm the validity of this assumption

The pressure of the system can be calculated from the volume derivatve of the Helmholtz energy

$$P = -\left(\frac{\partial F}{\partial V}\right)_T = \sum_i P_i = \sum_i \frac{N_i k_B T}{V} \tag{6-41}$$

The Gibbs energy per atom is given by

$$G = F + PV = -\sum_i \frac{N_i k_B T}{N} \ln\left(\frac{Z}{N_i}\right) \tag{6-42}$$

from which the chemical potential for each constituent can be calculated and equated to satisfy the conditions of thermodynamic equilibrium. If this is done for the dimer reaction

$$2X \leftrightarrow X_2$$

then chemical equilibrium must satisfy

$$2\left(\frac{\partial G}{\partial N_1}\right) - \left(\frac{\partial G}{\partial N_2}\right) = \lambda^{\frac{1}{2}} \tag{6-43}$$

where $\lambda$ is a constant corresponding to the square root of the chemical potential of the diatomic. Two expressions result from this equilibrium equation $N_2 = \lambda Z_1$ and $N_2 = \lambda^2 Z_2$ The fraction of each atom in the gas phase may now be written as a function of $\lambda$

$$\frac{N_1}{N} = \lambda \zeta_1 \Omega_r \tag{6-44}$$

$$\frac{N_2}{N} = \lambda^2 \zeta_2 \Omega_v \tag{6-45}$$

which satisfies the requirement that the sum of the fractions of each constituent must be one

$$\left(\lambda \zeta_1 + 2\lambda^2 \zeta_2\right)\Omega_v = 1 \tag{6-46}$$

The system pressure can now be defined in terms of the partition function result

$$P_v = \left(\lambda \zeta_1 + \lambda^2 \zeta_2\right) k_B T , \tag{6-47}$$

and the Gibbs energy of the system is the simple expression

$$G_v = k_B T \ln\lambda \tag{6-48}$$

A computational procedure for the calculation of saturated conditions can now be outlined If the Gibbs energy of the liquid phase is equated with the Gibbs energy of the vapor phase, an expression for $\lambda$ at equilibrium is apparent, and given by

$$\lambda\left(\Omega_l\right) = \exp\left(\frac{F_l\left(\Omega_l\right) - \Omega_l\left(\frac{\partial F\left(\Omega_l\right)}{\partial \Omega_l}\right)_{T,n} - E_{ion}}{k_B T}\right) \tag{6-49}$$

where $E_{ion}$ is used to correct the liquid energy to the same reference as the monatomic vapor The pressure equation allows for construction of an equation that defines equilibrium for the system

$$-\left(\frac{\partial F_l(\Omega_l)}{\partial \Omega_l}\right)_{T,\mu} = \left(\lambda(\Omega_l)\zeta_1 + \lambda(\Omega_l)^2\zeta_2\right)k_B T \tag{6-50}$$

Since equation (6-50) is only a function of liquid volume, a solution can be found by bracketing a root and using a root finder to solve for liquid volume. Once the liquid volume is found, information on the pressure, monatomic and diatomic fractions, Gibbs energy, and vapor volumes immediately follows.

Extension of the theory to include trimers is straightforward. Again the partition function for the trimer will be of the form

$$Z_3 = \zeta_3 V \tag{6-51}$$

The contributions due to vibrational rotational states of the trimer depend on the structural configuration, linear or bent, of the trimer, but these contributions do not change the volume dependence of the partition function, nor do they affect the argument. Assuming the predominant reactions in the vapor phase are given by

$$2X \leftrightarrow X_2$$
$$X + X_2 \leftrightarrow X_3$$

and that the conservation of atom number in the vapor phase satisfies the relation $N = N_1 + 2N_2 + 3N_3$, the specific volume of the liquid phase can be found by finding the roots of

$$-\left(\frac{\partial F_l(\Omega_l)}{\partial \Omega_l}\right)_{T,\mu} = \left(\lambda(\Omega_l)\zeta_1 + \lambda(\Omega_l)^2\zeta_2 + \lambda(\Omega_l)^3\zeta_3\right)k_B T \tag{6-52}$$

where as before,

$$\lambda(\Omega_i) = \exp\left(\frac{F_i(\Omega_i) - \Omega_i\left(\frac{\partial F(\Omega_i)}{\partial \Omega_i}\right)_{T,n} - E_{ion}}{k_B T}\right) \tag{6-53}$$

Extension of this method to other n-mers is less straightforward, since different reaction pathways involving two species exist to form chains of four or more atoms, though calculation will still be possible if an independent set of reaction pathways exists

A method for saturated property calculation using the Gibbs-Bogoljubov inequality to estimate an upper bound to the Helmholtz energy of the liquid phase is outlined The reciprocal space formulation of the empty core pseudopotential model is coupled with the hard sphere structure factor to estimate the liquid Gibbs energy The energy of the vapor phase is model dependent, and expressions have been given for both an ideal gas model and a model incorporating terms for gas monomers and dimers After equating the Gibbs energy, temperatures, and pressures of the two systems, an equation is found that is a function of liquid specific volume only Thus equation is solved using a numerical root finding technique, and the remainder of the saturated properties follow The Gibbs-Bogoljubov method will be used to evaluate the value of the hard sphere model as a reference fluid for metal systems, and the possibility of using the empty core pseudopotential as a potential describing liquid systems.

reciprocal space formulation of the empty core pseudopotential model is coupled with the hard sphere structure factor to estimate the liquid Gibbs energy. The energy of the vapor phase is model dependent, and expressions have been given for both an ideal gas model and a model incorporating terms for gas monomers and dimers. After equating the Gibbs energy, temperatures, and pressures of the two systems, an equation is found that is a function of liquid specific volume only. This equation is solved using a numerical root finding technique, and the remainder of the saturated properties follow. The Gibbs-Bogoljubov method will be used to evaluate the value of the hard sphere model as a reference fluid for metal systems, and the possibility of using the empty core pseudopotential as a potential describing liquid systems.

# CHAPTER 7
# APPLICATION OF THE GIBBS ENSEMBLE METHOD

The Gibbs ensemble method has been applied to both the Lennard-Jones 6-12 potential and the empty-core pseudopotential representation for potential energy. The Lennard-Jones system was chosen to test the computer code developed for this dissertation, since data and parameters from previous simulations are available for comparison. Results of the simulation are presented, along with the phase data of some of the systems that are well represented by the Lennard-Jones 6-12 pair-potential energy representation. A more rigorous study is conducted for the empty-core pseudopotential model on two metal systems with qualitatively different pair-potentials. Phase coexistence properties are estimated using the Gibbs ensemble method for the sodium and aluminum systems. The vapor phase in both cases is modeled as a monatomic ideal gas. A breakdown of results, including examples of liquid structure, are used to explain the successes and failings of the empty-core pseudopotential representation of a liquid metal system within the Gibbs ensemble method.

## Implementation of the Gibbs Ensemble Technique

The Gibbs ensemble technique was implemented in the C++ programming language using the OS/2 operating system on a Gateway 2000 486DX2/50 computer. The language was chosen with a programming model in mind, object-oriented constructs would make the Gibbs ensemble simulation program flexible and easy to modify. Data

objects and their methods were chosen to mimic an experimental system, but this experimental system had access to all data defining the system, including atom configuration. Measurement devices implemented as objects were then able to keep track of the system potential, pressure, chemical potential, volume, density, and particle count A specialized object was implemented to store the data necessary to calculate the radial distribution function for an atomic system

Treating the potential energy function of a system as an object had its advantages Potential energy functions were implemented as lookup tables in the code, and modifying the potential energy was reduced to redefining the method which fills the lookup tables This code, as it is written, could be modified to survey the most popular simple model potentials by specifying the potential energy function, the parameters for this function, and the initial system conditions

The object-oriented approach to building the simulation program is used with a higher goal in mind The objects and methods, as defined, are easily manipulated Since the goal of the Gibbs Monte Carlo method is to calculate a large number of uncorrelated configurations, the concept is highly parallelizable Each processor in a parallel configuration can be passed a total Gibbs ensemble system, and each processor will then calculate the equilibrium averages When the processors are done, the averages will be passed back to a single processor for analysis and output Thus, $N$ processors should speed the calculation $N$ times

This was the theory In practice the C++ language was not a language widely used at the University of Florida, in fact, it was not used at all Though vector processors and

multiprocessing systems exist that are capable of compiling C++ programs, these machines were not available to calculate the results in this dissertation The code has not yet been adapted to parallel machines.

The Lennard-Jones One Component System

The Lennard-Jones system is the most studied of all interatomic pair potentials, and because it can be rewritten easily in a scaleable dimensionless form, the results obtained from a single simulation can be applied to any system for which the Lennard-Jones parameters $\sigma$ and $\varepsilon$ are known Since the temperature-density profiles for saturated Lennard-Jones systems have been studied using other methods, comparison data is available to check the results of the computer codes developed for this dissertation Panagiotopoulos [1] also conducts a study of the Lennard Jones system in his initial proposal of the Gibbs ensemble His data allows for comparison of initial system conditions, steps until the simulation reaches equilibrium, and the system size dependence

Since computer time was initially scarce, it was considered important to find conditions close to equilibrium quickly The number of particles in the simulated systems was very small compared to a "real" system, so fluctuations in the calculated properties can be large in comparison to the measured property itself Determination of a regime where equilibration took place quickly, and in which estimates of equilibrium properties could be determined in the smallest possible number of configurations was a special concern It was found through trial and error, that the volume change step and the creation-destruction step were the two steps that led most quickly to a Gibbs system near

equilibrium, and it was through the liberal over-application of these steps that a system could be forced to it equilibrium state.

The Gibbs simulation was divided into several stages. The goal of the first stage was to reach a simulation regime near equilibrium as quickly as possible. Excessive volume change and particle creation/destruction steps were attempted, all to force the system into the equilibrium state quickly. Statistics taken during this initial pre-equilibration phase had large standard deviations, which indicated that the system was rapidly moving toward equilibrium. A second equilibration phase returned the number of volume displacement steps and particle creation/destruction iterations to the value used throughout the simulation. The purpose of the second equilibration phase was to allow the parameters defining the maximum particle displacement and the maximum allowable volume change to stabilize near a value that permitted a 50% acceptance rate for both particle displacements and volume interchanges between systems. After the second equilibration phase, the sampling of the system took place.

For the single component Lennard-Jones fluid, the densities of the two systems were initially chosen to be equal...both sub-systems I and II had the same number of particles and the same volume, to ensure that phase splitting would occur spontaneously. The total particle count for the simulated system was 300, and the total system volume was chosen to be close, but not exactly the total system volume suggested by previous results. The system was pre-equilibrated for 1000 iterations using the philosophy that no number of volume displacement or creation-destruction steps was enough, and after a few simulations it was found that 100 particle displacement steps coupled with 20 volume

displacement steps and a single particle displacement phase allowed equilibrium to be attained quickly for all the test cases. After the pre-equilibration, the system was equilibrated for 9000 more iterations using a more computationally conservative approach, only ten total particle creation and destruction steps and one volume displacement was attempted per iteration. These numbers were also used throughout the calculation phase, since changing these numbers would introduce a discontinuity in the statistics kept for the system.

The calculated results were very close to previous Gibbs ensemble results, and compared well with previous NVT Monte Carlo and perturbation calculations for the Lennard-Jones system. The standard deviations for system properties calculated by using only uncorrelated samples were remarkably similar to those found by Panagiotopoulos [1] over his simulations consisting of $10^6$ iterations, indicating that the previous work accumulated statistics over both correlated and uncorrelated configurations. Simulations near the critical point did not stabilize or approach a single equilibrium value as expected. Calculation on the Gateway 2000 486DX2/50 typically took three days for a single data point with 11000 equilibrium steps and 10000 calculation steps.

The calculated reduced temperature-reduced density profile is presented in figure 7-1. The pressure-temperature data is presented in a $\log_{10}$(reduced pressure)-inverse reduced temperature, and is shown in figure 7-2. Plotting the pressure-temperature data in this manner shows the linearity of the transformed data, indicating a nearly constant heat of vaporization over the entire range of the simulation. Thermodynamic data for several fluids that obey near Lennard-Jones behavior are included in figure 7-3 and figure 7-4 for

comparison. The Lennard-Jones parameters used for data reduction to dimensionless form, and their respective sources in literature, are included in Table 7-1. Error bars representing two standard deviations of the calculated average for this study are not included in any of the figures, since they would not extend beyond the edges of the data point markers.

The results of Panagiotopolous [1,26] and those calculated for this dissertation disagree at temperatures near the critical temperature. In light of the analysis presented by Smit *et al.* [37], it appears that the results presented in this dissertation more accurately reflect the problems associated with the Gibbs ensemble simulation near the critical point. In the simulations conducted for this dissertation, the phases near the critical point continually changed their character, switching from a low density vapor phase to a high density liquid phase regularly. As a result, the average properties calculated over the length of the simulation run did not represent the true properties of the system, but instead represented a more homogeneous metastable phase, as predicted by Smit.

Though the Lennard-Jones potential describes many simple materials well, the accuracy of this potential fails as a representation of the metallic liquid-vapor system. The critical exponent of a single component system is defined as the exponent $\beta$ in the equation

$$\rho_L - \rho_V = k\left(T_c - T\right)^{\beta} \tag{7-1}$$

where $\rho_L$ is liquid density, $\rho_V$ is the vapor density, $k$ is a constant, $T_c$ is the critical temperature, and $T$ the temperature of the system. The Van der Waals equation of state gives a critical exponent of exactly 1/2, the value of $\beta$ for metals found from theory and

experiment is nearer to 1/3 [58] The value of the critical exponent for the Lennard-Jones fluid found with the Gibbs ensemble simulation lies somewhere in between these two values, greater that the value for metals, but less than the value for a pure Van der Waals fluid A least squares fit through the data calculated for this dissertation near the critical point calculated with the Gibbs ensemble method results estimates $\beta$ to be 0 38, though this value may be influenced by the problems associated with the Gibbs simulation method near the critical point of the system.

Metal Systems—General Features

It has been shown experimentally that at a certain liquid density metal systems have a metal-insulator transition [59] and this transition is expected to lie on the high density liquid arm of the temperature-density curve The metal insulator transition suggests a qualitative change in character of the potential energy function as the density of the metal system decreases On the high density side of the temperature-density curve the potential will be metallic in character, exhibiting nearly free electron behavior On the low density portion of the curve, the metal phase will consist of a non-conducting mixture that interacts through multipole-multipole interactions, multiple-induced multipole interactions, and induced multipole-induced multipole interactions As the density of the vapor phase drops further, the metal atoms will approach the non-interacting behavior of an ideal monatomic gas. Based on this evidence, two different models were needed for metals in the liquid phase and metals in the vapor phase. Since it is expected that the qualitative switch in potential energy functions does not occur exactly at the critical point, accurate

calculations of phase properties near the critical point of the metal system are unlikely, since the choice of potential is ambiguous

The metal vapor phase is modeled as an ideal gas An offset is introduced to correct for the different energy references chosen for the vapor and liquid phase: this offset corresponds to the ionization energy of the vapor, $E_{ion}$ Initially the experimental ionization energy was chosen to represent the difference in energy due to ionization between the liquid and vapor phase but this is not strictly true for a liquid represented by the empty-core pseudopotential In fact model potentials should have different ionization energy corrections corresponding to their deviation from the true potential of the system. Since metal potentials have not been studied in this manner no data are available for corrections included in the $E_{ion}$ term The ionization energy can be considered an adjustable parameter in Gibbs simulation

The choice of whether to include $E_{ion}$ as an energy correction in the liquid or vapor phase is arbitrary but this choice determines the sign of the energy contribution. In this simulation, $E_{ion}$ is assumed to correct for the zero of energy in the Gibbs ensemble's vapor phase, defining $E_{ion}$ to be a negative quantity Each particle in the vapor phase contributes $E_{ion}$ to the total energy of the vapor phase, and since the vapor is ideal, no other potential contributions are considered As a result, particle displacements and volume changes that modify the vapor system do not change the overall energy The only vapor phase internal energy changes that need to be considered are during particle interchange steps A particle insertion in the vapor phase dictates that $E_{ion}$ must be added to the total system energy,

likewise, a particle destruction in the vapor phase removes $E_{kin}$ from the total system energy

Various trends are evident for the empty-core pseudopotential when traversing the periodic table of the elements At the melting temperature solid density, the Group IA metals have first pair potential minimum that lies very close to the principal peak as given by the radial distribution function. In these metals, the first pair potential minimum is also the global minimum for the pair potential function Group IIA elements exhibit the same behavior Group IIIA elements begin to show a deviation from this behavior the principal peak of the radial distribution function still lies at the first pair potential minimum, but this minimum is no longer the global minimum for the pair potential function The second potential minimum is the global minimum for these systems. This behavior is also evident in the Group IVA, VA, and VIA metals Different results are obtained when attempting to simulate these two classes of systems with the Gibbs method

This behavior does not hold as the liquid metal system is heated As the temperature of a metal system rises, the liquid density drops. Calculations show that as the liquid density drops, so does the value of the pair potential at the first pair potential minimum For a system such as the sodium system, the position of the global minimum on the pair potential curve changes very little, but for metals to the left of Group IIB on the periodic table of the elements, the position of the global minimum changes drastically, from the position of the second potential minimum at the melting temperature to a position near the principal peak of the radial distribution function Figures 7-5 and 7-6 illustrate the deepening of the first potential well as density decreases for the sodium and aluminum

systems, respectively. This behavior affects the characteristics of the simulations performed using the Gibbs ensemble.

Initial Conditions for Metal Simulation in the Gibbs Ensemble

The Gibbs ensemble simulations for the metal systems were conducted using 300 total particles. Simulation were restricted to regions near the metal melting temperature, where the metal melt would be expected to most resemble the solid phase. It was assumed that linear response theory would begin to break down at higher liquid densities, so simulations were conservatively conducted in regimes where the theory would be able to represent liquid phase interactions, if the theory worked at all. The volume of one phase was always disproportionately large in these simulations, since the vapor pressures of these metal systems are extremely low near the melting temperature. Since the potential energy function was different for the liquid and the gas phases, one phase was started with a large initial volume. This phase interacted with ideal gas behavior. Atoms in the much smaller initial volume interacted with the empty-core pseudopotential model. The initial vapor volume was chosen as the volume of an ideal gas consisting of 150 particles at the simulation temperature. The density of the liquid phase was initially chosen to be the experimental density of the liquid metal at its melting temperature.

Initially, 100 creation/destruction steps were attempted for every set of 300 displacement steps and one volume change. The number of creation/destruction steps was dropped to fifty as soon as the system approached equilibrium. Systems were simulated over $10^5$ iterations, with a pre-equilibration stage of $10^5$ steps and an equilibration stage of $10^5$ steps. Any step that changed the liquid system density warranted the recalculation of

the electron-ion core contribution to the potential energy and the pair-potential function To conserve computer time, creation and destruction steps were lumped together Rejected creation and destruction attempts did not change the projected density of the liquid metal system if the creation/destruction was accepted, so there was no need to recalculate the pair-potential for the liquid system after a rejected creation/destruction move

The Sodium System

Simulation of the sodium system encountered unexpected difficulty Originally, the experimental ionization energy found through experiment to be 5 139 eV, was used to correct the zero of the vapor phase potential energy It was originally expected that there would be an interplay between the two terms contributing to the potential energy of the system, the terms solely due to the density of the metal system and the pair-potential contribution As the pair-potential of the system dropped the volume energy would rise, counteracting decreasing system energy due to density-dependent changes in the magnitude of the pair potential minimum Instead, once the simulation was started the density of the liquid-phase began to drop, and did not stop The potential energy of the system also dropped steadily, obviously not affected by the increasing energy contribution due to the volume energy of the system

There is a simple explanation for this behavior First, the first pair-potential minimum is deep enough that the formation of clusters in a low-density liquid phase is likely, a fact supported by extraordinarily high peaks in the calculated radial distribution function, as shown in figure 7-7 , and plotted atomic configuration snapshots taken during

simulations The distance between atoms in these clusters corresponds to the position of the first minimum in the pair-potential for the system. If the system density decreases, the value of the first minimum of the pair-potential also decreases, and if most of the atoms lie near this minimum, the total system energy decreases. In a real metal system, this drop in the first pair-potential minimum is countered by a rise in the volume energy contributions due to the electron gas and the ion core-electron gas interaction. The compensation is enough to prevent the liquid system from continually dropping in energy The volume energy calculated using the empty-core pseudopotential, shown in figure 7-9 , does not vary enough with density to prevent the consistent drop in system energy with a drop in density It is unlikely, then, that a volume change step that allows a drop in system density will be rejected If every drop in density as defined by the volume change step is accepted, the system will drop in density uncontrollably more clusters will be allowed to form, and eventually the liquid phase will completely misrepresent reality The density of the clusters themselves can be near the experimental saturated liquid density, but the volume of the metal system has grown so large that large voids are present in the cubic system cell, as shown in figure 7-8

The most likely candidate for inaccuracy is the description of the volume energy of the system. The pair-potential energy function determines the microscopic liquid structure of a system, but the volume energy determines the effective cube size of a simulated system The electron gas in a metal system provides electroneutrality to the system, and thus the restoring forces needed to keep the positive ion cores from flying apart It appears in this simulation that the slope of the restoring energy of the electron gas for the liquid

system is too low in magnitude. The rejection and acceptance of volume change moves in the Gibbs ensemble method depends on the difference in volume energies between two states, and thus the slope of the volume energy versus density curve. In figure 7-9, the volume energy versus density curve shows a minimum near the number density for sodium solid ($2.54 \times 10^{28}$ / m$^3$ at 300 K), and a gently rising curve as number density decreases. Though the volume energy rises with decreasing liquid density, the rise is not enough to overcome the changes in system energy due to decreases in the pair potential as the number density of the system decreases. A steeper rise would eventually halt the decrease in system density, by overcoming the decrease in energy due to pair-potential, and allow for equilibration of energy near the experimental value.

The volume energy calculated using the empty-core pseudopotential is a rough approximation at best. The exchange and correlation energies of the electron gas are calculated using the random phase approximation, and may be accurate only at high metallic densities ($R_s << 1$). The volume energy of the electron gas, without exchange and correlation effects, is a fit to experimental data taken over a limited experimental range. The core-electron energy contribution is exact for the empty-core pseudopotential model of core-electron interaction, but does not represent local effects that can contribute to energy in configurations in which the cores are very close. Finally, it is not known to what extent core-core exchange and correlation energies contribute to overall metal system energies, but even small energy changes can disturb the volume energy curve enough to compensate for pair-potential energy drops.

The continual decrease in system energy with a decrease in liquid density may indicate that there are also other problems with the empty-core pseudopotential model. Other workers have suggested that the alkali metal system may not be best described as a metal with valence one, as assumed in the calculation. Partial valences ($Z = 0.9$) have been defined for the related cesium system [60], and with the defined parameters moderate success has been achieved in describing the structure factor of the fluid. Thus, an effective valence may better represent the behavior of the metal fluid system. As the density of a liquid system drops, it is expected that electron will become more localized in space near atomic cores. Each ion will interact through a reduced effective charge, which drops as core ions spread apart and individual electrons are bound to a single core ion.

Artificial barriers stopped the uncontrollable decrease in energy. For instance, if the density argument to the potential energy function calculation was not allowed to drop below a certain value, the simulation density would drop only slightly below this value. In this manner, the simulation calculated the vapor pressure of the system at equilibrium, but since one of the parameters fixed for simulation is the liquid density, this simulation was far from predictive. The radial distribution function of this artificial fluid showed a sharp first peak, but since the liquid density was not allowed to drop below a certain minimum, atom clusters did not form. Fixing the metal potential in this manner will only work for metals with pair-potential global minimum that correspond to the distance to the first peak of the radial distribution function, since systems with pair-potential global minimum outside the first radial distribution function peak tend to spread out, lowering the system density below the experimental value.

The blame for the poor results may not be only in the pair-potential representation, but in the simulation method. It appears that the electron concentration in a liquid metal system is not homogeneous but depends on a local ion core density. As the metal cores cluster, the local density rises, and the value of the first pair-potential minimum rises. This higher energy will favor the spread of the ion cores, and the clustering of ions in the liquid phase will be prevented. This suggests that the pair-potential interactions in the metal system should be calculated using a local density of ion cores.

The Gibbs ensemble simulation could be modified to reflect this observation. The pair interaction between two atoms would be calculated according to the local density of atoms surrounding a straight line drawn between the atoms. This local density would be arbitrary, and depend on the geometry of a single bounding surface containing both interacting atoms, within which the local density would be calculated. This bounding surface will need to be developed heuristically, since theory points in no clear direction for this addition to simulation. A new pair-potential would need to be available for every pair interaction, since the local density for every pair interaction can be different. Thus, the calculation time for each iteration of steps will increase.

A better solution should be presented by using pair-potentials calculated from experimental structure factors within the simulation. These pair-potentials are potentials of mean force in the system, and the structure factor generated by the Gibbs ensemble should resemble the experimental structure factor closely, but not exactly. Though this method would again ruin the predictive nature of the Gibbs ensemble simulation, it would give

insight into the form of the potential energy function that will allow accurate calculation of phase properties.

The Aluminum System

Simulation of the aluminum system met with more success. When calculated using the parameters for the aluminum system, the pair-potential of the empty-core pseudopotential has a first local minimum that does not necessarily correspond with the global minimum of the system, as shown in figure 7-6. This raised first minimum was essentially a repulsive force at regions near the ion core which initially prevented the coupled density drop and formation of clusters characteristic of the sodium system. The first local minimum of the aluminum system did not drop below the global minimum until the liquid metal system reached a number density below $3 \times 10^{28}$ atoms/m$^3$, a number far below the experimental melting temperature liquid density, which was chosen to be $5.33 \times 10^{28}$ /m$^3$.

The simulations were conducted over a narrow temperature range from the melting temperature, 934 K, to 1400 K. Various values were chosen for the ionization energy of aluminum. For a fixed temperature, as the ionization energy dropped, the equilibrium liquid density rose. Calculations are shown for only one ionization energy. It is representative of systems with other ionization energies. Each simulation behaved as the sodium system did, but the simulation stopped dropping at liquid phase number densities around $1.6 \times 10^{28}$, well below the experimental aluminum density.

The volume energy of the aluminum system, shown in figure 7-10, shows a volume energy curve with a steeper slope than the sodium curve, but most of this increase

in slope comes from the dependence of ion-core volume on the square of ion core charge It appears that as the density of the liquid metal system drops during simulation, the change in volume energy finally overcomes the drop in pair potential energy characteristic of the empty-core pseudopotential systems This allows the simulation to take place, even if the calculated values do not lie close to experiment

This does not happen before some of the physics of the system is lost, however As stated earlier, the first maximum of the radial distribution function lies at a radial distance smaller than the global minimum of the pair-potential Because it is so much more favorable energetically for the ion cores to lie in the global minimum of the pair-potential, in the absence of restoring forces the atoms will do so at equilibrium. This is precisely what happens in simulation The restoring volume forces are again too small in magnitude, so the system energy drops by placing all the atom it can in configurations where all the atoms lie at the potential global minimum. The restoring forces present in the experimental aluminum system are not present in the simulated system, and although the volume energy eventually halts liquid system volume growth, it is too late to match experiment. The first peak of the calculated radial distribution function lies at the pair-potential global minimum, contrary to experimental analysis

The calculated density of the aluminum system is much too low, and this is reflected in the calculations of saturated liquid density as a function of temperature shown in figure 7-11 There is very little variation of liquid density with temperature Calculated pressure versus temperature curves for aluminum are shown in figure 7 12 A radial distribution function of the aluminum system, calculated at the melting temperature of 934

K is included in figure 7-13 The first peak coincides closely with the global minimum of the system's pair potential Finally a snapshot of the position of the ion cores characteristic to the simulated system is shown in figure 7-14 The snapshot shows that the aluminum atoms do not move very far from their solid phase face-centered cubic lattice positions at 934 K.

In a simulation in which the density of a liquid system is allowed to change, as in the Gibbs ensemble method, it appears that the empty core pseudopotential model is an inadequate representation for the liquid phase Restoring forces characteristic of the volume energy do not overcome the tendency of simulated metal systems to expand due to drops in the energy contribution due to pair contributions. The density of the sodium system, in which the first minimum and the global minimum of the pair potential coincide, does not stop dropping Atoms cluster in the liquid phase, forming regions with unrealistically high densities and regions with no atoms Aluminum, which at high densities has a pair potential with a global minimum beyond the position of the first local minimum, does stop expansion, but at a density too low to match experiment. The aluminum system forms an ordered lattice, very near the solid face-centered cubic structure characteristic of pure aluminum at room temperature Changes to the simulation may improve results, but problems in the simulation are more likely a result of the weaknesses of the empty core pseudopotential representation in describing a liquid system.

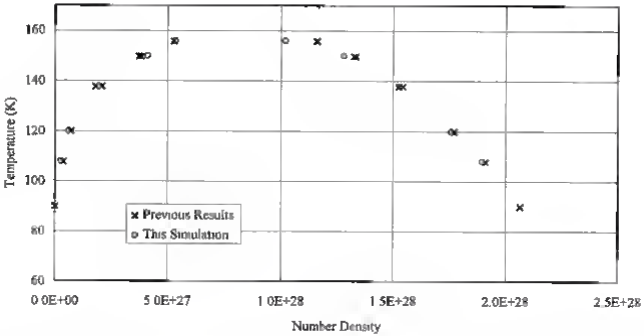


Figure 7-1 Reduced temperature versus reduced density plot for a pure Lennard-Jones fluid, calculated using the Gibbs ensemble simulation method Note that near the critical point the simulations do not match. Relative errors in the density calculations are very small (< 0 5 %) and are not shown to reduce the clutter at the data points. The simulations shown are results for 300 particle systems with $2 \times 10^5$ calculation iterations

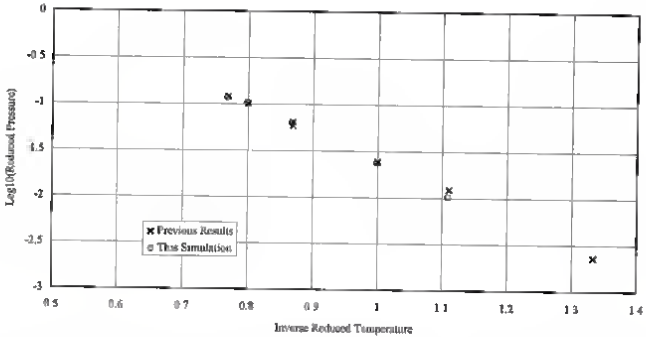


Figure 7-2 $Log_{10}$(reduced pressure) versus reduced temperature plot for a pure Lennard-Jones fluid calculated using the Gibbs ensemble simulation method Error bars are too small to be seen on the plot, and are no more than 0 3% The simulations shown are results for 300 particle systems, with $2 \times 10^5$ calculation iterations

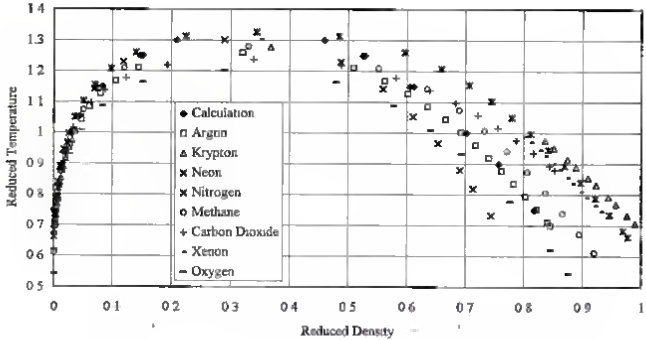


Figure 7-3 Reduced temperature versus reduced density plot for various materials Experimental data are taken from N.B Vargaftik [61].

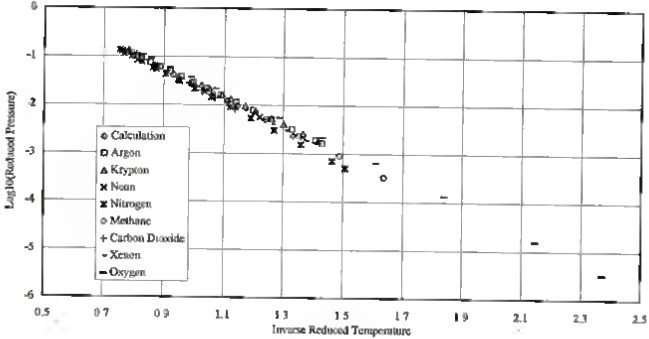


Figure 7-4 $Log_{10}$ (reduced pressure) versus inverse reduced temperature for various materials Experimental data are from N B Vargaftik [61]

Table 7-1 Lennard-Jones parameters for various systems. These parameters are used to reduce experimental quantities to dimensionless form

| | Argon [62] | Krypton [62] | Neon [62] | Nitrogen [63] | Methane [63] | Carbon Dioxide [63] | Xenon [63] | Oxygen [63] |
|---|---|---|---|---|---|---|---|---|
| $\varepsilon/k_B$ (K) | 119 8 | 164 0 | 34.2 | 95 2 | 148 9 | 246.1 | 222 3 | 128 8 |
| $\sigma$ (nm) | 0 341 | 0 383 | 0 272 | 0 375 | 0 378 | 0 375 | 0 410 | 0 336 |

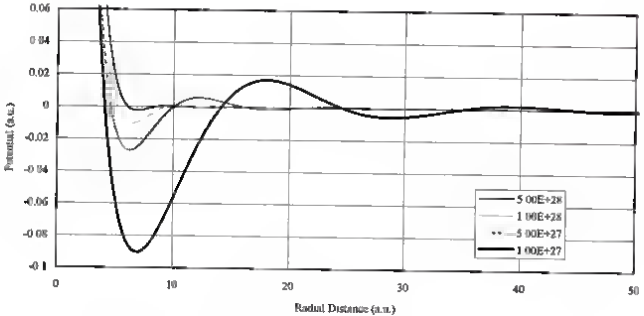


Figure 7-5 Sodium pair potential (a u ) versus radial distance (a.u ) for various densities.

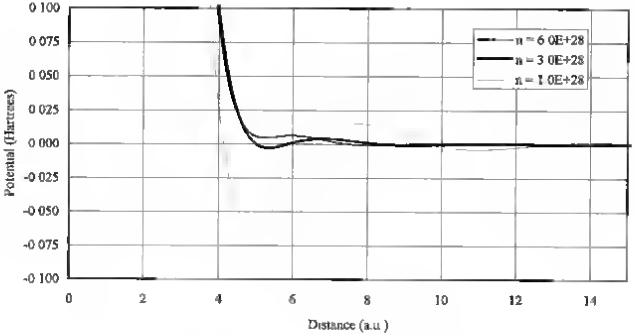


Figure 7-6 Pair potential (a.u ) versus radial distance for various densities of aluminum

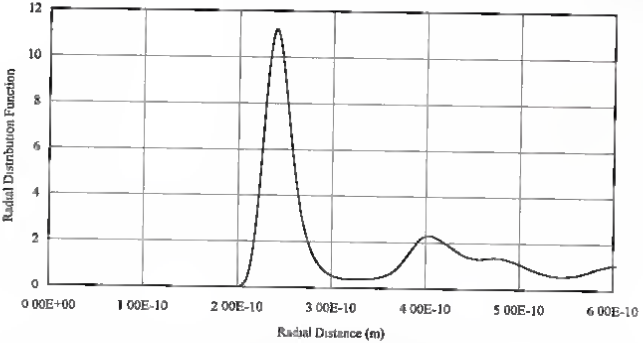


Figure 7-7 Typical calculated radial distribution function versus radial distance (m) for a simulated sodium system. The simulation temperature of this system was 373 K, and the ionization energy $E_{ion}$ = -5 143 eV. The tail end of the distribution function shows artifacts due to the method used to estimate the distribution.

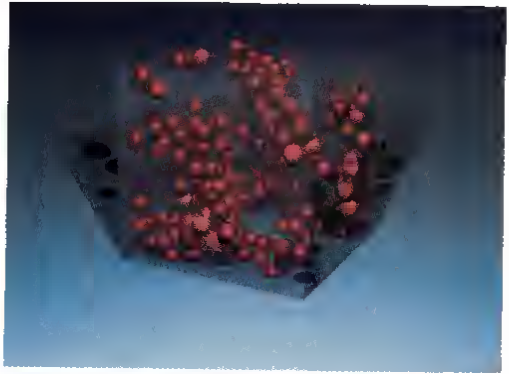

Figure 7-8 A snapshot of a sodium liquid configuration from a Gibbs ensemble simulation at 373 K The core radius, $R_c$ = 1 70 a.u., is used to size the spheres Note the voids in the system, which indicate that the liquid is not a homogeneous phase

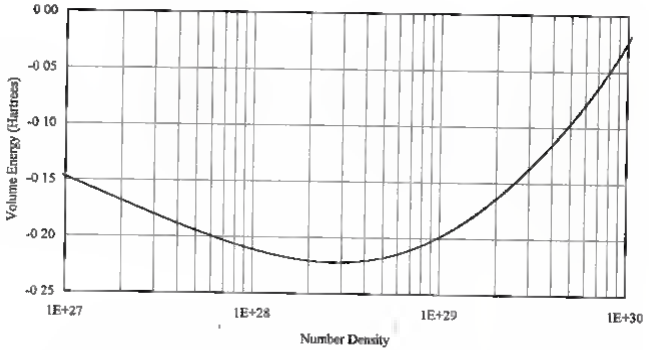


Figure 7-9 Potential energy contributions to the volume energy of sodium (Hartrees) versus number density (atoms/$m^3$)

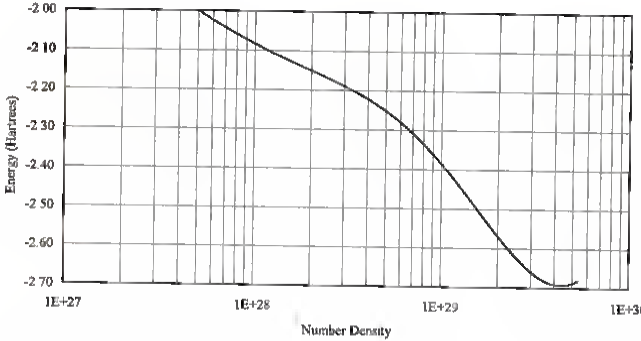


Figure 7-10 Potential energy contributions to the volume energy of aluminum (Hartrees) versus number density (atoms/$m^3$)

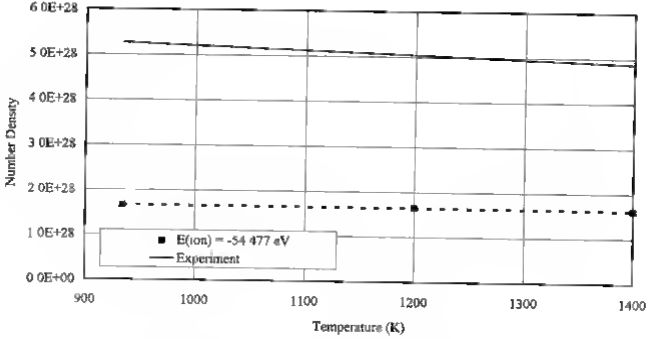


Figure 7-11 Aluminum number density (atoms/m$^3$) versus temperature (K) for $E_{ion}$ = -54 477 eV Experimental values are from the CRC Handbook of Chemistry and Physics [64]

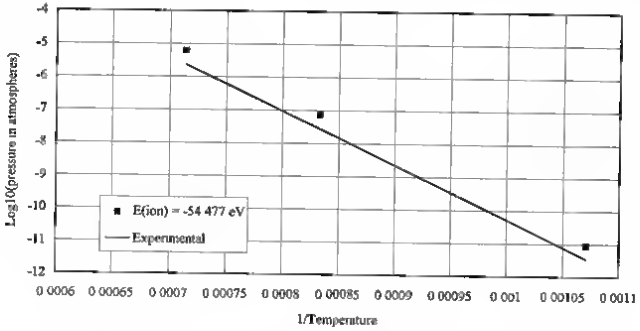


Figure 7-12 Aluminum $Log_{10}$(pressure in atmospheres) versus inverse temperature ($K^{-1}$) for $E_{ion}$ = -54 477 eV Selected values are from Hultgren *et al* [65]

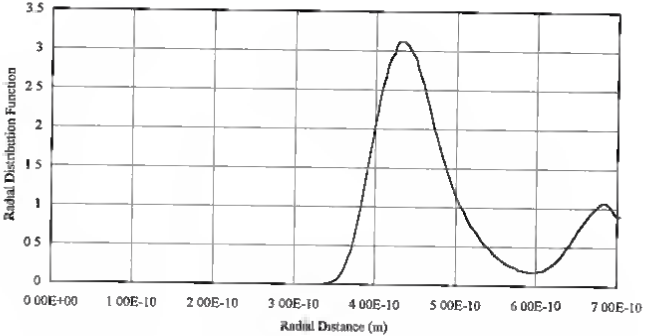


Figure 7-13 Radial distribution function versus radial distance in meters for the aluminum system This simulation was conducted with a 300 particle system at 934 K

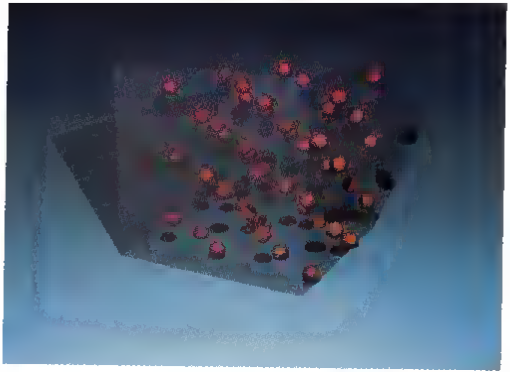

Figure 7-14 A snapshot of an aluminum liquid configuration from a Gibbs ensemble simulation at 934 K. The core radius, $R_c$ = 1.11 a.u., is used to size the spheres. The phase resembles solid aluminum.

# CHAPTER 8
# APPLICATION OF THE GIBBS-BOGOLJUBOV METHOD

The analysis of the phase results obtained using the Gibbs Bogoljubov method begins by dividing the elements into groups with similar liquid structures. Since liquid behavior is dependent on electronic shell configuration, the columns of the periodic table of the elements provide the most convenient means of categorizing the phase behavior of metal systems. This chapter will begin by discussing the trends in structure observed when traversing the periodic table of elements, using the hard-sphere fluid as a basis for comparison. This analysis will help to interpret the success of the results. Next, the Gibbs-Bogoljubov calculation will be outlined. Results will then be presented for the four groups most accurately represented by the empty-core pseudopotential coupled with the hard sphere fluid approximation. Groups IA, IIA, IIIA, and IVA. A final section will discuss the predicted boiling temperatures and ionization energies for the examined systems.

## Structure Trends in the Periodic Table of the Elements

Metallic liquids are often sorted into three qualitative categories when considering structure [66]. The first of these categories shows a symmetric first peak of the structure factor. The coordination number, calculated by integrating over the symmetric part of the first peak of the radial distribution function and multiplying by metal density, is between nine and eleven. The ratio of the positions of the second peak to the first peak of the radial

distribution function is near 1 91 Elements that approximately obey this behavior are the group IA and IIA elements, as well as aluminum, indium, tellurium, and lead The assumption of a hard sphere reference fluid is physically justifiable for these metals, since the coordination number of the hard sphere fluid is also between nine and eleven, and the first peak of the radial distribution function is symmetric.

The second category includes metals with asymmetric first peaks in their structure factor The coordination number of these metals is still essentially metallic in character with values between nine and eleven The ratio of the distance to the second peak over the distance to the first peak of the radial distribution function has a value greater than the hard-sphere value of 1 91 The group IIB elements, zinc, cadmium, and mercury, behave in this manner Though parameters for an empty-core pseudopotential description of the group IIB elements are available, the empty-core theory does a poor job of describing the binding energies in these metals Because there is such poor agreement between experiment and calculation for even the simplest of experimental quantities, no attempts were made to describe these metals with the Gibbs-Bogoljubov method

The final category for classifying the structure of liquid metal melts is for the liquids that deviate significantly from hard sphere behavior The coordination number of these liquids drops to values between six and eight Shoulders appear on the high-q side of the structure factor and the ratio of the distance to the second peak over the distance to the first peak of the radial distribution function is between 2 0-2 3 indicating a more loosely packed arrangement of atoms Silicon, germanium, gallium, and tin exhibit this behavior

The same trends in the empty core pair-potential that produced problems in simulating the liquid metals using the Gibbs ensemble method can be used to explain the differences in the structure factors of the metals. The local minimum of the empty-core pair potentials for elements in the same row of the periodic table essentially lie in the same position, and the core radii for elements in the same row are for the sake of argument, the same. For metals in the first column, a deeply attractive global minimum coincides with the first peak of the radial distribution function. Valence increases as one moves to the right across the table, and with increasing valance comes a rise in electron gas density. For higher electron densities, the Coulombic energy from the repulsive core, which is proportional to atomic charge, begins to cover the first minimum of the potential, creating a situation where the first minimum in the pair potential is higher in energy than the bottom of the second minimum. Since the atoms of the systems seek a low energy configuration, the atoms are spread apart toward the second minimum in the pair-potential, lowering the coordination number and distorting the liquid structure.

A second effect must be considered with increase of the core radius of an element, as in top to bottom traversal of the periodic table. As the valence of a metal increases, the peak of the radial distribution function will be pushed outward, but there will come a point where the core radius begins to limit whether this distortion can take place at all. The geometry of sphere packing for metallic systems with large ion core radii will ensure that the system retains the characteristics of a hard-sphere system, if only because the atoms are restricted from moving to what would be a lower energy configuration. This behavior is demonstrated most dramatically in group IVA. Silicon is a loosely packed metal with

covalent character, as is germanium. Tin begins a transition to the structure expected from a hard sphere fluid, and lead can be simulated as a pure hard-sphere fluid. As the core radius of the metals increase, the metals return from a loosely packed arrangement to a hard-sphere arrangement.

Hence, trends for the liquid structure of metals may be efficiently summarized. As the periodic table is traversed from left to right, the structure factor found by X-ray diffraction becomes less like that of a hard sphere fluid. Low electron densities characterize the metal to the left of the periodic table; high electron densities characterize those metals to the right. When the periodic table is traversed top to bottom, the structure of the fluid becomes more like that of a hard sphere fluid. The lower the metal resides on the periodic table, the larger the empty core radius of that atom, and the larger the effects of geometry alone.

## Outline of the Gibbs-Bogoljubov Calculation

The algorithm which allowed the calculation of saturated metal properties can be divided into three major tasks. The first task is the calculation of the slope for the first Fourier contribution to energy, using experimental data for the melting temperature, internal energy, liquid specific volume, and temperature. The new slope adjusts the calculated liquid internal energy at the melting temperature to the experimental value. The next step fits the ionization energy to liquid boiling temperature data, allowing the calculated pressure to be exact at the boiling temperature. A temperature is assumed for the final step, and a root-finding routine is used to find the specific volumes for which the

equilibrium equations are satisfied. The last step is repeated over several temperatures to gather the data necessary for a saturated properties curve.

Computer code was written to calculate saturated thermodynamic properties for liquid metals in the C++ programming language. QUADPACK [67] numerical integration routines were modified to allow calculation of the Helmholtz free energies for the liquid systems. The code was implemented in the OS/2 operating environment on a Gateway 2000 486DX/50. The calculation of saturated conditions for a single temperature took 8-12 minutes, with longer times necessary to calculate points with increased tolerance. Although data throughout the calculation were maintained accurate to seven decimal places, it is expected that the propagation of numerical errors has reduced this accuracy somewhat. Calculations at temperatures near the melting temperature often required ten or twelve significant figures of accuracy, but the integrator tolerances could only be set to seven significant digits before their own numerical error routines reported spurious results. Results were obtained at each temperature for saturated liquid density, vapor density, system pressure, Gibbs energy, and monomer and dimer fractions where appropriate.

Group IA Metals

Neutron diffraction studies [68] show that the Group IA elements have structure factors qualitatively resembling those of a hard sphere fluid, but studies examining the liquid pair potential suggest that subtle qualitative differences exist between the two systems. The potential energy function of the hard-sphere fluid has a steeply repulsive wall at the cut-off radius, which is in fact infinite in slope. Group I metals do not have this wall, and if the wall from the origin down to the first minimum of all metals is examined, the

Group I metals show repulsive portions of the potential with the smallest slope, suggesting that better reference systems than the hard-sphere fluid could exist [69]. A second reference system has been proposed [70] that can represent the structure of the alkali metals more accurately, that of a system of positive point charges interacting by a pure Coulombic potential in a negative compensating background. This model is known as the one component plasma (OCP) model, and accurate structure factors for various values of temperature and specific volume calculated from a Monte Carlo scheme have been tabulated [71]. It has also been shown [72] that the physical properties calculated from this model agree more closely with experimental values for Group I metals than those derived from the hard-sphere model. Structure factors calculated from the OCP scheme more closely match experiment, and the OCP structure factors yields a lower variational energy when coupled with the Gibbs-Bogoljubov inequality though differences are slight. With this in mind, the purpose of this study becomes one of determining whether the hard sphere approximation to liquid structure is an adequate description of the alkali metals for the purpose of coexistence calculation, or if the subtle gains from using the OCP approach are needed to calculate liquid-vapor equilibrium.

A previous calculation determining liquid-vapor coexistence properties for a sodium system by S. M. Osman *et al.* [73] uses a cubic polynomial fit in liquid density to approximate the zeroth Fourier component $F_0$ in the liquid pseudopotential. The polynomial fit was a trial-and-error procedure, adjusted to match experimental data. Since the eventual goal of this project will be the predictive modeling of phase behavior for mixtures and alloys, results were not adjusted by empirically chosen polynomial fits to

match available experimental data. Instead, the models have been chosen to minimize the parameters that would have to be acquired through experiment to calculate the liquid-vapor equilibria. All the parameters used throughout the thesis are readily available for most metal systems. The most difficult parameter to obtain experimentally, and perhaps the parameter with the most experimental uncertainty, is the internal energy of the liquid at the metal melting temperature. In this calculation, the first Fourier component of the empty-core pseudopotential is adjusted so that the internal energy of the modeled system matches the experimental internal energy of the liquid metal system at the system's melting temperature.

Calculations were performed for lithium, potassium, sodium, rubidium, and cesium systems. The parameters representative of each of the studied metals are listed in Table 8-1. Plots for sodium are included to show agreement with experimental data for the liquid density (figure 8-1), system pressure (figure 8-2), diatomic and monatomic vapor fractions (figure 8-3), and absolute Gibbs energy for the liquid system (figure 8-4), all as a function of temperature. It can be noted that the dimer fraction at high temperatures exceeds that measured in experiment, and this is characteristic of all the simulations for each metal.

In all the systems where data are available, the addition of a model for dimerization improves the quality of the calculated liquid-vapor equilibrium. Since diatomic spectroscopic data is not available, rubidium is modeled as a monomer only in the vapor phase, and agreement with experiment is still reasonable, especially at temperatures close to the system melting temperature. The liquid density for the remaining systems is summarized by least-squares linear data fits in table 8-2, and compared with experimental

data fits Also calculated and included in table 8-3 are the Antoine equation constants for saturated vapor pressure Note that the $r^2$ value for the vapor pressure fits are very close to unity, indicating that the heat of vaporization for the alkali metal systems is nearly constant over the temperature range simulated

Group IIA Metals

The structure factor for each of the Group IIA metals closely resembles that of hard sphere fluid The first peak in the structure factor is symmetric about the maximum, as it would be in a hard-sphere fluid, and the position of the oscillations in the structure factor nearly match those found through diffraction experiments It was assumed, therefore, that if good results were to be obtained for any of the calculated systems, the Group IIA metals should give the best agreement Calculations backed this assertion Calculations for the beryllium, magnesium, and calcium systems are shown in this thesis. Agreement is very good with experiment

Detailed results are presented for the magnesium system. The density versus temperature curve, figure 8-5, shows excellent agreement with experiment The corresponding vapor pressure curve is shown in figure 8-6, the vapor fractions of monomer and dimer are examined in figure 8-7, and the Gibbs energy of each of the phases is given in figure 8-8 The dimer fraction in the magnesium system is very low, and corresponds closely with experimental dimer fractions The hard sphere fluid introduced just the right structure to the liquid system to ensure the best results for the Gibbs-Bogoljubov calculation.

Group IIIA Metals

Calculation were performed for the aluminum system. Liquid densities for the aluminum system are very high, and it is probable that the nearly-free electron approximation assumed in the empty-core pseudopotential model begins to break down as the mean free path for electrons in the liquid phase begins to shorten with rising number density. Nevertheless, it appears that the effects of a decreasingly accurate pseudopotential model and a fairly good representation of aluminum liquid structure yield results close to experimental values. Aluminum is a liquid at very high temperatures, so little experimental data exist that describes liquid density for the aluminum system, and the data that do exist disagree [64]. A representative curve calculated over a short temperature range is included on the temperature-density plot for aluminum.

In the temperature-liquid density plot for aluminum, shown in figure 8-9, it appears that the hard sphere fluid model begins to misrepresent the true structure of the liquid metal. If the a line is drawn through the liquid density as a function of melt temperature, the slope of the line is a qualitative representation of the coordination number of the liquid phase. Liquid melts with high coordination numbers, such as the hard sphere fluid, will show smaller slopes that those fluids with lower coordination numbers. The experimental density of aluminum has a higher slope than the Gibbs-Bogoljubov calculation, indicating that the coordination number of the aluminum fluid is less than the hard-sphere representation. The aluminum empty-core pseudopotential at the liquid melting temperature density explains this behavior. As shown and discussed in the previous chapter, the aluminum pair-potential is more repulsive at the minimum neighbor distance defined by the radial distribution function than it is at the global minimum. As atoms

attempt to move toward the position of the global minimum of the system, which coincides with the second potential minimum, the coordination number of the system drops Aluminum reflects this drop experimentally as shown by the slope of the liquid density versus temperature curve, but the calculations, because of the imposed structure of the hard sphere system, do not

The detailed pressure versus temperature plot for the aluminum system is given in figure 8-10 Vapor fraction of dimer and monomer versus temperature is given in figure 8-11, and the Gibbs energy versus temperature is shown in figure 8-12 Deviations are larger in all cases from experimental data than calculations for the group IA and IIA metals

Group IVA Metals

The structure factors of group IVA metals deviate substantially from hard-sphere behavior Shoulders appear on the high-angle (high-q) side of the static structure factor, indicating a loosely packed structure Loose packed arrangements, and the resulting low coordination numbers, suggest the existence of strong multi-body forces, due to the increasingly covalent nature of bonding in the metal It is expected, therefore, that the result for liquid density predicted for the group IVA systems by a assuming a hard-sphere structure will be too high, as will be the lowest variational bound to the Helmholtz free-energy Experimental results for the liquid density as a function of temperature are scarce, and do not agree well [64] All the experimental results though, show that the density of the liquid phase is consistently lower than calculation (see figure 8-13), and that the temperature dependence of the silicon liquid density can be qualitatively wrong, with too low a slope given for a linear fit of liquid density to temperature The inclusion of

dimerization in the model does improve the agreement of the melting temperature density with experiment

Crystalline silicon has four nearest neighbors, and as the solid melts transforms into a liquid, the coordination number rises, but not enough to justify the use of the hard sphere model Again, the pair potential shows a global minimum beyond the first peak of the radial distribution function, which energetically favors lower coordination numbers.

Though the density of the system is not well represented, it appears that the saturated pressure of the system as a function of temperature, shown in figure 8-14, is close to experiment, indicating that the pressure calculations are not as sensitive to liquid structure as are the density calculations. This suggests that the Gibbs-Bogoljubov calculations can still be used to give pressure estimates of a pure metal system, even though the liquid structure is not that of a hard-sphere fluid Calculation of the saturated pressure of the system depends strongly on the difference between the Gibbs energy of the system and the ionization energy of the system This difference does not vary as quickly as the derivative of energy as a function of liquid specific volume at saturated conditions If the ionization energy is fit properly the pressure should be calculated to exactly match experiment at the boiling temperature, with only slight deviation as the temperature moves away at the boiling temperature, this deviation defined more by the difference in energy between the liquid and vapor phase than the derivative of that energy The silicon Gibbs energy versus temperature curve is shown in figure 8-16

The results for the calculation of monomer and dimer fraction, shown in figure 8-14, reflect observations in the experimental system Silicon has a strong tendency to form

dimers in the vapor phase, and trimer species have also been observed in the vapor phase The dimer fraction is overestimated in the calculation results, since the experimental dimer contribution to pressure at the boiling temperature is 0 0417 atmospheres It is doubtful that the introduction of a model for silicon trimer will improve results until a better structure factor representation can be found for silicon

The silicon system has also been used to examine the effect of varying the experimental internal energy of the system at the melting temperature as an input parameter This study was conducted to show how a small difference in the experimental value for internal energy could have profound effect on calculated liquid density In figure 8-17, variations in the third decimal place of internal energy show as offsets in density in the first significant figure Variations in the pressure-temperature curve, figure 8-18, are less pronounced, but are still unacceptably large.

Summary of Results

Tables have been constructed that allow for quick calculation of the liquid metal densities and saturated pressures given a temperature for coexistence. Liquid density is listed as a linear function of temperature in Table 8-2, and experimental curve fits are also included in the table for comparison. Liquid density is not linear over the entire temperature range of calculation, so the curve fits are over limited temperature ranges starting at the metal melting temperature These temperature ranges are chosen to correspond to the range over which the experimental data curve fits are valid By comparing the slope and intercept of the curve fits it is apparent that the Gibbs-Bogoljubov calculation can be used as a representation of the group IA and IIA metals for

temperature ranges between the melting temperature and the boiling temperature. The curve fits also exaggerate the problem of representing the group IIIA and IVA metals using a simple hard-sphere representation.

Table 8-3 gives the Antoine pressure equation coefficients for all the simulated metals. A value of $r^2$ near one indicates that the heat of vaporization over the entire temperature range of calculation is nearly constant, and all the linear fits of $\log_{10}$(pressure in atmospheres) versus 1/temperature show a value for $r^2$ near unity. One check for the accuracy of the Antoine equation coefficients is an estimation of the boiling temperature, and this thermodynamic consistency check is included in table 8-4. Agreement is again very good, with the largest deviation in the calculation for the silicon system, as expected.

During the Gibbs-Bogoljubov calculation, two parameters are fitted to experimental data at the melting temperature; the first of these is the ionization energy, or the difference between the references for energy in the liquid phase and the vapor phase, and the second the first Fourier coefficient for the Helmholtz energy calculation. The fitted ionization energy is also included in table 8-4. The values calculated are very close to experimental values, with the largest deviation again in the group IIIA and IVA elements. The lightest elements, lithium and beryllium, also show large deviations from experimental data.

The fitting of the first Fourier component to experimental internal energy corrects for the very inadequacy that prevented the Gibbs ensemble method from determining phase coexistence for the empty-core pseudopotential. Changing the first Fourier component which is a linear term in ion core density, is a change in the slope of the linear

contribution in ion core density to the real-space formulation of the volume energy. This correction may change the empty-core pseudopotential so that it is not representative of the band-structure of a solid, but it is a better representation of the true Helmholtz energy of the liquid melt, since the band-structure of the continuously moving liquid phase really has no meaning.

Table 8-1 Parameters used for the Gibbs-Bogoljubov calculation. Where parameters are not available for the diatomic vapor species the vapor is assumed to be an ideal monatomic gas. The experimental internal energies are from J M Ziman [73]. Diatomic spectral data are from Huber and Herzberg [74]. Core radii are the values given by Hafner [41]. All other property data are taken from the CRC Handbook of Chemistry and Physics, 74th Edition [64].

| | Molecular Weight | Charge | Core Radius | Melting temperature Internal Energy | Melting Temperature | Boiling Temperature | Diatomic Ground State Energy | Diatomic Bond Length | Diatomic Vibrational Frequency |
|---|---|---|---|---|---|---|---|---|---|
| | | (a.u) | (a.u.) | (Hartrees) | (K) | (K) | (eV) | ($10^{-10}$ m) | ($cm^{-1}$) |
| Li | 6 939 | 1 0 | 1 31 | -0 1362 | 453 0 | 1615 | 1 046 | 2 673 | 351 43 |
| Na | 22 98 | 1 0 | 1 70 | -0 1144 | 373 0 | 1156 | 0 720 | 3 079 | 159 124 |
| K | 39 10 | 1 0 | 2 12 | -0 0954 | 336 4 | 1033 | 0 514 | 3 900 | 92.3 |
| Rb | 85 47 | 1 0 | 2 47 | -0 0886 | 312.6 | 961 | - | - | - |
| Cs | 132 91 | 1 0 | 2 72 | -0 0836 | 301 6 | 944 | 0 394 | 4 47 | 42 022 |
| Be | 9 0122 | 2 0 | 0 76 | -0 6368 | 1560 0 | 2745 | - | - | - |
| Mg | 24 31 | 2 0 | 1 31 | -0 449 | 922 | 1363 | 0 0501 | 3 891 | 51 12 |
| Ca | 40 08 | 2 0 | 1 73 | -0 368 | 1112 | 1757 | 0 12 | 4 2773 | 64 92 |
| Al | 26 98 | 3 0 | 1 11 | -1 044 | 933 3 | 2793 | 1 5 | 2 295 | 378 0 |
| Si | 28 09 | 4 0 | 1 21 | -1 745 | 1685 | 3540 | 3 21 | 2 246 | 510 98 |

Table 8-2 Regression fits for liquid density Density is given in g/cm$^3$ Experimental curves are from the CRC Handbook of Chemistry and Physics, 74th edition [64]

| Element | Liquid Density (g/cm$^3$) | $r^2$ (corrected) | Experimental | Range |
|---|---|---|---|---|
| Li | 0 5137 - 9 24x10$^{-5}$ (T-453 0) | 0 9931 | 0 515 - 1 01x10$^{-4}$ (T-453 0) | 1600 K |
| Na | 0 9309 - 2 304x10$^{-4}$ (T-373 0) | 0 9966 | 0 927 - 2.24x10$^{-4}$ (T-373 0) | 600 K |
| K | 0 8256 - 2.717x10$^{-4}$ (T-373 0) | 0 9872 | 0 828 - 2 32x10$^{-4}$ (T-373 0) | 600 K |
| Rb | 1 4501 - 4 640x10$^{-4}$ (T-312 6) | 0 9925 | 1 463 - 4 51x10$^{-4}$ (T-312.6) | 600 K |
| Cs | 1 8630 - 6 051x10$^{-4}$ (T-301 6) | 0 9993 | 1 851 - 5 71x10$^{-4}$ (T-301 6) | 750 K |
| Be | 1 7360 - 1 249x10$^{-4}$ (T-1560) | 0 9750 | 1 690 - 1 1x10$^{-4}$ (T-1560) | 1700 K |
| Mg | 1 5784 - 2 217x10$^{-4}$ (T-923 0) | 0 9953 | 1 584 - 2.34x10$^{-4}$ (T-923 0) | 900 K |
| Ca | 1 3644 - 2.332x10$^{-4}$ (T-1112) | 0 9930 | 1 367 - 2 21x10$^{-4}$(T-1112) | 1200 K |
| Al | 2.3745 - 1 905x10$^{-4}$ (T-938 0) | 0 9967 | 2 368 - 2 65x10$^{-4}$ (T-938 0) | 900 K |
| Si | 2.5422 - 9 657x10$^{-5}$ (T-1683) | 0 9989 | 2 52 - 3 51x10$^{-4}$ (T-1683) | 1650 K |

Table 8-3 Regression fits for saturated vapor pressure described by the Antoine equation, given by $\log_{10}(P) = A + B/T$, where the pressure is in atmospheres, and the temperature in K.

| Element | A | B | Corrected r squared |
|---|---|---|---|
| Li | 4 7763 | -7698 5 | 0 9999 |
| Na | 4 5058 | -5240 0 | 0 9999 |
| K | 3 9715 | -4184 3 | 0 9940 |
| Rb | 3 7407 | -3666 2 | 0 9985 |
| Cs | 3 9474 | -3758 0 | 0 9999 |
| Be | 5 2202 | -14224 | 0 9984 |
| Mg | 4 8243 | -6660 1 | 0 9994 |
| Ca | 4 2010 | -7428 7 | 0 9989 |
| Al | 5 1489 | -13935 | 0 9999 |
| Si | 6 4501 | -23384 | 0 9998 |

Table 8-4 Ionization energy values, calculated to fit experimental data at the boiling temperature. Also included are the predicted melting temperatures from the Antoine equation curve fits listed in table 8-3. Experimental curves are from the CRC Handbook of Chemistry and Physics, 74th edition [64]

| Element | Experimental Ionization Energy (eV) | Calculated Ionization Energy (eV) | Experimental Boiling temperature (K) | Calculated Boiling temperature (K) |
|---|---|---|---|---|
| Li | 5 392 | 5 945 | 1615 | 1611 |
| Na | 5 139 | 5 235 | 1156 | 1163 |
| K | 4 341 | 4 410 | 1032 | 1053 |
| Rb | 4 177 | 4 095 | 961 | 980 |
| Cs | 3 894 | 3 824 | 944 | 952 |
| Be | 27 533 | 32 06 | 2745 | 2724 |
| Mg | 22 681 | 23 22 | 1363 | 1380 |
| Ca | 17 984 | 18 62 | 1757 | 1768 |
| Al | 53 261 | 54 48 | 2793 | 2718 |
| Si | 103.129 | 90 91 | 3540 | 3625 |

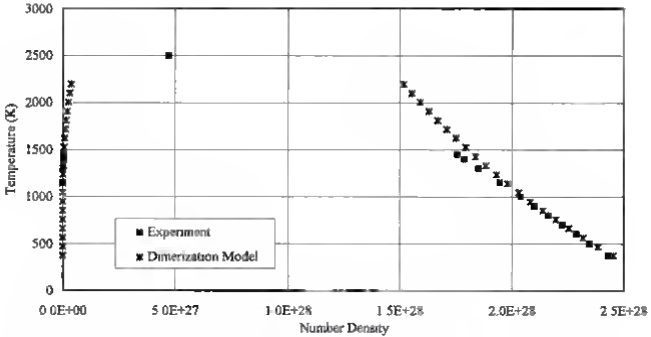


Figure 8-1 Temperature (K) versus number density (atoms/m$^3$) phase diagram for sodium. Experimental data are from N B Vargaftik [61]

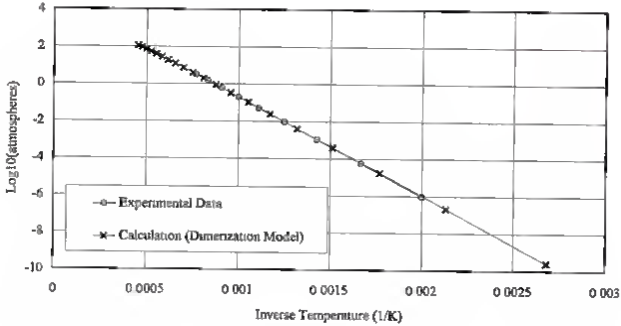


Figure 8-2 $Log_{10}$ (pressure in atmospheres) versus inverse temperature ($K^{-1}$) for sodium. Experimental data are from N B Vargaftik [61]

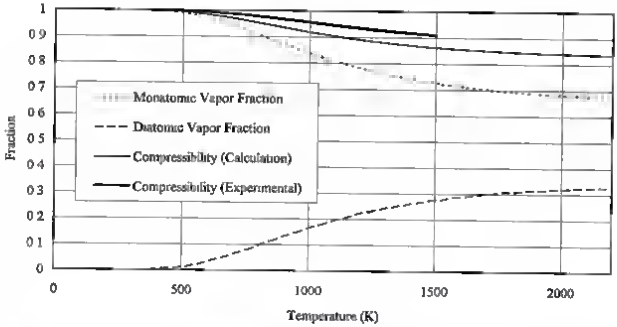


Figure 8-3 Vapor fraction of monatomic and diatomic species for sodium plotted versus temperature in Kelvin. Also included is the experimental and calculated compressibility $Z$ of the vapor phase. Selected values are from Hultgren *et al.* [65].

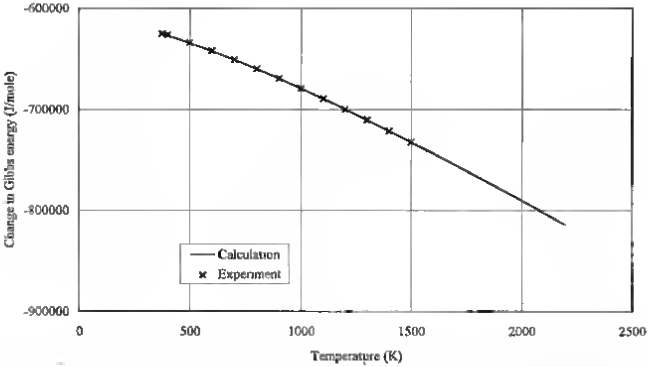


Figure 8-4 Calculated upper bound for the Gibbs energy per atom (J) versus temperature (K) for sodium. The Gibbs energy at the melting temperature is chosen as the reference energy. Selected values are from Hultgren *et al.* [65]

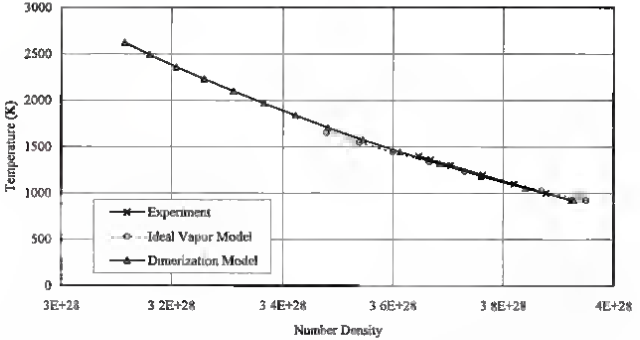


Figure 8-5: Temperature (K) versus number density (atoms/$m^3$) for magnesium. The experimental curve is from the CRC Handbook of Chemistry and Physics [64]

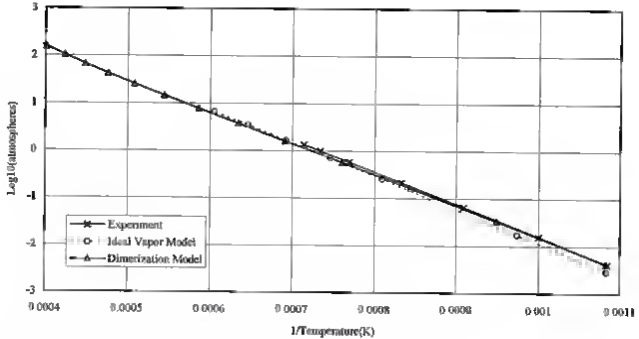


Figure 8-6 $Log_{10}$ (pressure in atmospheres) versus inverse temperature ($K^{-1}$) for magnesium. Selected values are from Hultgren *et al* [65]

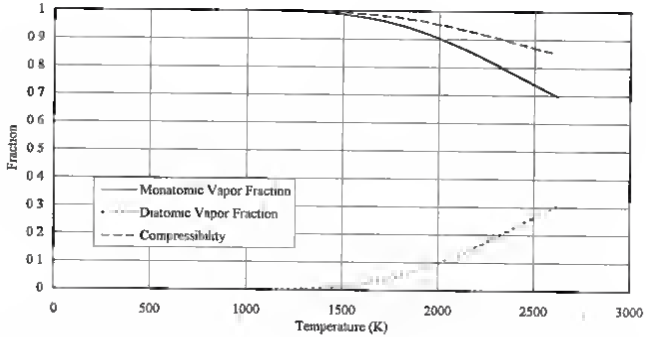


Figure 8-7 Vapor fractions of species versus temperature for magnesium Also shown is the compressibility Z for the system.

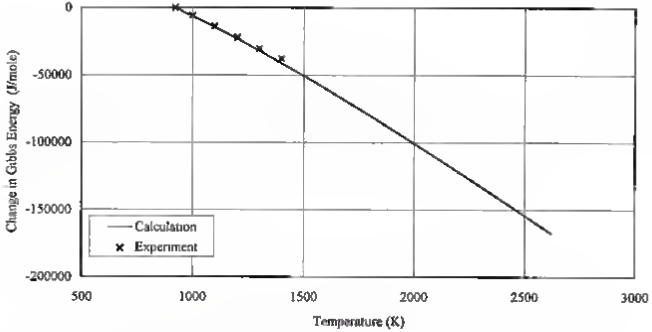


Figure 8-8 Gibbs energy (J) versus temperature (K) for magnesium The Gibbs energy at the melting temperature is chosen as the reference energy Selected values are from Hultgren *et al* [65]

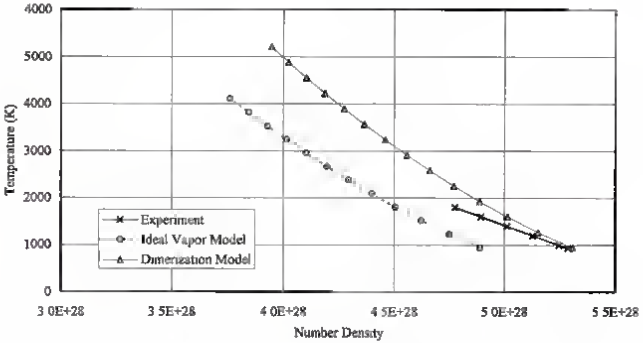


Figure 8-9 Temperature (K) versus liquid number density (atoms/m$^3$) for aluminum. The experimental curve is from the CRC Handbook of Chemistry and Physics [64]

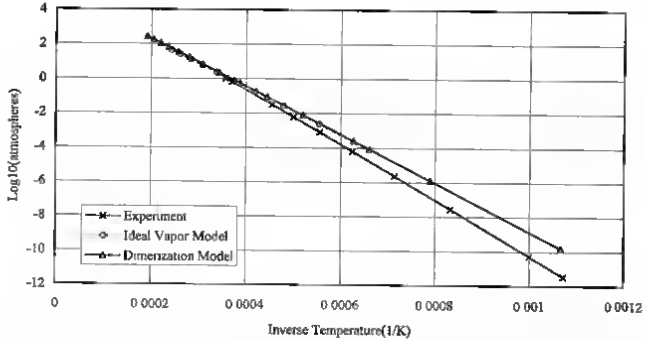


Figure 8-10 $Log_{10}$ (pressure in atmospheres) versus inverse temperature ($K^{-1}$) for aluminum. Selected values are from Hultgren *et al.* [65]

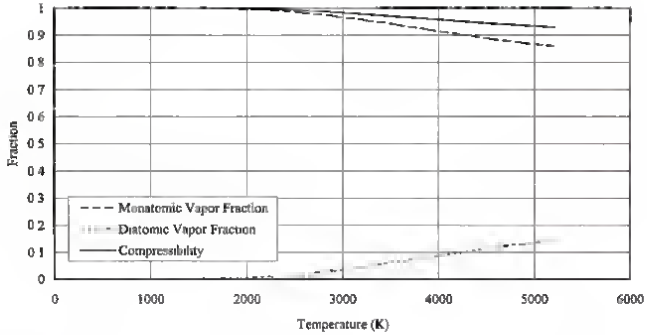


Figure 8-11 Calculated fraction of atomic species versus temperature (K) for aluminum. The calculated compressibility $Z$ is also shown.

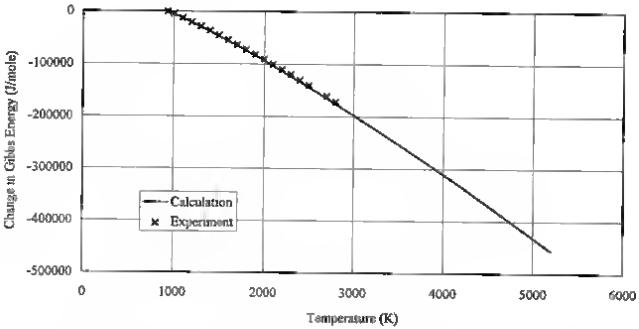


Figure 8-12 Calculated Gibbs energy per atom (J) versus temperature (K) for aluminum. The Gibbs energy at the melting temperature is chosen as the reference energy. Selected values are from Hultgren *et al.* [65]

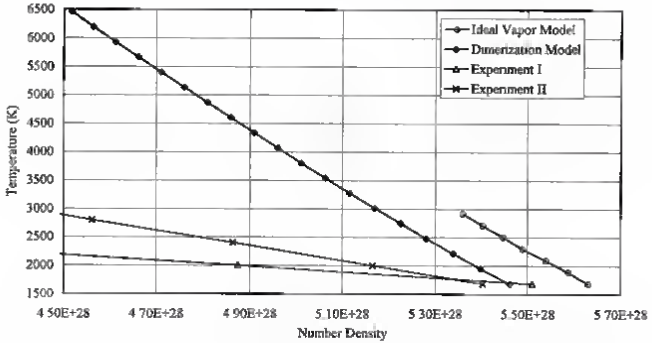


Figure 8-13 Temperature (K) versus liquid phase density (atoms/m$^3$) for silicon. Note the difference between the experimental curve fits. The experimental curves (Experiment I and Experiment II) are from the CRC Handbook of Chemistry and Physics [64]

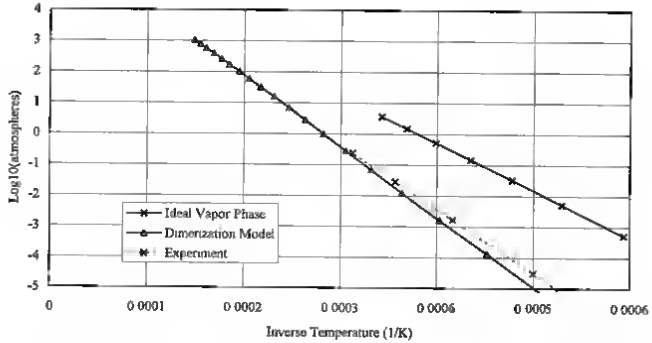


Figure 8-14 $Log_{10}$ (pressure in atmospheres ) versus inverse temperature for silicon. Selected values are from Hultgren *et al.* [65]

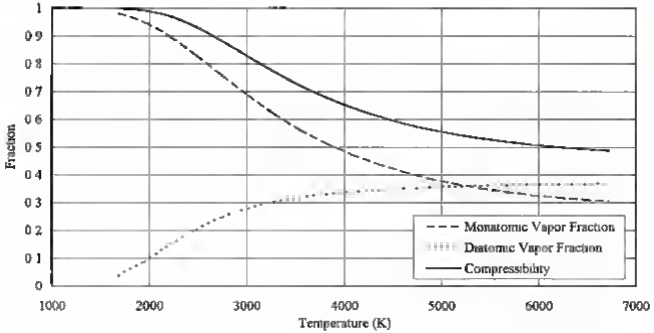


Figure 8-15 Calculated vapor fraction of species versus temperature (K) for silicon. The compressibility *Z* for the vapor phase is also shown

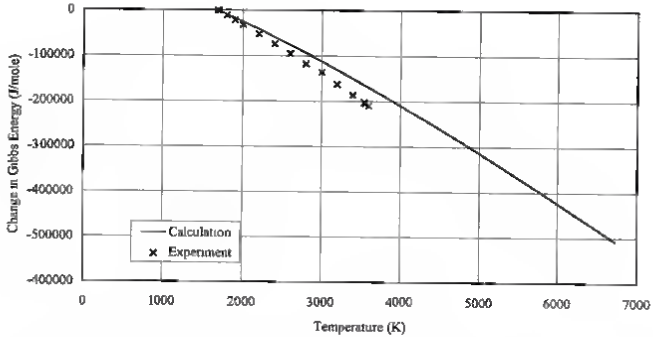


Figure 8-16 Calculated Gibbs energy per atom (J) versus temperature (K) for silicon The Gibbs energy at the melting temperature is chosen as the reference energy Selected values are from Hultgren *et al* [65]

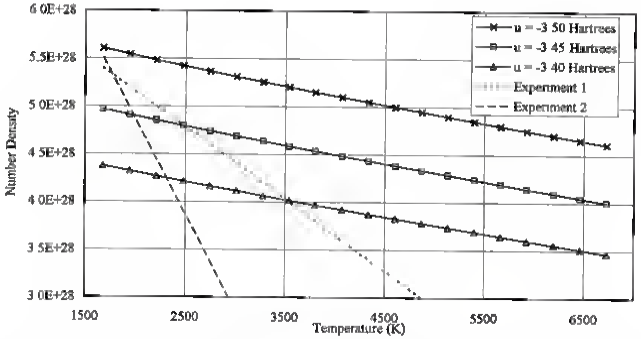


Figure 8-17 Calculated number density (atoms/m$^3$) versus temperature (K) for silicon. It appears that experimental error in the measurement of the internal energy of the silicon system at its melting temperature (internal energy u in Hartrees) can have a profound effect on the calculated value for liquid density

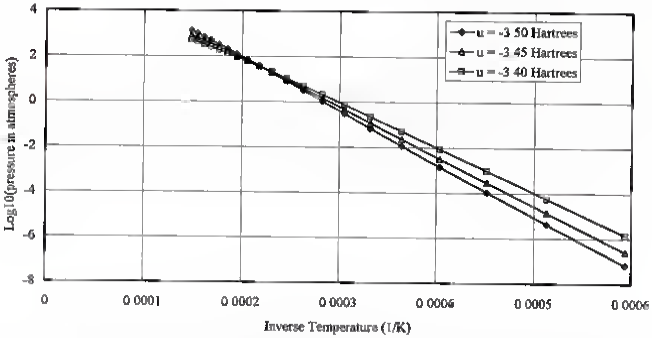


Figure 8-18 $Log_{10}$(pressure in atmospheres) versus inverse temperature ($K^{-1}$) for the saturated sodium system for several values of internal energy. Higher internal energies raise the slope of the vapor pressure curve, indicating a rise in the magnitude of the heat of vaporization for the system. The Experiment 1 and Experiment 2 curves are from the *CRC Handbook of Chemistry and Physics* [64]

## CHAPTER 9
## FUTURE CONSIDERATIONS

Since the Gibbs-Bogoljubov calculation is the more successful of the two methods implemented for describing actual systems, this method will be expanded through the modification of structure factors and potential energy functions to cover more metal and non-metal systems. The Gibbs-Bogoljubov calculation can be extended to binary mixtures, as a theory for the description of the binary alloy hard sphere structure factor already exists. Implementing the binary system structure factors will allow calculation of both liquid-vapor and liquid-liquid equilibrium curves. Finally, Monte Carlo and molecular dynamics simulation methods will allow rigorous fundamental study of potential energy functions as representations of real systems.

The purpose of this dissertation is to assess methods currently available to calculate properties of pure metal systems in liquid-vapor phase equilibrium. So far, results using the Gibbs-Bogoljubov inequality are accurate only for group IA and IIA metals, which leaves eighty-eight percent of the periodic table without a suitable model for liquid and vapor phase energy and structure properties. As shown in this thesis, the major weakness in representing a group IIIA and IVA liquid metals lies in choosing a suitable structure factor for the liquid metal system. Finding an adequate structure factor is also a problem when describing the transition metals, rare-earth elements, and non-metal melts,

but in the case of these elements, little work has been done to describe the potential energy functions of the system. Before calculations of the thermodynamic properties of alloys and mixtures of elements can be performed, the structure and potential energy of interaction for pure systems should be understood.

Alternate liquid structure descriptions are necessary to describe the Group IIIA and IVA liquid systems. The liquid phase of these metals retains some of the strong covalent bonding present in the solid, which reduces the coordination number of the melts. More complicated descriptions of liquid structure are available for reference fluids that increase the number of variational parameters for the Gibbs-Bogoljubov method. Properly chosen reference systems decrease the difference between the calculated upper bound to the Helmholtz energy and the Helmholtz energy of the actual metal system. One example of a liquid phase reference fluid that increases the number of variational parameters, and thus the possibilities for a better energy estimate, is the binary system of two hard spheres with different diameters. The introduction of a second hard sphere with a different diameter than the first allows more degrees of freedom in a Gibbs-Bogoljubov calculation. More degrees of freedom increase the possibility of calculating a more accurate upper bound to the Helmholtz energy for liquids with coordination numbers lower than a single component hard sphere fluid. Two additional variational parameters are introduced, one representing the concentrations of each type of sphere in the liquid melt, and a second representing the diameter of an introduced sphere representing the clustering of atoms.

If simple models for clustering do not work, then molecular dynamics simulation will be used to calculate structure factors and reference properties for more complex

systems. Structure factors with shoulders and peaks such as those obtained from neutron diffraction experiments on molten silicon, are probably more realistically represented by a mixture of atomic clusters than by a fluid of hard spheres. For instance, rigid rotors or dumbbells consisting of hard sphere monomers are better models of dimerization in the liquid phase than two independent hard spheres. Introducing four atoms in a pyramid will exclude some nearest neighbors, and even the simple dumbbell arrangement will introduce an order in the fluid not introduced by spheres. The exclusion of nearest neighbors due to geometric considerations will lower the value of liquid coordination number, a goal of any attempt to model the silicon melt.

New molecular dynamics codes will show whether simple arrangements of atoms will change the structure factor in a way representative of liquid melts with covalent character. The new parameters, which will correspond to the concentrations of each type of geometric cluster introduced into the melt, will be used as variational parameters in a Gibbs-Bogoljubov calculation. These calculations will take large amounts of computer time, since a simulation is performed to calculate each structure factor for the fluid, but the new representation of the liquid phase is worth studying to see if restrictive atomic cluster arrangements produce more realistic average energy calculations.

The Gibbs-Bogoljubov inequality itself will provide some valuable information on liquid energy properties in thermodynamically unstable regions where experiment is not possible. One possible application is in the estimation of supercooled liquid properties, the quantities necessary for the calculation of metastable regions in metal phase diagrams. Calculation of superheated and supercritical liquid properties is also possible if accurate

structure and potential energy functions can be chosen to represent all thermodynamic regimes

Many transition metals have structures resembling a hard sphere fluid, so their structure can be described with the techniques described in this dissertation However, the form of the potential energy function will be different , since d electrons will enter the conduction band in the liquid metal melt Some attempts at extending the empty-core pseudopotential to metals with valence electron contributions from d-orbitals have already been modestly successful [75] These potentials are in a form easily applied to the Gibbs-Bogoljubov calculation. No such attempts at parameterizing the empty-core pseudopotential have been made for higher angular momentum orbitals

The empty-core pseudopotential seems to represent the concentration dependence of the electron gas adequately in a confined system, but allowances have to be made to correct the density dependence of the Helmholtz energy at the melting temperature It is hoped that further advances in liquid potential theory will allow the calculation of saturated properties with little or no reference to quantities obtained experimentally, and that experiment will only be used as a check for the calculated properties Macroscopic behavior such as the metal-insulator transition should be predicted by the potential energy function before thermodynamic properties near the metal system's critical point can be calculated

The hard sphere structure factor for binary liquids is well known [76], and this will allow the immediate calculation of liquid-vapor coexistence curves for simple metal mixtures of group IA and IIA elements In addition, binary melts introduce another

phenomenon that can be studied with the Gibbs-Bogoljubov method Some mixtures have a miscibility gap, or a region in the temperature-composition phase diagram where two liquids of different composition coexist It is not known whether the hard-sphere representation with the empty-core pseudopotential model will show this miscibility gap for suitable liquid mixtures, but attempting this calculation will be a substantial test of the Gibbs-Bogoljubov method

The construction of a flexible Gibbs ensemble method code will allow for more fundamental studies in the future. For example, there is theoretical interest in how certain potential energy rules contribute to critical exponents of vapor liquid systems. These potential energy rules can be examined in detail by changing the input to the Gibbs ensemble simulation The Gibbs ensemble system will also be able to test a potential energy function for its ability to accurately represent a real system with free boundaries So far, the applications of the Gibbs ensemble method are limited by the construction of accurate potential energy representations of the metal system Only the simplest of potential energy functions can be assessed with this method

Potential energy function mixing rules are often arbitrary, and their contributions to the entropy of a system are usually not known before the rules are implemented. Systematic studies of mixing rules have not been attempted, since neither the computer time nor the code has existed until recently The written Gibbs ensemble code will allow for examination of the effects of mixing rules on saturated system properties, and thus allow a more fundamental understanding of interatomic potential effects in binary mixtures. It is also expected that the liquid-liquid miscibility gap can again be examined in

the context of an atomistic simulation method, within a quantitative framework. Studying the basic Lennard-Jones interaction will allow construction of a generalized binary and ternary phase diagram for the simple model potentials.

Various strategies have been outlined to further the calculation of saturated properties for pure elements and mixtures of these elements. Foremost in these strategies is implementing a program to understand more about liquid structure, or at least refine the current models to adequately describe the structure of liquids. Second, new potential energy functions will be analyzed, and potential energy models will be found that will minimize the need for parameters derived from experiment. Binary systems will be studied with the Gibbs-Bogoljubov method, breaking ground for calculation of ternary and quaternary liquid-vapor and liquid-liquid phase diagrams. The Gibbs ensemble method will allow for fundamental investigation of the contributions of various potential energy terms to phase diagram structure, which will eventually allow for the construction of an adequate equation of state for liquid metal systems.

# CHAPTER 10
# SUMMARY AND CONCLUSIONS

Two methods of calculating liquid-vapor phase coexistence curves for pure liquid metals have been assessed. The Gibbs ensemble method has shown through its generality that the empty-core pseudopotential is not an adequate representation for all nearly free electron metals for the purpose of calculating saturated conditions. Calculation with the Gibbs-Bogoljubov inequality proved more successful, by the imposition of liquid structure on the liquid metal system some of the weaknesses of the empty-core pseudopotential representation were overcome. Results from the Gibbs-Bogoljubov inequality compared favorably with experiment for group IA, IIA, and IIIA metals. Ambiguities in experimental data prevented the assessment of the calculation for Group IVA, though it appears that reasonable engineering estimates to saturated pressure properties were obtained using this simple model. Density calculations for the group IVA metals deviated substantially from experiment at temperatures away from the melting temperature.

The Gibbs Ensemble Monte Carlo method has shown that more realistic representations of the potential energy functions of liquid metal melts are needed before calculations can be performed for all pure nearly free electron metal systems. Promising simulation results have been obtained for the aluminum system, which has a pair potential with a global minimum at a distance greater than the minimum neighbor distance given by

the radial distribution function of the system The liquid phase of the aluminum system shows stable long range order, and the simulation stabilizes at a particular liquid density, but this density is not near the experimental liquid density The simulation of sodium, which has a pair potential with a global minimum corresponding to the distance to the first peak of the radial distribution function does not give reasonable results, it is energetically favorable for the liquid metal system to drop to unrealistically low densities, since the magnitude of the restoring volume energy cannot overcome energy contributions from the rapid drop in the pair potential minimum as volume decreases Radial distribution functions calculated during sodium simulation show clustering of atoms in the liquid phase, and snapshots of configurations taken during the sodium simulation show the same behavior

The Gibbs-Bogolyubov methodology added a compensating effect that overcame the shortcoming of the empty-core pseudopotential. The pair-potential representation of the empty-core pseudopotential is known to be inaccurate at short distances from the atomic core centers, in the region near the first minimum of potential The form of the pair-potential in this region is highly dependent on the model chosen to represent the dielectric function of an electron gas By coupling the hard-sphere structure factor with the empty-core pseudopotential a portion of the short-range contribution of the pair-potential to the Helmholtz free-energy of the system is truncated eliminating some of the ambiguity introduced by the modeling the liquid phase with the simplistic empty-core pseudopotential model coupled with the Itoh-Utsumi approximation to the dielectric function Once structure is imposed on the liquid system, estimates to the Helmholtz free-

energy of the system become more accurate The unposed structure of the Gibbs-Bogoljubov method also overcomes problems in the calculated magnitude of the volume dependent energy in the real space formulation of the empty core pseudopotential The magnitude of the volume energy is not large enough to accurately model liquid density using the Gibbs ensemble method, but the assumption of liquid structure circumvents this problem by defining the volume and the distribution of particles within that volume.

Modeling the vapor phase using the Gibbs Ensemble also presented an obstacle that was not overcome in this dissertation Though a simple ideal gas model was chosen for the vapor phase, a parameter was needed to describe the ionization energy for the metal system, and the results of the simulations proved to be dependent on this parameter Dimerization was not simulated, since the algorithms had no contingencies for reactive systems, nor were potentials to simulate monomer dimer and dimer-dimer interactions readily available for calculating the potential energies of the vapor phase

Again, these problems were overcome in the application the Gibbs-Bogoljubov method The ionization energy of the empty-core pseudopotential system could be calculated from melting temperature data, and the approximated ionization energies were in good agreement with experimental data A vapor phase consisting of monomers and dimers was modeled using an associated solution model based on the canonical ensemble partition function, and when compared to calculations performed assuming an monatomic ideal gas vapor phase the associated solution model produced results in better agreement with experimental data

Conditions for phase equilibria calculated using the Gibbs-Bogoljubov approach appeared to be very close to experiment for temperatures from the melting temperature to temperatures short of the critical points of the pure metal systems, suggesting that this method can be used as a predictive tool for calculating saturated properties in regimes where experiment has yielded poor results. It is clear, however, that the current methods for estimating the Gibbs free energies of both the liquid and vapor systems have shortcomings as the critical temperature of the system is approached. The success of hard-sphere theory in representing liquid structure also suggests that the same theory should be used as a first approximation to binary liquid structure. Coupling the associated solution model with the appropriate description of the binary liquid metal Helmholtz energy should allow for the calculation of saturated conditions over binary melts of nearly free-electron metals.

Though not yet predictive, the Gibbs ensemble method gave qualitative insights that will be helpful in developing an atomistic simulation method for metal systems. In a pure form, the Gibbs ensemble method will not depend on experimental parameters, but will depend only on the supplied potentials of interaction for the system. The method has not yet reached this state of maturity. For the Gibbs Ensemble Monte Carlo technique to be a useful tool, dimerization in the gas phase must be taken into account. Probabilities for state to state transition for reactive systems based on the chemical potential of the species of the constituents of the vapor phase must be defined. More fundamental study will be needed to determine the conditions at which the metal-insulator transition in liquid metal

systems takes place before an attempt can be made to simulate systems near their critical point

Three approaches can be taken to correcting for the clustering characteristic in the liquid phase of the Gibbs-Ensemble method. A mean potential for the liquid phase based on liquid theory rather than the solid-state theory used to describe the empty-core pseudopotential can be developed. Progress in the development of liquid state potential energy functions is slow, and no real alternatives for perturbation theory models yet exist. If this approach does not work, a semi-empirical expression relating volume energy to density will probably allow the calculation of saturated metal properties, but the need for experimental parameters to calculate the corrections to the pseudopotential volume energy will reduce the predictive capability of this approach. The third approach is to continue using the empty-core pseudopotential model, but with a modification to the algorithm. The clustering observed in the sodium simulations is not exactly what the empty-core pseudopotential predicts, but it is the effect that should be observed in a simulation that assumes a homogeneous electron density in the liquid phase. Adjusting the interatomic pair-potential to account for the local density of the electron gas between interacting cores should allow clusters to break apart, and more accurate statistical sampling will take place.

It has been shown that two different methods are capable of calculating phase equilibria for real systems, provided the correct phenomenological models are introduced into the simulation systems. It is also evident that the theory of nearly-free electron metals has advanced enough to allow the estimation of saturated system properties in a predictive fashion. The toolbox is not nearly complete; most of the interesting semiconducting or

superconducting compounds have melts consisting of not only the nearly free-electron metals, but also transition metals and nonmetals It will be necessary to examine each class of material in an elementary fashion, determining potential energy functions and radial distribution functions that adequately describe the saturated properties of these systems before a comprehensive plan to generalize liquid-vapor phase calculations can begin

## APPENDIX A
## THE DIRECT CORRELATION FUNCTION OF A HARD-SPHERE FLUID

The direct correlation function for a one-component hard sphere fluid is often reported in literature in its integral [53,41], instead of its more convenient analytic form The direct correlation function for a hard-sphere fluid is

$$c(q\sigma) = -4\pi\sigma^3 \int_0^1 ds\, s^2 \frac{\sin(sq\sigma)}{sq\sigma}\left(\alpha + \beta\, s + \gamma\, s^2\right) \tag{A-1}$$

where $\alpha$, $\beta$, and $\gamma$ are functions of the packing density parameter $\eta$ given by

$$\eta = \frac{\pi n\sigma^3}{6}, \tag{A-2}$$

$$\alpha = \frac{(1+2\eta^2)}{(1-\eta)^4}, \tag{A-3}$$

$$\beta = \frac{-6\eta\left(1+\frac{\eta}{2}\right)^2}{(1-\eta)^4}, \tag{A-4}$$

and

$$\gamma = \frac{\eta(1+2\eta)^2}{2(1-\eta)^4}, \tag{A-5}$$

with $n$ representing the hard sphere liquid density. Evaluation of the direct correlation function integral yields

$$c(u) = \sigma^3\left\{\frac{\alpha}{u^2}\left(\frac{\sin u}{u} - \cos u\right) + \frac{\beta}{u^2}\left(\frac{2\sin u}{u} - \cos u + \frac{2\cos u - 1}{u^2}\right)\right. \\ \left. + \frac{\gamma}{u^2}\left(\sin u\left(\frac{4}{u} - \frac{24}{u^3}\right) + \cos u\left(\frac{12}{u} - 1\right)\right) + \frac{24(1-\cos u)}{u^4}\right\} \tag{A-6}$$

where $u = q\,\sigma$

## APPENDIX B
## APPROXIMATIONS TO THE EMPTY-CORE PSEUDOPOTENTIAL

The numerical calculation of the pair-potential integral for the empty-core pseudopotential proves to be the time limiting step in the Gibbs ensemble simulation of metallic systems. Numerical methods for dealing with oscillatory integrands are slow, especially when these integrands are spread over an infinite range. Both the pair-potential and energy of interaction between ion cores and the electron gas have integrands with both these characteristics. Even slower is the numerical evaluation of the long-range potential of the system, which can require several thousand evaluations of the pair potential integral. Each change in system density requires the calculation of a new pair-potential, thus each volume change or particle creation/destruction attempted is a computationally expensive proposition. Fortunately, several approximate methods exist to shorten the time necessary to calculate new pair-potentials, and these methods were employed not only to calculate the pair potential itself, but to estimate the long range corrections for the system.

The energy of interaction between electron gas and ion cores was calculated numerically over a range of liquid densities before simulation took place. Placing the pre-calculated values in a lookup table allowed the simulation to advance without the time-consuming step of calculating this interaction for every volume change. The pair-potentials

were treated in a different manner A rational polynomial was developed to approximate the static polarizability and the Ichimaru-Utsumi form of the local field correction for the dielectric function of an electron gas These two expressions allowed for the construction of a rational polynomial for the dielectric function The rational polynomial could then be substituted into the pair-potential integral and an integration in the complex plane yielded an analytic expression consisting of trigonometric and exponential functions The notation for each system has changed slightly in this appendix to match literature.

The pair potential for an empty-core pseudopotential model is

$$v(r,\rho)=\frac{2Z}{r}\left\{1-\frac{2}{\pi}\int_0^{\infty}\left(1-\frac{1}{\varepsilon(q,\rho)}\right)\cos^2(qR_c)\frac{\sin(qr)}{q}dq\right\} \tag{B-7}$$

where $\rho$ is the liquid number density The dielectric function for this potential is

$$\varepsilon(q,\rho)=1+\left(\frac{k_{TF}}{q}\right)^2\left(\frac{f_0\left(\frac{q}{2k_f}\right)}{1-G\left(\frac{q}{2k_f}\right)f_0\left(\frac{q}{2k_f}\right)}\right) \tag{B-8}$$

with $G$ the local field correction, and $k_{TF}$ the Thomas-Fermi wavevector given by

$$k_{TF}=\left(\frac{4k_F}{\pi}\right)^{\frac{1}{2}} \tag{B-9}$$

Previous results in literature [77] gave the rational function approximation to the Lindhard static polarizability $f_0(x)$ of the electron gas

$$f_0(x)=\frac{1+bx^2+\left(\frac{61}{315}+\frac{4b}{15}-\frac{3c}{35}\right)x^4+\left(\frac{16}{63}+\frac{b}{3}-\frac{8c}{35}\right)x^6+cx^8}{1+\left(b+\frac{1}{3}\right)x^2+\left(\frac{13}{35}+\frac{3b}{5}-\frac{3c}{35}\right)x^4+\left(\frac{3}{7}+\frac{3b}{5}-\frac{9c}{35}\right)x^6+\left(\frac{16}{21}+b-\frac{9c}{7}\right)x^8+3cx^{10}} \tag{B-10}$$

with $x = q/2k_f$ and the constants b = -0 5395 and c = 0 3333 chosen to minimize the r m.s. error between the rational polynomial and the actual Lindhard polarizability A rational polynomial approximation to the Ichimaru-Utsumi local field correction was created, and this approximation was combined with the rational function approximating static polarizability to give the a new rational function for the dielectric function

$$\varepsilon^{-1}(x) = \frac{\sum_{n=0}^{11} a_n x^{2n}}{\sum_{n=0}^{11} b_n x^{2n}} \tag{B-11}$$

Rational coefficients could be expressed in terms of the five constants A, B C D and E defined by

$$\begin{aligned} A &= 16(0.029) \\ B &= 4\left(\frac{9}{16}\gamma_0(r_s) - \frac{3}{64}[1-g(0)] - \frac{4}{15}A\right) \\ C &= -\frac{3}{4}\gamma_0(r_s) + \frac{9}{16}[1-g(0)] - \frac{4}{5}A \\ D &= B + \frac{2}{3}A \\ E &= \frac{1}{\pi k_F} \end{aligned} \tag{B-12}$$

where $\gamma_0$ and $g(0)$ are as given in the original Ichimaru Utsumi expression The coefficients to the numerator of equation (B-11) are given in table B-1 the coefficients for the denominator are given in table B-2 The coefficients are given in rational form to preserve accuracy

The pair potential is found by first finding the poles of the inverse dielectric function, which amounts to finding the roots of the denominator that lie in the upper half

of the complex plane After the eleven poles $q_n^2$ are found, the static polarizability can be rewritten

$$\varepsilon^{-1}(q,\rho)=\sum_{n=1}^{11}D_n\frac{q^2}{\left(q^2-q_n^2\right)} \tag{B-13}$$

with the weights $D_n$ found using a Heaviside expansion. The weights and poles of the dielectric function may now be incorporated into the solution of the integral representing the real space formulation of the empty-core pseudopotential, to give the result for the pair-potential of the system

$$v(r,\rho)=\left(\frac{2Z^2}{R}\right)\sum_{n=1}^{11}D_n v_{ps}^2(q_n)e^{iq_n r} \tag{B-14}$$

where

$$\hat{v}_{ps}(q)=\cos(qR_c) \tag{B-15}$$

is the pseudopotential matrix element characteristic of the empty-core pseudopotential. Note that the poles used within this formula are the square roots of the roots of the denominator of the dielectric function again, the valid root is the root that lies in the upper portion of the complex plane If the poles and weights calculated for this series are complex, they exist in complex conjugate pairs Real roots for the inverse static polarizability contribute an exponentially decaying real term to the pair potential The imaginary contributions to the real space potential all sum to zero The calculation of a pair potential is reduced from the numerical solution of a slowly converging integral to an easily evaluated series of trigonometric functions

From representation (B-14) of the potential, an approximation to the long-range correction for the empty-core pseudopotential can be derived. The contribution due to each root takes a different form depending on whether the given root came from a real pole, or a complex conjugate pair of poles. First, for the complex conjugate pair of poles, the weights will look like

$$D_{i1} = x_{i1} + i\,y_{i1} \tag{B-16}$$

and the square roots of the poles will be written in the form

$$q_{i2}^{\frac{1}{2}} = x_{i2} + iy_{i2} \tag{B-17}$$

where $x_{i1}$, $x_{i2}$, $y_{i1}$, and $y_{i2}$ are positive. Remember that the poles themselves are complex conjugates, so the square roots of the poles that lie in the upper half of the complex plane differ by sign in their real part only. The total long range correction to for the system is comprised of two sums, one sum corresponding to the contributions of each complex conjugate pair of poles, and the other the contribution of the negative real pole, of which there will always be one. The total long-range potential for a system in atomic units is then

$$V_{lrc}(r_{cut}) = 8\pi Z^2 \left( \sum_{\substack{\text{complex} \\ \text{conjugate} \\ \text{roots}}} h_i^{\text{complex}} + \sum_{\substack{\text{real} \\ \text{negative} \\ \text{roots}}} h_i^{\text{real}} \right) \tag{B-18}$$

Each pair of complex conjugate poles contributes one term to the summation, and this term is given by

$$h_i^{\text{complex}} = g_{i1} + g_{i2} + g_{i3} \tag{B-19}$$

where

$$g_{i1} = 2\cos^2(r_c x_{i2})\cosh^2(r_c y_{i2})\left(f_{i1}x_{i1} - f_{i2}y_{i1}\right), \tag{B-20}$$

$$g_{12} = 4\cos(r_c x_{12})\sin(r_c x_{12})\cosh(r_c y_{12})\cosh(r_c y_{12})(f_{11}y_{11} + f_{12}x_{11}), \tag{B-21}$$

$$g_{12} = 2\sin^2(r_c x_{12})\sinh^2(r_c y_{11})(f_{11}x_{11} - f_{12}y_{11}), \tag{B-22}$$

and

$$f_{11} = -\frac{r_{cut}\, y_{12}\cos(r_{cut}x_{12}) + \cos\left(r_{cut}x_{12} + 2\tan^{-1}\left|\frac{x_{12}}{y_{12}}\right|\right) - r_{cut}|x_{12}|\sin(r_{cut}x_{12})}{(x_{12}^2 + y_{12}^2)\exp(r_{cut}y_{12})} \tag{B-23}$$

$$f_{12} = -\frac{r_{cut}|x_{12}|\cos(r_{cut}x_{12}) + r_{cut}\, y_{12}\sin(r_{cut}x_{12}) + \sin\left(r_{cut}x_{12} + 2\tan^{-1}\left|\frac{x_{12}}{y_{12}}\right|\right)}{(x_{12}^2 + y_{12}^2)\exp(r_{cut}y_{12})} \tag{B-24}$$

For a root which has only the imaginary part $y_{11}$, the corresponding weight will make the real contribution $x_{11}$ and the contribution to the long-range correction will be

$$h_1^{cut} = -\frac{2|x_{11}|\cosh^2(r_c y_{12})\exp(-y_{12}r_{cut})(y_{12}r_{cut}+1)}{y_{12}^2} \tag{B-25}$$

The long range correction to the virial is divergent This means that the pressure of the metal system must be calculated by a means other that the summing of the individual contributions to the virial as outlined in Chapter 2 This does not present a major problem, since the pressure of the system is readily calculated in the vapor phase during a Gibbs simulation, and calculation of the liquid pressure would only be a redundant measure of the accuracy of the simulation If the pressure of the liquid phase is absolutely needed, the calculated distribution function can be converted to a structure factor and the

derivative of the Helmholtz free-energy with respect to liquid specific volume at constant temperature can be calculated, which is the method presented in chapter 6 for the Gibbs-Bogoliubov method.

Problems arise when using rational polynomials to approximate the dielectric function. Some metal systems have parameters that exhibit multiple poles for certain values of liquid density. Simulations that have this characteristic will "stick" at the density which exhibits the multiple roots, tainting simulation results. To remedy this situation, an arbitrarily small radius was defined around each pole in the upper-half of the imaginary plane. If multiple poles exist at a certain density, then an overlap of two of the radii will occur as the simulation moves toward the offending density. For the purposes of this simulation, a discontinuity is introduced, once overlap between poles is detected, a phantom density 0.1% greater than the density with overlap is used to calculate a new potential, which is used as an approximation to the potential with multiple roots. In most cases, this small nudge is enough to allow the system to negotiate the singularities and problems introduced by multiple roots. The introduced discontinuity is not expected to adversely affect simulations in regimes where the calculated average density is far from the density with degenerate roots.

Table B-1 Coefficients for the numerator of the rational polynomial representation of the dielectric function.

| | Value |
|---|---|
| $a_0$ | $0$ |
| $a_1$ | $1-E\left(B+\frac{2}{3}C+D\right)$ |
| $a_2$ | $-\frac{1237}{3000}+E\left(-2A+\frac{2237}{3000}B+\frac{1637}{4500}C+\frac{4237}{3000}D\right)$ |
| $a_3$ | $\frac{20366383}{252000000}+E\left(\frac{1079}{500}A-\frac{38202383}{252000000}B-\frac{22220783}{378000000}C+\frac{14430487}{28000000}D\right)$ |
| $a_4$ | $\frac{2129061}{70000000}+E\left(-\frac{84038383}{126000000}A-\frac{1292197}{540000000}B+\frac{390998267}{354375000}C+\frac{213162451}{378000000}D\right)$ |
| $a_5$ | $-\frac{6172022347}{14700000000}+E\left(\frac{4252439}{78750000}A-\frac{7783311521}{66150000000}B-\frac{278351043373}{99225000000}C-\frac{242308964083}{198450000000}D\right)$ |

Table B-1 (Continued) Coefficients for the numerator of the rational polynomial representation of the dielectric function

| | |
|---|---|
| $a_6$ | $\frac{22995320777}{11025000000}+E\left(-\frac{132829449323}{99225000000}A-\frac{22995320777}{22050000000}B+\frac{390998267}{354375000}C+\frac{349744199753}{198450000000}D\right)$ |
| $a_7$ | $-\frac{6172022347}{14700000000}+E\left(\frac{509951117}{708750000}A+\frac{2031852119}{3780000000}B-\frac{22220783}{378000000}C-\frac{6416388187}{11340000000}D\right)$ |
| $a_8$ | $\frac{2129061}{70000000}+E\left(-\frac{320831183}{1134000000}A-\frac{21184783}{756000000}B+\frac{1637}{4500}C+\frac{2584087}{84000000}D\right)$ |
| $a_9$ | $\frac{20366383}{252000000}+E\left(\frac{37}{13500}A+\frac{637}{9000}B-\frac{2}{3}C-\frac{293}{1000}D\right)$ |
| $a_{10}$ | $-\frac{1237}{9000}+E\left(-\frac{2}{9}A-\frac{1}{3}B+\frac{1}{3}D\right)$ |
| $a_{11}$ | 1 |

Table B.2 Coefficients for the denominator of the rational polynomial representation of the dielectric function

| | |
|---|---|
| $b_0$ | $E$ |
| $b_1$ | $1-E\left(\frac{2237}{3000}+B+\frac{2C}{3}+D\right)$ |
| $b_2$ | $-\frac{1237}{3000}+E\left(\frac{38202383}{252000000}-2A+\frac{2237}{3000}B+\frac{1637}{4500}C+\frac{4237}{3000}D\right)$ |
| $b_3$ | $\frac{20366383}{252000000}+E\left(\frac{1292197}{540000000}+\frac{1079}{500}A-\frac{38202383}{252000000}B+\frac{22220783}{378000000}C+\frac{14430487}{28000000}D\right)$ |
| $b_4$ | $\frac{2129061}{70000000}+E\left(\frac{7783311521}{66150000000}-\frac{84038383}{126000000}A-\frac{1292197}{540000000}B+\frac{390998267}{354375000}C+\frac{213162451}{3780000000}D\right)$ |
| $b_5$ | $-\frac{6172022347}{14700000000}+E\left(\frac{22995320777}{22050000000}+\frac{4252439}{78750000}A-\frac{7783311521}{66150000000}B-\frac{278351043373}{66150000000}C-\frac{242308964083}{198450000000}D\right)$ |
| $b_6$ | $\frac{22995320777}{11025000000}+E\left(-\frac{2031852119}{3780000000}-\frac{132829449323}{99225000000}A-\frac{22995320777}{22050000000}B+\frac{390998267}{354375000}C+\frac{349744199753}{198450000000}D\right)$ |

Table B-2 (continued) Coefficients for the denominator of the rational polynomial representation of the dielectric function

| | |
|---|---|
| $b_7$ | $\frac{6172022347}{14700000000}+E\left(\frac{21184783}{754000000}+\frac{509951117}{708750000}A+\frac{2031852119}{3780000000}B-\frac{22220783}{372000000}C-\frac{6416388187}{11340000000}D\right)$ |
| $b_8$ | $\frac{2129061}{70000000}+E\left(-\frac{637}{9000}-\frac{32083183}{1134000000}A-\frac{21184783}{756000000}B+\frac{1637}{4500}C+\frac{2584087}{84000000}D\right)$ |
| $b_9$ | $\frac{20364383}{252000000}+E\left(\frac{1}{3}+\frac{37}{13500}A+\frac{637}{9000}B-\frac{2}{3}C-\frac{293}{1000}D\right)$ |
| $b_{10}$ | $\frac{1237}{3000}+E\left(\frac{2}{9}A-\frac{1}{3}B+\frac{1}{3}D\right)$ |
| $b_{11}$ | 1 |

## APPENDIX C
## CALCULATION OF THE RADIAL DISTRIBUTION FUNCTION

The details of implementing an algorithm to calculate the radial distribution function of a fluid are often overlooked. This appendix presents the methods used to gather data for later calculation of the radial distribution function. Expressions are included that stretch the gathered data, allowing an estimate of the radial distribution function beyond the usual half-cell length limit imposed by conventional algorithms. Finally, the smoothing polynomials incorporated into the smoothing algorithm are presented.

Some preliminary bookkeeping is necessary in the calculation of the radial distribution function. A collection of bins is set up that contains MAXBIN bins, with each bin containing a counter. This collection of bins is usually implemented in the C programming language as a zero based array. Each bin represents a range of distances from a center atom. The width of the bin $\delta r$ is determined by dividing the distance $a\sqrt{3}/2$ by the maximum number of bins, where $a$ is length of a side of the cubic simulation cell. Bin 0 is then assigned to represent the range of distances from 0 to $\delta r$, bin 1 represents the distance from $\delta r$ to $2\delta r$, and so on.

A histogram can now be built during simulation that tracks the distribution of distances between pairs of atoms, based on the minimum image distance to other atoms.

Given a pair of atoms, the distance between the centers of the atoms is calculated, and the appropriate bin counter is incremented, if the distance lies within the range of distances represented by the bin. This procedure is repeated for each pair of atoms. Note that each pair makes two contributions to the appropriate bin, so each bin counter is incremented twice for a single pair of atoms. Conveniently, the formula for finding the array index of the bin which represents the distance between the two atoms is the number before the decimal point of the quotient (distance/$\delta r$). The resolution of the gathered radial distribution function thus depends on the resolution of the bins, which is determined by the number of bins and the cubic cell length of the simulated system. The accuracy of the histogram depends on the number of generated Monte Carlo configurations for which distance data has been gathered.

Once the data had been gathered, a method of normalization is employed that maximized the information available from the distance sorting and counting scheme. In the simplest of algorithms, only the data that lies within the largest sphere that can be placed entirely within the cubic simulation cell is considered useful, and this is the simplest normalization transformation. The calculated radial distribution function then has its outer limit at the length $a/2$. Two more geometric regions exist that also contain useful information, and these regions can be visualized as follows. Imagine the framework of a cube of side length $a$ with its origin at the center of the cube, and imagine a sphere of radius $a/2$ with its origin at the same point. The usual normalizing volume corresponds to concentric spherical shells with centers at the origin that lie within this sphere. The sphere touches the cube six times, in the center of each face. Now begin to increase the radius of

the sphere only, as if a balloon was being blown up inside the cube. The sphere now intersects the six faces with six circles. The surface of the sphere enclosed within the cube is the differential element of the second type of volume considered in a more complicated scheme of calculating the radial distribution function. When the radius of the unit sphere reaches the value $(a/2)^{1/2}$, a third differential element is defined by the surface of the sphere enclosed by the cube. The sphere intersects the faces of the cube in four partial arcs, each connected by the straight edge of the cube. This surface shape continues until the sphere gets large enough that there is no intersection with the cube, when the radius of the sphere reaches $a\sqrt{3}/2$.

Complex functions can be defined to calculate the normalizing function for each of the differential surfaces defined above, but since the data gathered in each of the bins is discrete, the differential elements are defined more conveniently in terms of shells of thickness $\delta r$. Using these definitions, the radial distribution function value for the bin representing distances between $r_{i-1}$ and $r_i$ with thickness $\delta r$ is defined by

$$g_{\alpha\beta}^{(i)}\left(r_{i-1}+\frac{\delta r}{2}\right)=\frac{V}{V\left(r_i\right)-V\left(r_{i-1}\right)}\frac{N_{\alpha\beta}^{(i)}}{N_{\alpha\beta}} \qquad \text{(C-1)}$$

where $V$ is the total volume of the system, $N_{\alpha\beta}$ is the total number of particles, $N^{(i)}_{\alpha\beta}$ is the average number of particles counted in this region of space, and $V(r)$ is the function defined by

(C-2)

$$V(r)=\begin{cases}\dfrac{4}{3}\pi r^3 & for \quad r\le\dfrac{a}{2}\\[2ex] 2\pi\left\{\dfrac{2}{3}r^2-\left(r-\dfrac{a}{2}\right)^2\left(2r+\dfrac{a}{2}\right)\right\} & for \quad \dfrac{a}{2}\le r\le\dfrac{a}{\sqrt{2}}\\[2ex] \alpha^3\left\{\left(\lambda^2-2\right)^{1/2}+\left(\lambda^2-\dfrac{1}{3}\right)\left[2\sin^{-1}\left(\dfrac{1}{\left(\lambda^2-1\right)^{1/2}}\right)-\sin^{-1}\left(\dfrac{\lambda^2-2}{\lambda^2-1}\right)^{1/2}-\dfrac{\pi}{4}\right]\right.\\ -\dfrac{\lambda^3}{3}\left[\sin^{-1}\left(\dfrac{\lambda-\left(\lambda^2-2\right)^{1/2}}{2\left(\lambda^2-1\right)^{1/2}}\right)-\sin^{-1}\left(\dfrac{\lambda+\left(\lambda^2-2\right)^{1/2}}{2\left(\lambda^2-1\right)^{1/2}}\right)-\sin^{-1}\left(\dfrac{\lambda^2-\lambda-1}{(\lambda-1)\left(\lambda^2-1\right)^{1/2}}\right)\right.\\ \left.\left.+\sin^{-1}\left(\dfrac{\lambda^2+\lambda-1}{(\lambda-1)\left(\lambda^2-1\right)^{1/2}}\right)\right]\right\} & for \quad \dfrac{a}{\sqrt{2}}\le r\le\dfrac{a\sqrt{3}}{2}\end{cases}$$

Note that $V(r)$ is defined for each of the three differential volume elements described above.

The latter two of the three differential surfaces have increasingly discontinuous edges. Data gathered in the continuous spherical region provides a fairly continuous radial distribution function. Less data is gathered within the other regions, and the accuracy of the calculated radial distribution function begins to become highly dependent on the number of configurations sampled. In simulations with a small number of samples, the extra data gathered can be useless, especially at distances approaching $a\sqrt{3}/2$.

In Monte Carlo simulations some statistical noise may remain in the gathered histogram data, even when a large number of configurations are sampled In order to perform a Fourier transform on the data to examine its structure factor, these random noise elements must be eliminated to avoid spurious peaks in the transformed data. Polynomial smoothing can be used remove some of this noise. A typical set of smoothing polynomials is given by

$$\tilde{g}_{n-2} = \frac{1}{70}\left(69g_{n-2} + 4g_{n-1} - 6g_n + 4g_{n+1} - g_{n-2}\right) \qquad \text{(C-3)}$$

$$\tilde{g}_{n-1} = \frac{1}{35}\left(2g_{n-2} + 27g_{n-1} + 12g_n - 8g_{n-1} + 2g_{n-2}\right)$$

$$\tilde{g}_n = \frac{1}{35}\left(-3g_{n-2} + 12g_{n-1} + 17g_n + 12g_{n+1} - 3g_{n-2}\right)$$

$$\tilde{g}_{n-1} = \frac{1}{35}\left(2g_{n-2} + 27g_{n+1} + 12g_n - 8g_{n-1} + 2g_{n-2}\right)$$

$$\tilde{g}_{n-2} = \frac{1}{70}\left(69g_{n-2} + 4g_{n+1} - 6g_n + 4g_{n-1} - g_{n-2}\right)$$

Radial distribution data presented in this dissertation is smoothed using (C-3)

## REFERENCES


1 A. Z Panagiotopoulos, *Molecular Physics*, **61** 813 (1987)

2 I H Umar, A. Meyer, M. Watabe, W H Young, *Journal of Physics F: Metal Physics*, **4**, 1691 (1974)

3 P. Minchin, M Watabe, and W H Young, *Journal of Physics F: Metal Physics*, **7**, 563 (1977)

4 C T Ewing, J P Stone, J R. Spann, and R. R. Miller, *Journal of Physical Chemistry*, **71**, 473 (1967)

5 N W Ashcroft, *Physics Letters* **23**, 48 (1966)

6 A. Arnold, N Mauser, and J Hafner, *Journal of Physics: Condensed Matter*, **1**, 965 (1980)

7 S M Osman and W H Young, *Physical Chemistry of Liquids*, **17**, 181 (1987)

8 D McQuarrie, *Statistical Mechanics* Harper & Row Publishing, New York, 1976

9 N. March, *Liquid Metals. Concepts and Theory*, Cambridge University Press, New York, 1990

10 N Metropolis, A. W Rosenbluth, M N Rosenbluth, A. H Teller and E Teller, *Journal of Chemical Physics*, **21** 1087 (1953)

11 L D Landau and E. M Lifschitz, *Statistical Physics*, Pergamon, New York, 1980

12 G Jacucci and A. Rahman, *Nuovo Cimento* **D4**, 341 (1984)

13 R Friedberg and J E Cameron, *Journal of Chemical Physics* **52**, 6049 (1970)

14 D Fincham, N Quirke, and D J Tildesley, *Journal of Chemical Physics* **84** 4535 (1986)

15 I R. McDonald and K Singer, *Molecular Physics* **23**, 29 (1972)

16 J P Hansen and L. Verlat, *Physical Review* **184** 151 (1969)

17 W W Wood, *Physics of Simple Liquids*, edited by H N V Temperley, J S Rowlinson, and G S Rushbrooke, North Holland, Amsterdam, 1968

18 I R. McDonald, *Molecular Physics*, **23**, 41 (1972)

19 G E Norman and V S Filinov, *High Temperature USSR*, 7, 216 (1969)

20 D J Adams, *Molecular Physics* **32**, 647 (1976).

21 D J Adams, *Molecular Physics* **37**, 211 (1979)

22 B Widom, *Journal of Chemical Physics* **39**, 2808 (1963)

23 K S Shing and K E Gubbins, *Molecular Physics* **49**, 1121 (1983)

24 S Romano and K Singer *Molecular Physics*, **37**, 1765 (1979)

25 J G Powles, W A B Evans, and N Quirke, *Molecular Physics*, **46** 1347 (1982)

26 A Z Panagiotopoulos, N Quirke, M Stapleton, and D J Tildesley, *Molecular Physics* **63** 527 (1988)

27 B Smit, Ph De Smedt, and D Frenkel, *Molecular Physics*, **68**, 931 (1989)

28 B Widom, *Journal of Chemical Physics*, **39**, 2808 (1963)

29 B Smit, C P Williams, E M Hendricks, and S W de Leeuw, *Molecular Physics*, **68**, 765 (1989)

30 M R. Stapleton, D J Tildesley, N Quirke, and A. Z Panagiotopoulos, *Molecular Simulation* **2**, 147 (1989)

31 B Smit and D Frenkel, *Molecular Physics* **74**, 35 (1991)

32. E. de Miguel, L F Rull, and K. E Gubbins, *Physica A*, **177**. 174 (1991)

33 J J de Pablo, J M Prausnitz, H J Strauch, and P T Cummings *Journal of Chemical Physics* **93** 7355 (1990)

34 G C A. M. Mooij D Frenkel and B Smit, *Journal of Physics: Condensed Matter* **4**, L255 (1992)

35 J J de Pablo, M Bonnin, J M Prausnitz, *Fluid Phase Equilibria* **73**, 187 (1992)

36 W L Jorgensen, J D Madura, C J Swenson, *Journal of the American Chemical Society*, **106**, 6638 (1984)

37 B Smit, Ph De Smedt, and D Frenkel, *Molecular Physics*, **68**, 931 (1989)

38 S Zhen and G J Davies, *Physica Status Solidi*, **78** 595 (1983)

39 I V Abarenkov and V Heine *Philosophical Magazine* **12**, 529 (1965)

40 B J Austin, V Heine, and L. J Sham, *Physical Review*, **127**, 276 (1962)

41 J Hafner, *From Hamiltonians to Phase Diagrams, Springer Series in Solid State Sciences* Springer, Berlin, 1987

42 J Hafner and G Kahl *Solid State Communications* **49** 1125 (1984)

43 M. Gell-Mann and K A. Brueckner, *Physical Review*, **106** 364 (1957)

44 S Ichimaru and K Utsumi *Physical Review B* **24**, 7285 (1981)

45 S Ichimaru *Reviews of Modern Physics* **54**, 1017 (1982)

46 J Hafner and V Heine *Journal of Physics F: Metallic Physics* **13**, 2479 (1983)

47 J Hafner and V Heine, *Journal of Physics F Metallic Physics* **16**, 1429 (1986)

48 D G Pettifor, *Physical Metallurgy vol 1* ed by R. W Cahn and P Haasen, North Holland, Amsterdam, 1983

49 J Lindhard *K Dan.Vidensk.Selsk.Mat.Fys.Medd. (8)*, 18 1 (1954)

50 D Pines, *The Theory of Quantum Liquids*, ed. by D F Brewer, Benjamin, New York, New York, 1966

51 S Ichimaru and K Utsumi *Physical Review B* **24**, 7285 (1981)

52 T Lukes, R. Jones, *Journal of Physics A*, **1**, 539 (1968)

53 N W Ashcroft and J Lekner, *Physical Review* **143**, 145 (1966)

54 N W Ashcroft and D C Langreth, *Physical Review*, **156**, 685 (1967).

55 M. Ross, H. E DeWitt, W B Hubbard, *Physical Review A* **24**, 1016 (1981)

56 P Nozieres and D Pines *Physical Review*, **111**, 442 (1958)

57 L Hedin and H Lundquist *Solid State Physics*, ed by F Seitz and D Turnbull, Academic Press, New York 1966

58 R. G. Chapman, *Reports on Progress in Physics*, **30**, 615 (1967).

59 F. Yonezawa and T. Ogawa, *Progress in Theoretical Physics Supplement*, **72**, 1 (1982).

60 T. Arai and I. Yokohama, *Physical Chemistry of Liquids*, **26**, 143, (1993).

61 N. B. Vargaftik, *Tables on the Thermophysical Properties of Liquids and Gases*, John Wiley and Sons, New York, 1975.

62 M. P. Allen and D. J. Tildesley, *Computer Simulation of Liquids*, Clarendon Press, Oxford, 1989.

63 G. C. Maitland, M. Rigby, E. B. Smith, and W. A. Wakeham, *Intermolecular Forces*, Clarendon Press, Oxford, 1981.

64 *CRC Handbook of Chemistry and Physics*, 74th Edition, CRC Press, Boca Raton, 1993.

65 R. Hultgren, P. Desai, D. Hawkins, M. Gleiser, K. Kelley, and D. Wagman, *Selected Values of the Thermodynamic Properties of the Elements*, American Society for Metals, Metals Park, 1973.

66 Y. Waseda, *The Structure of Non-Crystalline Materials-Liquids and Amorphous Solids*, McGraw-Hill, New York, 1980.

67 R. Piessens, E. De Doncker-Kapenga, C. W. Uberhuber, D. K. Kahaner, *QUADPACK-A Subroutine Package for Numerical Integration*, Springer-Verlag, New York, 1983.

68 N. S. Gingrich and L. Heaton, *Journal of Chemical Physics*, **34**, 873 (1961).

69 R. Kumaravadivel, R. Evans, *Journal of Physics C*, **9**, 2080 (1977).

70 M. Ross, H. E. de Witt, and W. B. Hubbard, *Physical Review A*, **26**, 2255 (1982).

71 W. L. Slattery, G. D. Doolen, and H. E. DeWitt, *Physical Review A*, **21**, 2087 (1980).

72 K. K. Mon, R. Gann, and D. Stroud, *Physical Review A*, **24**, 2145 (1981).

73 J. M. Ziman, *The Physics of Metals-1 Electrons*, Cambridge University Press, New York, 1969.

74 K. P. Huber, G. Herzberg, *Molecular Spectra and Molecular Structure - IV. Constants of Diatomic Molecules*, Van Nostrand Reinhold Company, New York, 1952.

75 R. Venkatesh, *Physica Status Solidi*, **176**, 91, (1993).

76 J E Enderby and D M North, *Physics and Chemistry of Liquids*, 1, 1, (1968).

77 D G Pettifor and M A Ward, *Solid State Communications* 49, 291 (1984)

## BIOGRAPHICAL SKETCH

Mark Montoya was born on August 21, 1965, in Las Cruces, New Mexico. It was there he developed his love for tortillas, tamales, and hot dry weather, despite the fact he was only a baby at the time and cannot remember exact details. After brief stints in Midland, Texas, and El Paso, Texas, Mark found his way to Northern New Mexico where he finally settled in Los Alamos at the age of ten. His long academic career led him through Los Alamos High School, and eventually to New Mexico State University in Las Cruces, where he studied chemical engineering, mathematics, and computer science. Undergraduate summers were spent at the Los Alamos National Laboratory, where Mark worked in the field of health physics. After graduation, Mark returned to Los Alamos for a brief stay with the now defunct laser isotope separation group. No connection between the demise of this important research group and Mark has been proven, however.

Shooting a basketball in the thin high altitude air of Los Alamos proved too much of a challenge for Mark, so he thought it best to attend a school near sea level, where the dense air would allow the "English" on his shots to have maximum effect. He ended up at the University of Florida, where he began six years of graduate study. This document is preventing a seventh. Mark's love for tortillas, tamales, and hot, dry weather has never been fully satisfied, and he will return to Las Cruces to begin teaching at New Mexico State University in the Fall of 1994.

I certify that I have read this study and that in my opinion it conforms to the acceptable standards of scholarly presentation and is fully accurate, in scope and quality, as a dissertation for the degree of Doctor of Philosophy

Timothy Anderson, Chair
Professor of Chemical Engineering

I certify that I have read this study and that in my opinion it conforms to the acceptable standards of scholarly presentation and is fully accurate, in scope and quality, as a dissertation for the degree of Doctor of Philosophy

Ioannis Bitsanis
Assistant Professor of
Chemical Engineering

I certify that I have read this study and that in my opinion it conforms to the acceptable standards of scholarly presentation and is fully accurate, in scope and quality, as a dissertation for the degree of Doctor of Philosophy

Gar Hoflund
Professor of Chemical Engineering

I certify that I have read this study and that in my opinion it conforms to the acceptable standards of scholarly presentation and is fully accurate, in scope and quality as a dissertation for the degree of Doctor of Philosophy

David Micha
Professor of Chemistry

I certify that I have read this study and that in my opinion it conforms to the acceptable standards of scholarly presentation and is fully accurate, in scope and quality as a dissertation for the degree of Doctor of Philosophy

Mark Orazem
Professor of Chemical Engineering

This dissertation was submitted to the Graduate Faculty of the College of Engineering and to the Graduate School and was accepted as partial fulfillment of the requirements for the degree of Doctor of Philosophy

August 1994

Winfred M. Phillips
Dean, College of Engineering

Karen A. Holbrook
Dean, Graduate School